Combined Design and Control Optimization: Application to Optimal PHEV Design and Control for Multiple Objectives

by

Rakesh M. Patil

A dissertation submitted in partial fulfillment
of the requirements for the degree of
Doctor of Philosophy
(Mechanical Engineering)
in The University of Michigan
2012

Doctoral Committee:

Professor Zoran S. Filipi, Co-Chair
Assistant Professor Hosam K. Fathy, Co-Chair
Professor Gregory A. Keoleian
Professor Huei Peng

I have yet to see any problem, however complicated, which, when looked at the right way, did not become still more complicated.

— Paul Alderson, in ”New Scientist”, 25 September 1969.

Inventions have long since reached their limit, and I see no hope for further development.

— Julius Sextus Frontinus, highly regarded engineer in Rome, 1st century AD.

This thesis is dedicated to my parents,
and to my younger brother, Vineeth.

Acknowledgments

I would like to thank my advisers, Profs. Zoran Filipi and Hosam Fathy. Their advice and pertinent questions directed the majority of my research. Prof. Filipi provided me the opportunity to work in the W.E. Lay Automotive Lab for my master's and PhD. His perspectives on hybrid vehicles research helped me define the questions for my PhD. He was also instrumental in providing necessary resources and the freedom to work on several topics with minimal restrictions.

Prof. Fathy spent several hours meeting and discussing the minute details of my work. He asked the questions, that made make me go back, dig into literature and think differently. He believed in my work and constantly encouraged me to aim higher. A major inspiration for my PhD research was his PhD work on combined design and control optimization.

I am extremely thankful to my committee members, Prof. Huei Peng and Prof. Gregory Keoleian, for asking tough questions and providing critical feedback at our meetings. Their insightful advice has been crucial towards creating a solid foundation for the work presented in this dissertation. I truly appreciate their time and effort in reviewing this work. I would also like to thank Prof. Jeffrey Stein, for his excellent questions and his constant support and appreciation of my research through the NSF-EFRI group.

Next, I would like to thank the many researchers I collaborated with. Brian Adornato and his work on characterizing drive cycles added a new dimension to my research. Brian also managed to point me towards some aspects of the 'American' way in research as well as in life. I would like to thank Prof. Timothy Gordon and Dr. Zevi Bareket of UMTRI for providing the naturalistic driving data used in my work. My communications with Dr. Jarod Kelly provided me with great insights and models regarding electric grid dispatch. This model, as described in chapter 3, has been extensively used to predict grid emissions for my research. Chiao-Ting Li, as a student member of the EFRI group also provided data on frequency regulation power demands. Most importantly, she and other members of the NSF-EFRI research group provided critical feedback of my work and helped me learn many things that are not in my domain of expertise.

None of this research would have been possible without the constant support and mentor-

ing from my lab mates. Scott Moura has questioned and encouraged my research by going to great lengths from which he had little to gain. His work and his approach to research inspired me to work harder and better. Rajit Johri was my go-to guy when I had worked on something for months to no avail. His affable nature and the tenacity with which he approached research deserves the utmost respect and my sincere gratitude. There are several lab mates that I cannot thank enough for their company, and for their ideas - Fernando Tavares, Joel Forman, Rahul Ahlawat, Tae-Kyung Lee, Andres Ivanco, Youngki Kim and Rohit Gupta.

Finally, I wish to thank all my friends in Ann Arbor, without whose company I could probably have finished my research a few years earlier. On a more serious note, the times I spent in Willowtree, Parc Pointe and Island Drive apartments with countless friends exploring the world that has been and will be, was nothing short of extraordinary. All the great food cooked at these places merits special mention. I am also extremely grateful for the 'good times' that I had at Josh's Miller times. Leah and Mark invited me to their lovely home for the most sumptuous thanksgiving meals and words can do no service for that. I would also like to thank my wonderful girlfriend Alexandra. Her American ways and her questions about all things graduate school were inspiring and humbling. Her company has truly enriched my PhD journey. I would also like to thank her parents for all the great food.

My Parents believed in me and they constantly supported and encouraged all my academic endeavours and I thank them for that. Without their sensible guidance at various points in my life, all this research would not be possible.

Table of Contents

List of Tables

Table

List of Figures

Figure

List of Appendices

Appendix

Abstract

This dissertation develops algorithms and frameworks to obtain the optimal design and control solutions for a non-linear dynamic system in a computationally efficient manner. These methods and their advantages are demonstrated by applying them to a Plug-in Hybrid Electric Vehicle (PHEV) powertrain's optimal design and supervisory control. Since a PHEV draws energy from the electric grid it is important to consider these interactions in optimal design and control decisions of the PHEV. At the same time the battery size significantly affects the amount of grid energy transferred to propulsion and consequently the on-road power management decisions. Thus, we develop and apply algorithms capable of highlighting the optimal PHEV battery size and control decisions that result in a synergistic interaction with the electric grid.

First, we develop a Dynamic Programming (DP) based optimal control algorithm capable of evaluating optimal on-road power management for a series PHEV. This algorithm was based on a backward looking implementation of the PHEV powertrain's dynamic model. Such an implementation of the DP algorithm avoided the need to interpolate the value function or enforce constraints through penalty functions, thereby alleviating crucial computational concerns. The performance of two supervisory control strategies for series PHEVs was compared using this algorithm. For a series PHEV, the results show that a charge deplete and sustain approach is comparable in performance (in $ costs) to the optimal strategy in most cases (esp. when gasoline is more expensive per mile than electricity).

Then, we extend this algorithm to consider optimal charging on the electric grid. This extension was made possible by understanding and utilizing the conditions at the boundaries of the optimal charging and driving problems, and the computational attractiveness offered by the above DP algorithm. The results showed the tradeoffs between optimal charging and power management decisions depending on grid mix and driving conditions, thereby highlighting the need for such an approach. This algorithm was further applied to understand the possible optimal CO_2 reduction benefit translated to propulsion depending on increased wind power on the grid.

Since PHEVs are expected to be instrumental in reducing emissions while offering

operational cost benefits to the owner, and are expected to participate in grid services such as storage and regulation, we develop a multi-objective dynamic programming (MODP) algorithm. This algorithm utilizes the idea of crowding distance from Non-Dominated Sort Genetic Algorithms (NSGA) literature to represent the Pareto front with fewer points thereby easing the computational time and memory requirements for such problems. For the grid mix and driving behavior assumed, tradeoffs in achieving minimum CO_2 vs. minimum operational costs are discussed.

Finally, we extend and utilize the theory on the combined optimization of a dynamic system's design and control to size the PHEV battery by taking its optimal charging and power management decisions into account. This approach is computationally efficient through the use of a coupling term that captures the dependence between the design and the optimal control. The salient features of the algorithm such as the calculation and use of the coupling term and the accompanied reduction of computational effort is first demonstrated by solving a beam mass reduction and vibration attenuation problem. Then, this algorithm is applied for optimal battery sizing of a PHEV while considering the dependence of the optimal supervisory control solution on the battery size. The coupling term provided insights into this dependence and helped obtain the optimal battery sizes while considering the optimal control with low computational effort.

Chapter 1
Introduction

This dissertation develops algorithms and frameworks to obtain the optimal design and control solutions for nonlinear dynamic systems in a computationally efficient manner. These methods and their advantages are demonstrated by applying them to a Plug-in Hybrid Electric Vehicle (PHEV) powertrain's optimal design and supervisory control. Currently, PHEVs are touted as the next step in vehicle powertrain technology due to their ability to draw power from the electric grid, store it in batteries, and use it for transportation [1] as well as electric grid related services [2, 3]. A PHEV's battery size significantly affects its charging and on-road power management decisions [4, 5, 6]. Hence, this work is motivated by the problem of optimizing the design (e.g., component sizing) and supervisory control (e.g., power management and charging) of PHEVs.

There are two major technical challenges that are resolved in this dissertation. The first challenge is related to the optimization of supervisory control of a PHEV. PHEVs, unlike HEVs or conventional vehicles interact with the electric grid. Therefore, we have to consider the optimal charging control and the optimal on-road control problems and their dependence on each other. At the same time, this optimization algorithm has to be flexible to address the multiple objectives and services that a PHEV is targeted to be used for. Developing an integrated framework capable of including multiple objectives for a nonlinear dynamic system such as a PHEV powertrain is conceptually challenging and necessitates computational efficiency. The second major challenge is to obtain the optimal PHEV battery sizes accounting for its usage (the supervisory control actions). For this purpose, the dependence between the static nature of the optimal design problem and dynamic nature of the optimal control problem has to be rigorously characterized and assimilated in the optimization, while retaining computational feasibility.

These challenges were resolved through innovative approaches in optimization methods and by understanding the PHEV's system dynamics. The two optimal control problems for a PHEV (charging and on-road power management) were integrated by exploiting the constraints at the boundaries of these two problems. The results showed that considering the

dependence between the charging decisions and on-road power management is essential. For example, it is shown that it is not always optimal to fully charge the battery before each driving trip, as it is assumed in most of the literature [7, 8, 9]. To solve the combined design and control optimization problem, our approach was to define and calculate the sensitivity of the optimal control solutions to the size of the battery. By capturing this sensitivity in a computationally efficient manner, the coupling term was demonstrated to reduce the function evaluations necessary to attain the combined optimum. Through the insight provided by this sensitivity (or coupling term), we inferred the combined optimal battery sizes that result in minimum CO_2 emissions throughout the PHEV's manufacturing and usage. Under our grid mix and driving behavior assumptions, the results showed that a larger battery size does not necessarily result in lower lifecycle CO_2 emissions. Ultimately, these methods integrating the two control optimization problems as well as the design optimization problem can also be applied more generally to other dynamic systems.

The remainder of the introduction section is organized as follows. First, the big picture motivation for this research is presented. Next, the related literature is reviewed and the research gaps that this dissertation addresses are identified. Finally, we summarize the unique contributions of this dissertation and outline their development in the remaining chapters.

1.1 Motivation

Plug-in hybrid electric vehicles (PHEVs) are hybrid vehicles that can draw energy from the electric grid and supply propulsive energy for transportation. This functional change allows a plug-in hybrid to displace petroleum energy with multi-source electrical energy. The interconnection between the transportation and the electric grid infrastructures through the PHEV presents opportunities to reduce emissions in transportation including green house gas emissions, lower costs to the consumer and use battery energy storage for grid services [2, 3].

There are many challenges in achieving these multitude of objectives. There are challenges at the subsystem or component levels (e.g. battery technology, smart metering), at the system level (*e.g.* PHEV design, integrating intermittent renewable power) and at the interconnections of these systems (*e.g.* fleet charging, demand side control). Battery technology is essential for efficient energy storage and transportation. In this aspect, there are challenges related to battery charge and health estimation [10], improving energy density through chemistry [11], and costs reduction through sizing and other avenues [12]. Smart

grid technology faces challenges related to communication networks [13], security and privacy issues [14] and reliability [15]. Successful integration of renewable power sources requires increased storage [10], and regulation capability on the electric grid [16]. It is also vital that all the pieces of the puzzle fit together in a symbiotic fashion [17, 18]. Furthermore, at each of these subsystem and system levels, many interesting questions remain unanswered. Thus, it is imperative to clearly define the areas of focus of this dissertation.

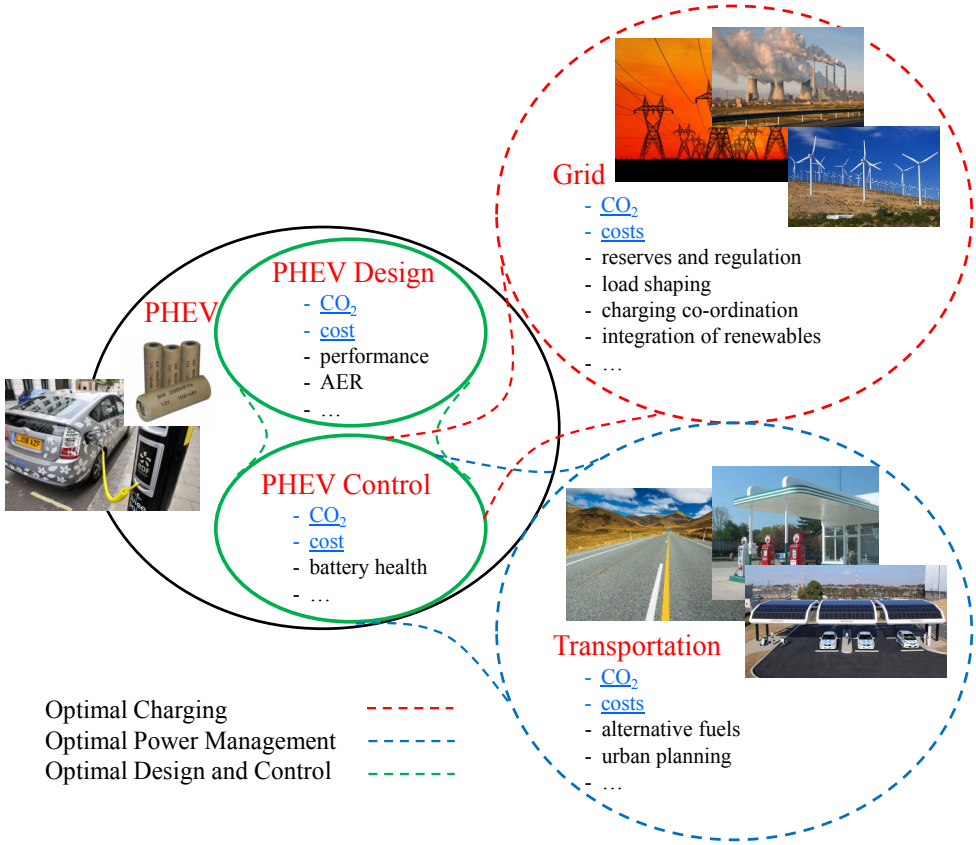

Figure 1.1 Interconnections between different systems, the optimization problems, and the goals (underlined) considered

The research in this dissertation specifically focuses on the PHEV system, optimizing its battery size and control strategies to maximize its synergistic interaction with the electric grid (Fig. 1.1). It is understood that the loading of the PHEV on the electric grid can result in excessive stress or instability of the infrastructures [17, 18]. Studies that looked at different PHEV charging scenarios show that charging based on intuitive rules might exacerbate grid load, increase emissions and in extreme cases may also result in catastrophic events such as blackouts [19, 20]. In addition, the costs of vehicle electrification, along with the

uncertainties related to new technologies might significantly affect consumer adoption [22]. Thus, our objective in this dissertation is to develop optimization methods that highlight opportunities from an individual PHEV's perspective for a series PHEV powertrain's design and control while including information about its interactions with the electric grid.

These goals will be accomplished through the development of computationally efficient optimization methods. In Fig. 1.1, the connections between different systems, the goals of each subsystem, and the boundaries of different optimization problems are shown. The solid boundaries indicate the systems and problems considered in this dissertation. The dashed boundaries indicate the systems that are affected by the PHEV and whose operational constraints will be instrumental in the design and control of a PHEV. It is clear that the PHEV can be designed and optimized for endless objectives and scenarios. In this dissertation, we restrict ourselves to meaningfully tackle the goals that are underlined in Fig. 1.1.

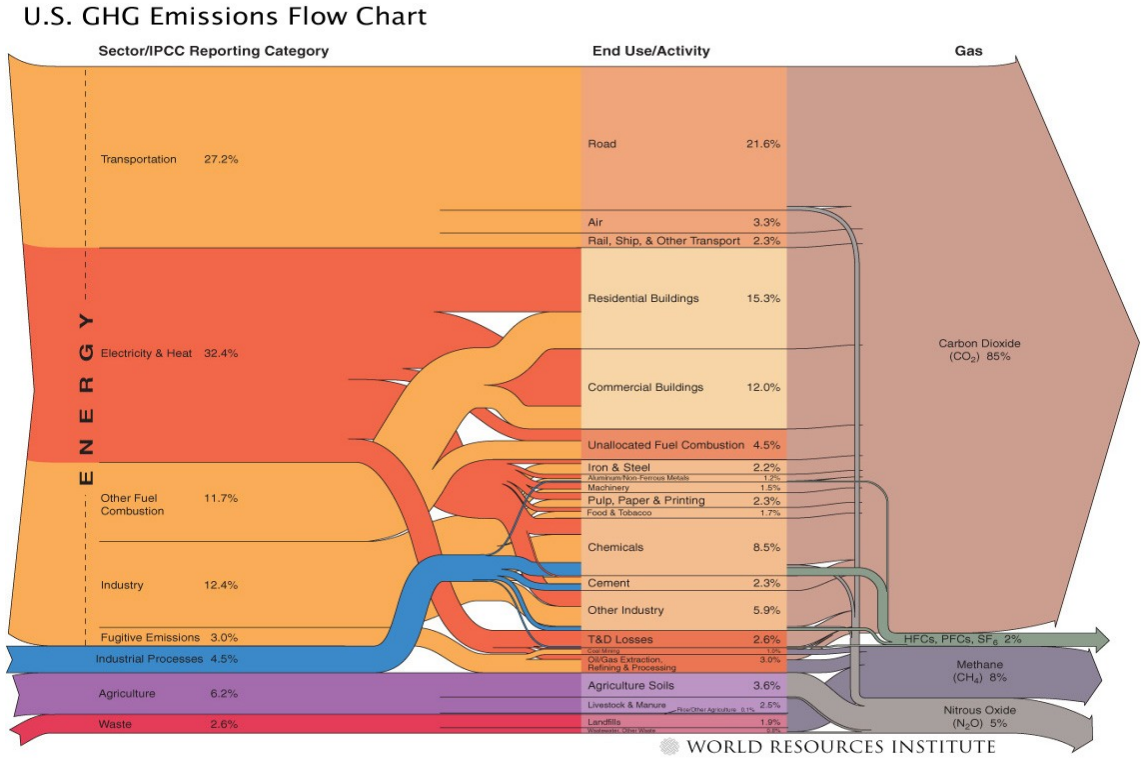

Figure 1.2 Flowchart for GHG Emissions in the US (1990-2003) [21]

Of the goals mentioned in Fig. 1.1, particular importance is given to minimizing CO_2 emissions and the dollar costs incurred by a PHEV owner. This is because the electric grid and the transportation sector result in more than 60% of US greenhouse gas emissions (GHG), of which a significant portion is due to CO_2 emissions, as shown in Fig. 1.2. At the same time, the dollar costs incurred by a customer are a major influence on a consumer's

decisions to buy and to charge/fuel a PHEV [22, 23]. Thus, minimizing CO_2 emissions and dollar costs are the objectives considered in our optimization studies. The coupling of the electric grid with the PHEV not only provides cleaner fuels for transportation through renewable sources like wind and solar but also provides opportunities for using PHEV for electric grid services such as storage and regulation. These services are termed 'Vehicle-to-Grid' or V2G services [2, 3]. The idea is to use the energy stored in the PHEV battery for grid services because the PHEV is stationary for a majority of the time. Major V2G services currently discussed are spinning reserves, frequency and voltage regulation, valley filling and peak shaving [3, 16, 23]. Thus it is necessary to optimize PHEV activity on the grid, along with its activity on the road in order to maximize the benefits of PHEV introduction. Optimizing the charging and on-road power management in a single framework also helps understand the impacts of V2G services on the PHEVs on-road usage.

At the same time it is necessary to size the PHEV components appropriately to facilitate its usage for the above services and objectives. The batteries used in PHEVs are electrochemical storage devices. The battery in a PHEV is substantially larger than in an HEV, in order to draw and store electric energy from the grid rather than act as a buffer only [3, 23]. Several advantages of using a battery are outlined in the previous paragraphs. Some weaknesses of electrochemical energy storage relative to conventional petroleum-based fuels include low specific energy, low energy density, low refuelling/recharging rate and high initial costs [25]. Thus, for widespread introduction and usage of PHEVs for multiple goals, battery sizing is an important task. In addition, optimal battery sizing requires the consideration of how the battery will be used or controlled. For example, using a large battery can ensure all-electric driving for a certain driving distance during the day (say 40 miles), or a smaller battery with multiple charging events can also ensure all-electric driving for the same distance. Such tradeoffs motivate us to consider the problem of optimal battery usage together with optimal battery sizing in order to not sacrifice total system level optimality.

1.2 Literature

This section highlights the research gaps that will be addressed in this dissertation by briefly discussing the relevant literature. A more detailed discussion of literature on each topic will be presented in the respective chapters. Previous work on the development and application of optimal control algorithms, and combined design and control optimization as applied to vehicle powertrains is briefly discussed. In addition, some of the literature related to V2G

services and multi-objective optimization is also presented to motivate the research in this dissertation.

1.2.1 Optimal Control Objectives and Methods

There are two optimal control problems for PHEVs considered in the literature. First, is on-road power management, which refers to the best combination of engine and battery usage to achieve a chosen objective [26, 27]. Some of the objectives considered for on-road HEV and PHEV power management are MPG [26, 27, 28, 29] , emissions [30, 31, 32], drivability [33], battery health [34] and combined fuel and electricity consumption [35, 36]. Previous research has mostly addressed power management for parallel and power split configuration hybrids [26, 27, 28, 29, 30, 31, 32, 35]. In order to obtain minimum fuel and electricity consumption, it is shown that smartly battery power with the aid of IC engine power (blending) produces optimal results [36]. For a series PHEV, the configuration lends itself to a control strategy where battery charge is depleted first and then the engine is used to sustain battery charge around a threshold and power the vehicle [37]. Though this control strategy is easier to implement and it exploits some obvious design features of the series configuration, the optimality of such a control strategy has not been discussed in the literature. Thus, one of the goals of this dissertation is to calculate and analyze optimal power management solutions for a *series* PHEV.

The second optimal control problem for PHEVs considered in the literature is charging. Optimal charging refers to the amount of charge and the charging times to minimize some environmental or economic objective for a given PHEV over the span of a day. The goals addressed in the literature are minimization of dollar costs of electricity consumed by the PHEV [7, 8], minimize emissions [9], maximize battery health [38] and/or provide V2G services to the grid [39, 40]. Researchers have also developed optimal control solutions to charge fleets of PHEVs while maintaining suitable grid operation [9, 40, 41, 42]. Existing studies on optimal charging assume the need for a full charged PHEV battery and optimize the charging to satisfy these driving needs [8, 9, 40, 41, 42, 43]. PHEV charging activities, especially when used for V2G services, strongly influence the initial conditions for on-road power management [41, 44]. Studying the optimal charging and driving problems separately restricts the exploration of the total optimality of PHEV usage [38, 45]. In this dissertation, we study the two optimization problems together for an individual PHEV, thereby considering the dependence between its charging and on-road power management.

Several optimal control methods have been applied to PHEV charging and power management problems. A list of these methods includes dynamic programming (DP) [27, 30, 31],

predictive control [40, 46, 47], Equivalent Consumption Minimization Strategy (ECMS) [28, 32, 35], Evolutionary Algorithms (EA) [9, 38, 48], game theory [39], and intelligent rule based optimization methods [29, 49]. ECMS is based on Pontryagin Minimum Principle (PMP) and provides optimal solutions for power management under certain assumptions [28]. EA and rule based control methods represent the dynamic controller through static variables and optimize for the values of these static variables. ECMS, EA and rule based methods provide controllers that are easy to implement. The dynamic programming approach explicitly uses Bellmans principle for optimal control, and thus guarantees global optimality. Stochastic DP is used to obtain optimal solutions over all realizations of stochastic variables such as driving power and/or grid mix [30, 31, 36]. In our studies we use deterministic DP because we wish to analyze and understand the nature of the optimal control for different scenarios on the grid and driving. The output of this process is a supervisory control trajectory that can be used to gain important physical insights and extract implementable rules for subsequent online power management [50, 51].

1.2.2 Vehicle to Grid (V2G) Applications

The idea of using PHEVs for V2G services was introduced and studied in detail by Kempton *et al.* [2, 3]. As the electric grid includes more renewable power sources through economic and policy requirements [16, 52, 53], there is an increased need for storage and regulation (frequency and voltage) [1, 2, 16]. The use of PHEV batteries for storage and spinning reserves has been investigated in [3, 24]. Though these are services that the PHEV can be used for, it is understood that frequency regulation and demand-side control are more attractive services for the following reasons. First, several analyses show that allowing a PHEV to be used for regulation can provide a PHEV owner with higher revenue than most other V2G services [24, 54]. Second, discharging and charging PHEV batteries at a low rate resulting in small amounts of total energy flow is less harmful to battery health than its use for storage [55, 56]. In this dissertation, we will demonstrate the use of our integrated optimal charging and power management framework (Chapter 3) to study impacts of using PHEVs for services with low power demands and high financial potential.

1.2.3 Multi-Objective Control Optimization

PHEVs create significant opportunities for emissions reduction, reduction of operational costs to utilities and consumers and will be required to provide several V2G services [1, 2]. To best utilize a PHEV for these multiple purposes, it is necessary to obtain optimal control

solutions considering multiple objectives. Previous research in optimal PHEV supervisory control has mostly considered single objective optimization [27] - [30] and [32] - [9].

To consider multiple objectives in control optimization of vehicle powertrains, two approaches have been adopted previously. One is using Multi Objective Evolutionary Algorithms (MOEA) [57, 58]. Since EAs work with populations of points in each iteration, a number of Pareto-optimal solutions may be captured in an efficient manner using non-domination operators [59, 60]. However, the controller has to be parametrized in order to use such algorithms due to their static nature. The second approach is to combine multiple objectives into a single objective through a weighting scheme, and use the optimal control methods mentioned in section 1.2.1. This method requires multiple optimizations to obtain the Pareto front [34] and is not conducive to reveal the non-convex regions of the front [61]. Thus there is a need to develop an optimal control method capable of addressing multiple objectives efficiently (like MOEA) while retaining the dynamic nature of rigorous optimal control methods.

1.2.4 Combined Design and Control Optimization

In PHEVs, the dependence between design and control is more pronounced than other powertrains due to the sensitivity of the supervisory control to the battery size. For example, in [6], authors show that smarter power management algorithms can reduce vehicle energy consumption and hence reduce battery energy capacity requirements. At the same time, a larger battery capacity means more flexibility with charging times [38, 45]. In addition to the above considerations, batteries are expensive and their sizing is an important concern for consumer acceptance of PHEVs [25, 62]. Thus there is a need for the combined battery sizing and supervisory control optimization of a PHEV powertrain.

At the same time, solving the plant design and control optimization problems through a simultaneous or a combined approach 1) guarantees complete dynamic system optimality [63, 64, 65, 66] and 2) considers the dependence of the controller design problem on the plant design [63, 67, 68, 69, 70]. The computational cost of simultaneous plant/control optimization can be quite prohibitive [71, 72, 73]. In addition, the PHEV powertrain model does not lend itself to optimization with fast gradient based algorithms. This is because the model is non-linear (due to component efficiency maps) and discontinuous (due to different modes of operation). Hence, there is need for an efficient yet rigorous computational plant/control optimization framework.

Several methods address both design and control issues and some of them have been applied for a vehicle powertrain's design. The major challenge these methods seek to address is

to reconcile the dynamic nature of the controller optimization problem with the static nature of the design optimization problem in a computationally attractive manner [74]. Parametric studies (varying battery size) are helpful in understanding the impacts of varying the design on the available control solutions [6, 75], but they do not provide the optimal solutions. The most common combined optimization approach is to develop a surrogate controller model, which represents a rule based control [29, 57, 58], or simplifications of optimal control solutions [66]. This surrogate model is then included in the design optimization process to obtain a combined optimum. These methods ensure computational feasibility but sacrifice optimality due to the simplifications involved in obtaining the surrogate control model. Finally, a nested optimization method with or without a sensitivity term (quantifying the dependence of the optimal control solution on the design) obtains the combined optimal solution [70, 76] in a rigorous manner with fewer assumptions on the controller structure. Such methods are computationally demanding [71, 72]. This is due to the need to optimize the controller several times for each design optimization iteration. Hence, such methods have been applied to hybrid powertrain design and control sparingly [77], due to the non-linear and discontinuous nature of the models involved. Thus our research will develop a computationally efficient yet rigorous combined optimization procedure and demonstrate its application to optimal PHEV battery sizing and control.

1.3 Research Challenges

In summary, the unanswered research questions from above sections 1.2.1- 1.2.4 that will be addressed in this dissertation are:

- To develop optimal power management algorithms for series PHEVs over a range of driving distances and study the nature of the optimal control solution. Though there are intuitive power management solutions for series PHEVs, a rigorous comparison of these solutions through optimal control of series PHEV has not been performed.
- To develop an integrated optimal charging and optimal power management algorithm. Previous studies consider these problems separately and assume initial/final conditions associated with both these problems. These assumptions result in loss of optimality and flexibility to expose tradeoffs. Furthermore, such a framework can be utilized to understand the on-road power management implications of using PHEVs for V2G services.
- To develop an optimal control method capable of addressing multiple objectives effi-

ciently (like MOEA) while retaining the dynamic nature of rigorous optimal control methods. PHEVs can create multiple economic and environmental opportunities for consumers and utilities, necessitating the development of such an algorithm.

- To develop a computationally efficient yet rigorous combined design and control optimization procedure and apply it to PHEV battery sizing and supervisory control. In PHEVs, the dependence between design and control is more pronounced than other powertrains due to the sensitivity of the charging and driving control to the battery size. Addressing such dependencies in an optimal way is computationally burdensome due to both, the nature of the PHEV powertrain model and the existing nested/iterative combined design and control optimization algorithms.

1.4 Unique Contributions

The overarching goal of this dissertation is to develop optimization algorithms for the design and control of a PHEV for multiple objectives and V2G services. These unique contributions follow directly from the research gaps addressed.

1. **Optimal Power Management for a Series PHEV**
    - A computationally efficient dynamic programming (DP) algorithm capable of handling a finely meshed state space is developed. Computational intractability issues were resolved using a backward looking model implementation. (see Section 2.3.1)
    - A fair comparison of two supervisory control strategies for series PHEVs, namely Blending and EV/CS (Electric Vehicle/ Charge Sustenance) was performed using this algorithm. Results showed that irrespective of trip distances, when gasoline is more expensive than electricity per mile, there is no significant difference in the performance of the two popular control strategies for a series PHEV. (see Section 2.5)

2. **Integrated Optimization of Charging and Power Management for a Single PHEV**
    - An optimization algorithm which exploits the boundary conditions between the

two optimal control problems is developed. Results show that such an approach is necessary because the battery is not always fully charged at the start of a driving trip, as assumed in the literature. (see Sections 3.3, 3.4)

- This algorithm was applied to investigate the CO_2 reduction impact and power management implications of charging a PHEV from a grid mix with a significant amount of wind power. (see Section 3.5)

3. **Computationally Efficient Multi-Objective Dynamic Programming (MODP) to Minimize Costs and CO_2 Emissions of a Single PHEV**

   - A computationally efficient MODP algorithm is developed by integrating the concept of crowding distance from the MOEA literature. The computational time and memory requirements were drastically reduced while obtaining a Pareto front with no a priori weighting of objectives. (see Section 4.3.1)
   - This algorithm is applied to obtain the optimal supervisory control for a PHEV to minimize two objectives - CO_2 emissions and operational dollar costs to an individual PHEV owner. (see Section 4.4)

4. **Combined Design and Control Optimization of a PHEV**

   - The coupling between the plant design and controller optimization problems is captured by considering the dependence of the control optimization problem on the design variables. The use of this coupling term is also demonstrated to improve computational performance of the optimization. (see Chapter 5)
   - Application of the above theoretical method for the design and control of a complex nonlinear system such as a PHEV is demonstrated. Results elucidate the insights offered by the coupling term. These observations are then used to decide on the combined optimal battery sizes under different assumptions. (see Chapter 6)

1.5 Dissertation Outline

This dissertation is organized as follows. Chapter 2 explains the development of an optimal power management algorithm and its application to a series PHEV powertrain. The results present a comparison of two optimal strategies for a series PHEVs power management. The results study the impact of different driving distances and electricity to gasoline price ratios.

Chapter 3 develops an integrated optimal charging and power management algorithm and its application to a PHEV powertrain for various grid mix scenarios is explained. The integrated framework is further applied to understand the optimal CO_2 emissions reduction benefit that can transferred to propulsion due to increased wind penetration on the grid. Chapter 4 develops a multi-objective dynamic programming algorithm and obtains the Pareto set illustrating the tradeoffs between dollar costs and CO_2 emissions for a PHEV owner.

Chapter 5 develops a novel combined design and control optimization framework and its application is demonstrated for a beam mass reduction and vibration attenuation problem. Chapter 6 demonstrates the application of the framework developed in Chapter 5 for PHEV battery sizing and optimal control.

Chapter 2

Optimal Power Management of a PHEV

This chapter develops a unique dynamic programming algorithm that is employed to obtain optimal on-road power management solutions for a series PHEV powertrain. First, the literature is discussed in detail. Then the dynamic system model used to represent the PHEV powertrain is presented. This model will also be used in future chapters. Next, the dynamic programming algorithm is presented. Finally, the results highlight the nature of the optimal control solutions for varying ratios of gasoline and electricity prices and driving distances.

2.1 Literature and Motivation

This chapter examines the problem of optimizing the cost of the fuel and electricity consumed by a plug-in hybrid electric vehicle. The work is motivated by the fact that PHEVs make it possible for two major infrastructures, the transportation infrastructure and the power grid, to exchange significant amounts of energy. In doing so, PHEVs make it possible to replace some of the petroleum currently being used for propulsion with other sources of energy [1]. To maximize this synergy, our overarching goal is to optimize the cost of fuel and electricity consumption for a PHEV.

In pursuit of the above goal, we compare the optimal fuel and electricity consumption costs associated with two supervisory control strategies for PHEVs. The first strategy, **Blending**, uses fuel and electricity together for propulsion throughout a given drive cycle [27, 35, 78]. The second strategy is dubbed **EV/CS** because it operates in "**E**lectric **V**ehicle" mode first, then switches to "**C**harge **S**ustenance" at a predefined SOC threshold [37, 78]. We compare these strategies using Deterministic Dynamic Programming (DDP) to ensure fairness, and implement the DDP algorithm in a novel manner using a backward-looking powertrain model instead of forward-looking models used in previous research [27, 35, 36].

Previous research has shown that blending optimizes combined fuel and electricity costs for parallel and power split HEVs and PHEVs [27, 35, 36, 79]. Blending attains

this optimality by employing the engine to slow down battery charge depletion, thereby minimizing the amount of time spent in charge sustenance. This is important because in the charge sustenance mode, the engine must (*i*) meet driver power demand, (*ii*) regulate battery SOC, while (*iii*) being mechanically coupled to the final drive. This combination of three requirements and constraints can tax engine efficiency significantly, making charge sustenance undesirable [36, 80]. In a series powertrain, the engine is mechanically decoupled from the final drive. In this chapter, we show that the difference in fuel and electricity cost between the blending and EV/CS strategies is not as pronounced for a *series* vehicle.

Research on optimal supervisory control strategies for hybrid vehicle powertrains has focused on optimization methods [27, 35, 36, 37, 47, 49, 78, 79], the impact of different powertrain architectures [75, 81], and driving scenarios [36, 75]. Optimal control methods applied for HEV and PHEV control are reviewed in section 1.2.1. A recent article by Pisu and Rizzoni compares some of these methods and the subsequent results obtained by using them to control a parallel hybrid powertrain [79]. Regardless of the optimization method used, the goal in hybrid power management is to minimize vehicle-level objective(s), such as fuel consumption, by optimally allocating driver power demand among different propulsion devices. The dynamic programming approach explicitly uses Bellmans principle for optimal control, and thus guarantees global optimality. The output of this process is a supervisory control trajectory that can be used to gain important physical insights and extract implementable rules for subsequent online power management [50, 51]. In [35, 78], authors compare the EV/CS and Blended control strategies for series, parallel and power-split architectures. They obtain implementable control rules and discuss the pros and cons of each architecture based on simulation results. They also assert the need for using globally optimal methods for a fair comparison. This motivates us to apply optimal control by using DDP for the series architecture.

Applications of dynamic programming in optimal powertrain control have followed the numerical methods outlined in [82]. These methods use a forward looking model of the system under consideration and interpolates to obtain the cost-to-go function. As exhaustive as this method is, depending on the system under consideration, computational challenges arise. We did not experience the more popular problem of the curse of dimensionality [83], as our system was modeled with two states and two inputs. However, due to the large size of the battery in a series PHEV, its state-of-charge (*SOC*) dynamics are very slow in terms percentage change in *SOC*, requiring a very fine state space gridding. This resulted in a higher number of interpolations to obtain value function estimates and an exaggerated effect of the propagation of penalties used to handle constraints. These two effects required a higher amount of computational time and memory, rendering the problem computationally

challenging.

There have been several attempts to overcome these particular computational challenges. In [84], authors present a novel procedure to consider constraints that bound the states of a system with only one state and one input. Several authors [34, 85], evaluate feasible sets of controls offline, before performing the optimization. The approach in [85] is geared towards reducing computational time only. The issue of propagation of large penalty values associated with constraints is not considered. Further, the approaches outlined in [34, 85] are well suited for stochastic DP. To implement the ideas from [34, 85] at every time step of deterministic DP would require significant offline calculations and storage.

Our approach of using a backward looking powertrain model to implement DDP helps evaluate the constraints at every time step on the go in a computationally efficient manner with no requirement for storage. In [86], a preliminary version of this approach is presented. This chapter explains the advantages of our approach in more detail and the approach is applied to a wider range of cases that allow us to examine the impact of driving distance on the optimal EV/CS and optimal blending strategies. In the next section, the PHEV powertrain model is described in detail. We also show that the powertrain model under consideration is invertible, thereby allowing us to use a backward looking model.

2.2 PHEV Powertrain Model

2.2.1 Model Overview

The series electric powertrain model considered for this study is schematically shown in Fig. 2.1 and the component specifications are listed in Table 2.1. The arrows indicate the

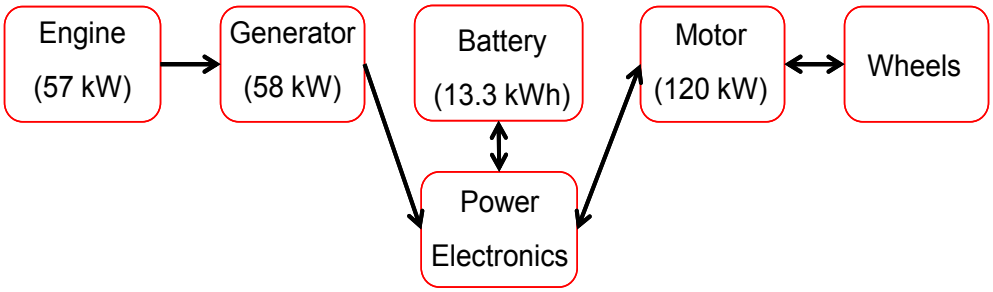

Figure 2.1 Series Hybrid Powertrain Model

Table 2.1 Component Specifications for the Powertrain

Component	Specification
Engine	MY04 Prius 1.497 L gasoline, 57 kW, 110 Nm max torque at 4000 RPM.
Generator	Permanent magnet. 400 Nm max torque, 58kW peak power.
Battery	Li-ion Chemistry. 7.035Ah, 75 cell SAFT model scaled by current capacity to 13.3 kWh total energy.
Motor	Permanent magnet. 715 Nm max torque, 130 kW peak power.
Final Drive	Ratio = 3.07
Resistance Coefficients	f_0 = 88.6 N, f_1 = 0.14 N-s/m, f_2 = 0.36 N-s^2/m^2

possible directions of power flow. The power electronics are a parallel bus which split the electric current between the generator, battery and the motor. Thus the engine power is converted to electrical power in the generator and is split between the driving motor and the battery in the power electronics depending on the wheel power demand.

The Engine, Generator and the Motor are static map based models. The maps are obtained from Powertrain System Analysis Toolkit (PSAT) [87] through testing at Argonne National Laboratory (ANL) and they provide the operating efficiencies of the components. The battery is an equivalent circuit model where its open circuit voltage and internal resistance are functions of the battery state of charge (SOC). The maps for voltage and internal resistance are based on Li-ion battery chemistry and are also obtained from PSAT.

2.2.2 Model Equations

Equations governing the powertrain model dynamics are represented as nonlinear ODEs. This powertrain model has 3 state variables: vehicle velocity (v), engine speed (ω_e) and battery state-of-charge (SOC). The three inputs used to control the model are the power demand by the driver at the wheels ($P_{wh,dmd}$), fuel flow rate to the engine ($\dot{m}_f$) and the torque demand from the generator (τ_g).

We use a dynamic programming approach in which the driving cycle for which the operation costs have to be minimized is chosen a priori. Such an approach is called "Deterministic" Dynamic Programming (DDP) in the literature [27, 79]. For a chosen drive cycle (i.e. reference velocity trajectory), the vehicle velocity (v) and the wheel power demand ($P_{wh,dmd}$) can be calculated before the optimization using Eqs. 2.1 and 2.2. Thus, these

variables ($v_{act}, P_{wh,dmd}$) are not considered as variables in the optimization.

$$\Delta v = v_{ref} - v_{act} \tag{2.1a}$$

$$F_{wh,dmd} = K_p \Delta v + K_i \int_0^t \Delta v dt + f_0 + f_1 v_{ref} + f_2 v_{ref}^2 \tag{2.1b}$$

$$P_{wh,dmd} = F_{wh,dmd} v_{ref} \tag{2.1c}$$

The vehicle velocity at a given time step is v_{act} and the deviation from the reference velocity, v_{ref}, is used to calculate the force ($F_{wh,dmd}$) and power demand ($P_{wh,dmd}$) at the wheels. The resistance coefficients f_0, f_1, f_2 represent the rolling resistance and aerodynamic drag and their values are given in Table 2.1. The differential equation describing the rate of change of vehicle speed is given as

$$\frac{dv_{act}}{dt} = \frac{r_{wh}}{J_{wh}} (\tau_{wh} - \tau_{loss}) \tag{2.2a}$$

$$\tau_{wh} = \tau_m \eta_{fd} \tag{2.2b}$$

$$\tau_{loss} = r_{wh} \left(f_0 + f_1 v_{act} + f_2 v_{act}^2 \right) \tag{2.2c}$$

where r_{wh} is the wheel radius, J_{wh} is the vehicle moment of inertia as seen at the wheels and τ_{loss} represents the torque lost due to rolling resistance and aerodynamic drag losses. The torque produced by the powertrain and supplied to the wheels by the motor is τ_{wh} . In the remainder of this section, we present the equations governing the other two state variables (SOC and ω_e) and the two inputs ($\dot{m}_f$ and τ_g), which will be optimized.

The motor power demand at the wheels ($P_{m,mech}$) can be calculated by Eq. 2.3. The final drive is assumed to have a constant efficiency (η_{fd}) of 97%.

$$P_{m,mech} = \frac{P_{wh,dmd}}{\eta_{fd}} \tag{2.3}$$

The motor torque demand (τ_m) is in turn related to the mechanical power demand through the motor speed (ω_m)

$$\tau_m = \frac{P_{m,mech}}{\omega_m} \tag{2.4}$$

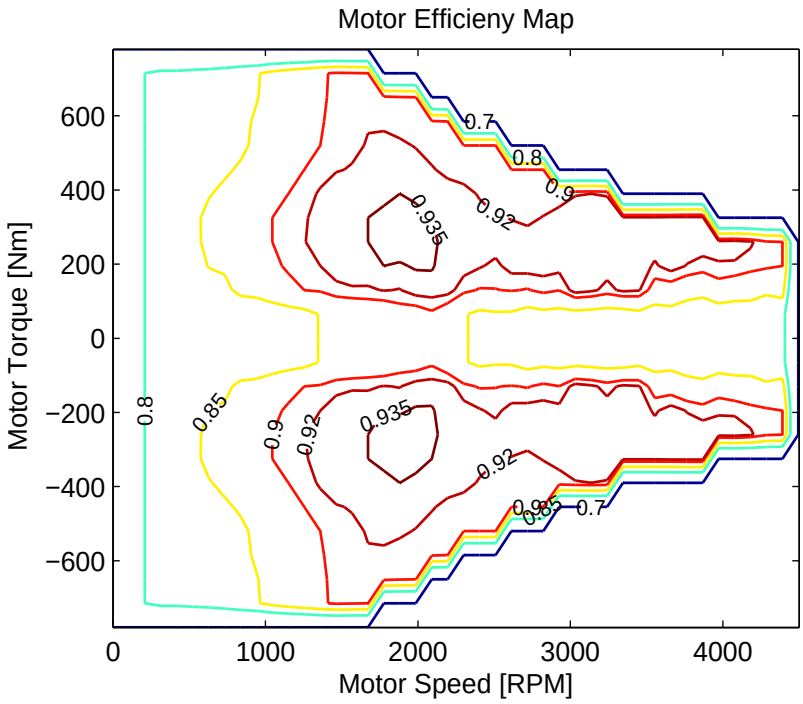

Figure 2.2 Motor Efficiency Map

$$\eta_m = f_m(\tau_m, \omega_m) \tag{2.5a}$$

$$P_{m,elec} = \begin{cases} \frac{P_{m,mech}}{\eta_m} & \text{if } P_{m,elec} \geq 0 \\ P_{m,mech}\eta_m & \text{else} \end{cases} \tag{2.5b}$$

This torque is used to calculate the motor operating efficiency (η_m) and the electrical power that has to be supplied to the motor ($P_{m,elec}$). In Eq. 2.5, f_m is the motor efficiency map, shown in Fig. 2.2.

The electrical power supplied to the motor by the power electronics comes from the battery and the generator. Power electronics acts as a parallel bus connecting the battery, motor and the generator and it is assumed that there are no losses in its operation. Thus we get Eq 2.6 relating the electrical power in the two machines ($P_{m,elec}$ and P_g) and the battery (P_b).

$$P_b = P_{m,elec} + P_g \tag{2.6}$$

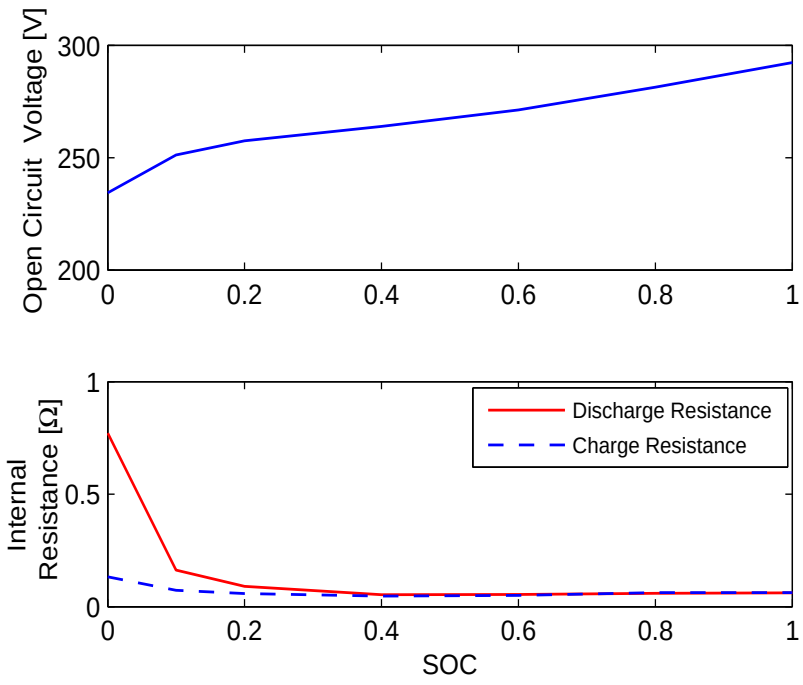

Figure 2.3 Battery Open Circuit Voltage and Internal Resistance as a Function of *SOC*

As the battery is an equivalent circuit model, the equations describing its current flow (I_b) and rate of change of *SOC* are given as

$$I_b = \frac{V_{oc} - \sqrt{V_{oc}^2 - 4R_i P_b}}{2R_i} \tag{2.7a}$$

$$\frac{dSOC}{dt} = -\frac{I_b}{Q_{max}} \tag{2.7b}$$

where V_{oc} and R_i are the open-circuit voltage and internal resistance of the battery, which are functions of *SOC* (Fig. 2.3). Q_{max} is the maximum current capacity of the battery.

The equations describing the generator are similar to that of the motor with only one-way (mechanical to electrical) power conversion.

$$\eta_g = f_g(\tau_g, \omega_g) \tag{2.8a}$$

$$P_g = \eta_g \tau_g \omega_g \tag{2.8b}$$

where τ_g and ω_g are the generator torque and speed respectively. The generator torque is an input to the model while its rotational speed is proportional to the engine speed. In

Eq. 2.8, f_g is the generator efficiency map, shown in Fig. 2.4.

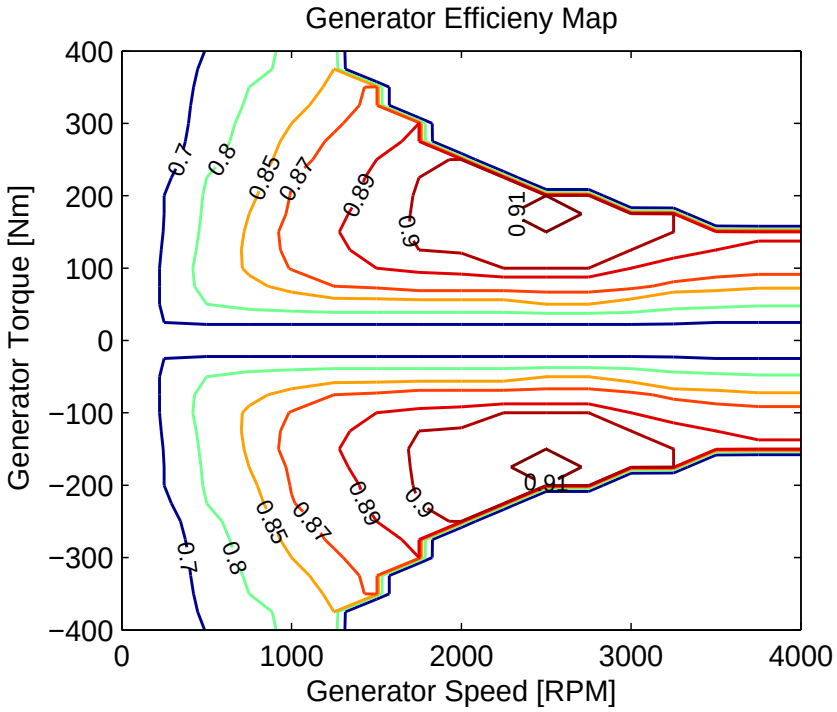

Figure 2.4 Generator Efficiency Map

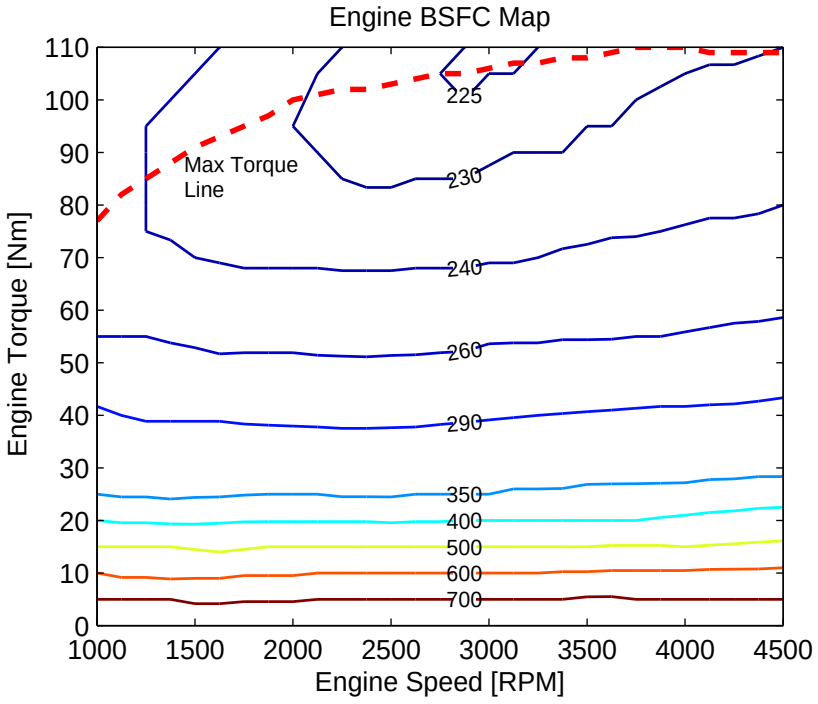

Figure 2.5 Engine BSFC Map

The engine speed dynamics are governed by its flywheel, which is affected by both the engine and generator torque. The equations describing engine operation are

$$\tau_e = f_e(\dot{m}_f, \omega_e) \tag{2.9a}$$

$$\frac{d\omega_e}{dt} = \frac{\tau_e - \tau_g}{J_{flwhl}} \tag{2.9b}$$

where the engine fueling rate ($\dot{m}_f$) is an input to the model, ω_e is the engine speed, which is a state variable, τ_e is the engine torque and J_{flwhl} is the inertia of the flywheel. The torque output for a given fueling rate is obtained through the fueling rate map f_e. The fueling rate map is obtained from the BSFC map, shown in Fig. 2.5. Equations 2.3 - 2.9 along with the constraints described in the next section represent the vehicle model.

2.2.3 Model Constraints

There are physical constraints on the states and inputs described in Eqs. 2.10 and 2.11. Sets Z and U represent the feasible values of the states and inputs respectively.

$$\omega_{e,min} \leq \omega_e \leq \omega_{e,max} \tag{2.10a}$$

$$SOC_{min} \leq SOC \leq SOC_{max} \tag{2.10b}$$

$$0 \leq \dot{m}_f \leq \dot{m}_{f,max}(\omega_e) \tag{2.11a}$$

$$0 \leq \tau_g \leq \tau_{g,max}(\omega_g) \tag{2.11b}$$

The chosen engine model has a maximum speed rating of 4500 RPM. The SOC is restricted to be within 0.9 and 0.3 at all times. The engine fueling rate ($\dot{m}_f$) has a maximum value which varies with engine speed and the maximum generator torque output is also a function of its speed. In addition, The powertrain model has constraints related to the ratings of the components and to the power flow between the components (Eq. 2.12). For example, the battery has limits on its charging and discharging power available, depending on its SOC and its capacity (Eq. 2.12a).

$$P_{c,max}(SOC) \leq P_b \leq P_{d,max}(SOC) \tag{2.12a}$$

$$0 \leq \tau_e \leq \tau_{e,max}(\omega_e) \tag{2.12b}$$

$$-\dot{\omega}_{e,min} \leq \dot{\omega}_e \leq \dot{\omega}_{e,max} \tag{2.12c}$$

$$\omega_{g,min} \leq \omega_g \leq \omega_{g,max} \tag{2.12d}$$

2.2.4 Backward Looking (Inverted) Powertrain Model

The system model represented by Eqs. 2.3 - 2.9 is discretized for simulation using an Euler discretization. The model is then simulated as a backward looking model, *i.e.* the model is of the form

$$u(k) = g(x(k), x(k+1)) \tag{2.13}$$

where, given the current and future states of the model (i.e. $x(k)$ and $x(k+1)$ respectively) the inputs required for that transition can be calculated. This is in contrast with the more popular approach of using a forward looking model which calculates the future states given the current states and inputs (Eq. 2.14).

$$x(k+1) = f(x(k), u(k)) \tag{2.14}$$

A backward looking model can be used because the powertrain components are appropriately sized (Table 2.1) ensuring that the vehicle model satisfies all the power demands at the wheels for the chosen drive cycles. Furthermore, we show that the forward looking model is invertible, or equivalently that the set of inputs maps to the set of future states with a one-to-one correspondence (i.e. one-to-one and onto). This one-to-one correspondence of the model and a discussion on its invertibility is presented in Appendix A. Such a one-to-one correspondence might not extend to other PHEV configurations such as parallel and power-split. This might result in different numerical challenges in implementing the DP algorithm through our approach. However, the invertibility of a series PHEV configuration is shown in Appendix A, allowing us to use the novel DP implementation presented in 2.3.1.

In Eq. 2.13, for given current states ($x(k)$), the input is the future states $x(k+1)$, and the

equation outputs $u(k)$, or equivalently the input required to transition from $x(k)$ to $x(k+1)$. This model is essential to implement our novel DP algorithm presented in the next section (2.3.1).

2.3 Optimal Control Problem

The optimal control problem is formulated as follows:

$$\min_{z(t),u(t)} J = \sum_{k=0}^{T} \left(c_G \dot{m}_f + c_E P_b \right) \tag{2.15a}$$

$$\text{subject to} \quad u(k) = g(x(k), x(k+1)) \tag{2.15b}$$

$$x \in Z \quad \textit{and} \quad u \in U \tag{2.15c}$$

where J represents the cost function to be minimized. It is given by the total dollar costs of the gasoline and electric power used during a chosen trip. The cost of gasoline is $\$c_G$/gallon and the cost of electricity is $\$cE$/kWh. The engine fuel usage rate is given by $(\dot{m}_f)$ and the battery power is given by P_b. The total time for the driving trip under consideration is T. The states and inputs of the system are x and u respectively. The system equations are implemented in a backward looking fashion (Eq. 2.13), rather than the more common forward looking model (Eq. 2.14). The admissible ranges of x and u are Z and U, which are governed by state and input constraints discussed in section 2.2.3. In the remainder of this section, our dynamic programming implementation and its advantages are presented.

2.3.1 Dynamic Programming Implementation

The theory behind dynamic programming as a tool for calculating the optimal control is well understood. However, numerical problems arise when implementing the algorithm. Equation 2.16 shows the discretized form of the Hamilton-Bellman-Jacobi (HBJ) equation.

$$V(k, x^i(k)) = \min_{U} \left[c(x^i(k), u^j(k)) + V(k+1, x^{ij}(k+1)) \right] \tag{2.16}$$

Previously, this equation has been used to solve optimal powertrain control problems [27, 36, 79] and is introduced in more detail in [82]. Here, we briefly explain how Eq. 2.16

has been used by researchers in order to justify the need for our novel DP implementation.

The i^{th} point on the state grid is represented by x^i. Given a current state $x^i(k)$, applying an input $u^j(k)$, results in a future state $x^{ij}(k+1)$ and one-step cost $c(x^i(k),u^j(k))$. The optimal cost-to-go (or value function) from state $x^i(k)$, at time step k, is given by $V(k,x^i(k))$. It should be noted that to obtain $V(k+1,x^{ij}(k+1))$, an interpolation is required as $x^{ij}(k+1)$ may not lie on the state grid. Another important computational aspect that is not represented in Eq. 2.16 is that the constraints are usually implemented through penalty functions. With this understanding of the previous DP implementations, we now discuss the numerical issues arising from the use of Eq. 2.16.

These numerical problems are specific to the system under consideration. For the series PHEV powertrain model, the following are the two major issues that arise during the implementation of the DP algorithm given by Eq. 2.16. First, due to the large size of the battery in a series PHEV, its *SOC* dynamics are very slow in terms of percentage change in *SOC*. For example, drawing 32.2 kW of power (which is higher than the average power demand at the wheels) from the battery causes its *SOC* to drop by only 0.13% over two seconds. To accurately capture the system dynamics the *SOC* grid has to be "fine" (4500 grid points in our case). This large number of grid points exacerbates the computational processor requirements due to the interpolations to calculate the value function. Furthermore, the large number of grid points also result in prohibitive computer memory requirements.

The second numerical issue arises due to the implementation of constraints that bound the state variables (i.e. the constraints given by Eq. 2.10. Penalty functions are used in previous approaches to characterize constraint violations [27, 36, 50, 85]. Due to the interpolations of the value function, there is a leaking effect, or propagation of the large penalties imposed. Due to the long time horizon (on the order of thousands of times steps), and a finer state grid for our control optimization, the leaking effect of the penalties is more pronounced. This results in a sub-optimal solution. Thus, even though imposing penalty functions does not increase computational time or memory requirements, it produces solutions that are not optimal.

To overcome these two major challenges we use the backward looking powertrain model and implement the DP algorithm as presented in Eq. 2.17.

$$V(k,x^i(k)) = \min_{X(k+1,x^i(k))} \left[c(x^i(k),x^j(k+1)) + V(k+1,x^j(k+1))\right] \tag{2.17}$$

In Eq. 2.17, $c(x^i(k),x^j(k+1))$ is the cost of transitioning from state x^i at time k to x^j at time $k+1$ and $V(k,x^i(k))$ is the optimal cost to go from state x^i at time k to the final time. To

obtain the cost of transitioning from state x^i at time k to x^j at time $k+1$, we have to simulate the backward looking model, given by Eq. 2.13. The set $X(k+1,x^i(k))$ defines the set of all feasible reachable points in the discretized state space at time $k+1$, given the current state x^i. It is a subset of the set Z (section 2.2.3). The major difference in our approach is the minimization of the costs over this set $X(k+1,x^i(k))$ and not the set $U(k)$ as is the case in Eq. 2.16, *i.e.* we consider the minimization of costs over all possible transitions to future states rather than the minimization of costs over all possible inputs. Since Eq. 2.17 is an interpretation of the HBJ equation, this formulation still results in optimal solutions. However, in this approach the optimality of the solution is dependent on the discretization $X(k+1)$, rather than on $U(k)$, which affects the optimality of previous approaches.

There are three major advantages of this approach which overcome the numerical issues outlined above in this section. First, we can evaluate all the constraints *a priori* without any model simulation, knowing only the current and future states ($x^i(k)$ and $x^j(k+1)$ respectively). After evaluating the constraints, we obtain the set of future states that are feasible, $X(k+1,x^i(k))$. This set is a very small subset of the discretized state space. This results in a lower number of model simulations at every time step as compared to the previous approaches and hence a computational advantage. Second, since only transitions to states in $X(k+1,x^i(k))$ are evaluated, we do not require interpolations to obtain the optimal value function at $k+1$. This results in further reduction in computational time and memory. Finally, as the constraints are evaluated *a priori*, penalty functions are not necessary to describe constraint violations, thereby eliminating the propagation of penalties.

2.4 Optimization Conditions

Two PHEV power management strategies are optimized and compared: Blending and EV/CS. Note that the definition of blending in this study differs from its previous usage for parallel and power-split PHEVs. In our study the optimal blending solution simply refers to a solution that allows the optimal usage of engine and battery irrespective of the battery *SOC*. On the other hand the EV/CS solution restricts the first engine usage event to occur only after an *SOC* of 0.4 is reached. This restriction thus results in no opportunity for blended usage of engine and battery power till an *SOC* of 0.4 is achieved. Note that when the optimal blending determines that it is not favorable to utilize engine power (when gasoline is more expensive than electricity), the optimal blended solution might be similar to EV/CS. This difference in the definition of blending in our discussion is due to the arrangement of power sources in a series PHEV. In summary, blending in this dissertation refers to the freedom

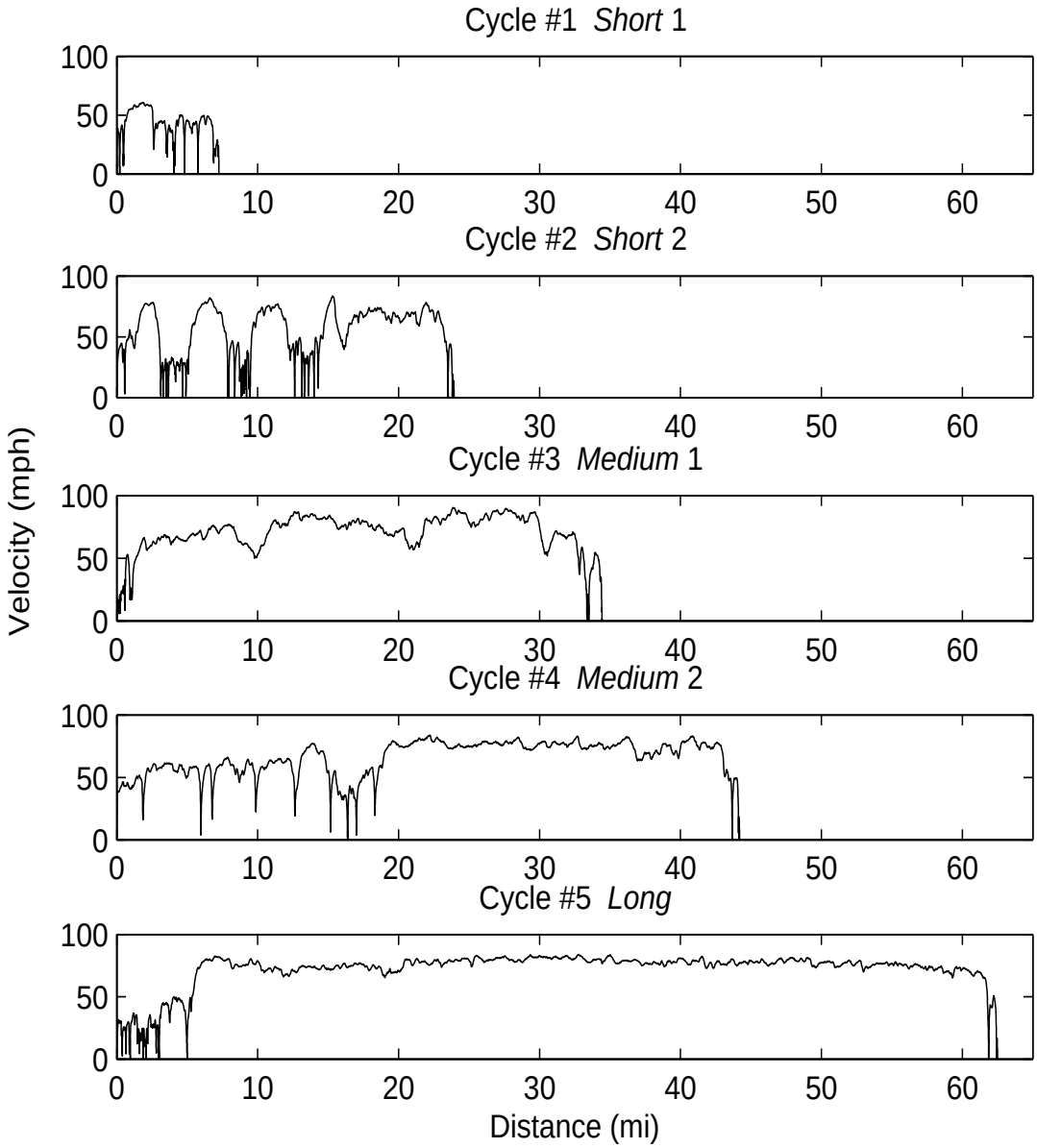

Figure 2.6 Drive Cycles used for Optimization graphed as Function of Distance

to blend the usage of the two power sources, and does not necessitate the blending of the power sources.

To ensure fairness in the comparison of blending and EV/CS, we optimize both strategies for: (*i*) identical drive cycles, (*ii*) the same optimization constraints, and (*iii*) the same optimization objective (namely, the total cost of fuel and electricity). The only difference

between the two strategies is the fact that we allow (though not necessitate) the blending strategy to tap into combustion engine power any time, while barring EV/CS from using the engine until battery *SOC* reaches a threshold of 0.4.

One important goal of this research is to quantify the impact of the relative cost of fuel and electricity on the optimality of Blending vs. EV/CS. To do this, we repeat the optimization-based comparison of blending and EV/CS for fuel costs ranging from \$1/gallon to \$4/gallon, keeping the price of electricity constant at \$0.1/kWh. A second important goal of this research is to quantify the impact of driving distance on the relative optimality of Blending vs. EV/CS. Previous research shows that longer driving distances are statistically correlated with higher average vehicle speeds and propulsion energy needs per mile [75, 88]. We perform our optimization study using naturalistic driving cycles that capture this important correlation. These drive cycles are obtained from Field Operation Tests at the University of Michigan Transportation Research Institute [89]. Fig. 2.6 plots five naturalistic driving cycles used in this study, showing both their speed profiles and the total distances travelled.

2.5 Optimization Results

Examining the results presented in Appendix B and the associated optimal trajectories leads to the following six major observations:

Observation #1: *For long driving cycles, in a scenario where gasoline is more expensive per mile than electricity, the blending and EV/CS strategies have almost identical total optimal energy costs*. Figure 2.7 illustrates this result for Cycle #5 and a fuel cost of \$2.5/gallon. The blending strategy consumes fuel and electricity at a relatively uniform rate over the course of the entire cycle. EV/CS, in comparison, is unable to tap into engine power till the *SOC* reaches the threshold of 0.4, but compensates for that by using the engine more aggressively afterwards. The ultimate effect over the entire cycle is that both strategies consume the same amounts of fuel and electricity. This result stands in sharp contrast to similar studies for power split vehicles, where blending outperforms EV/CS [36, 79].

Observation #2: *Observation #1 can be explained by the fact that the series powertrain mechanically decouples the internal combustion engine from the PHEV wheels, thereby allowing both blending and EV/CS to operate the PHEVs combustion engine at minimum BSFC*. Figure 2.8 illustrates this by showing the fuel consumption for both strategies superimposed on the engine BSFC map. Both strategies are clearly burn the most amount of fuel in the desirable low BSFC range.

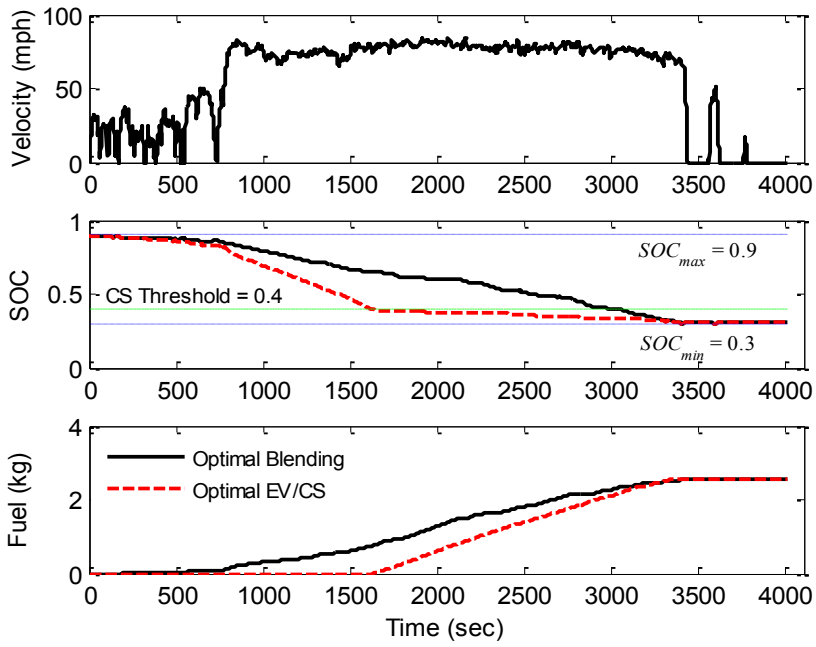

Figure 2.7 Comparison of Optimal Solutions for Minimizing Total Dollar Costs (Highway Cycle, $c_G = 2.5$ \$/gallon, $c_E = 10$c/kWh)

Observation #3: *The ability of EV/CS to match blending in terms of total fuel and electricity cost over long trips is maintained even when gasoline is relatively cheap*. Figure 2.9 illustrates this for Cycle #5 for an unrealistically cheap gasoline price of \$1/gallon. In this case, the relative cost of fuel vs. electricity favors charge sustenance. The blending strategy operates in a charge sustenance mode. The EV/CS strategy is unable to do so initially because of its inability to tap into combustion power. Once the EV/CS strategy is, however, able to tap into combustion power, it recharges the battery and attains an overall fuel and electricity consumption cost almost identical to blending.

Observation #4: *The ability of optimal EV/CS performance to match optimal blending in terms of total fuel and electricity cost is insensitive to total driving distance, as long as gasoline is more expensive per mile than electricity*. The definition of blending is discussed in the previous section 2.4. Optimal blending has the option to utilize engine power at any *SOC*, though it is not a necessity to blend the usage of the power sources. Figure 2.10 illustrates this by repeating the optimization study from Fig. 2.7 for drive Cycles 1-5. Please note that for the shorter drive cycles, blending and EV/CS trajectories (for expensive gasoline) are identical and neither invoke combustion power, and therefore the cost of fuel consumption for both strategies is zero.

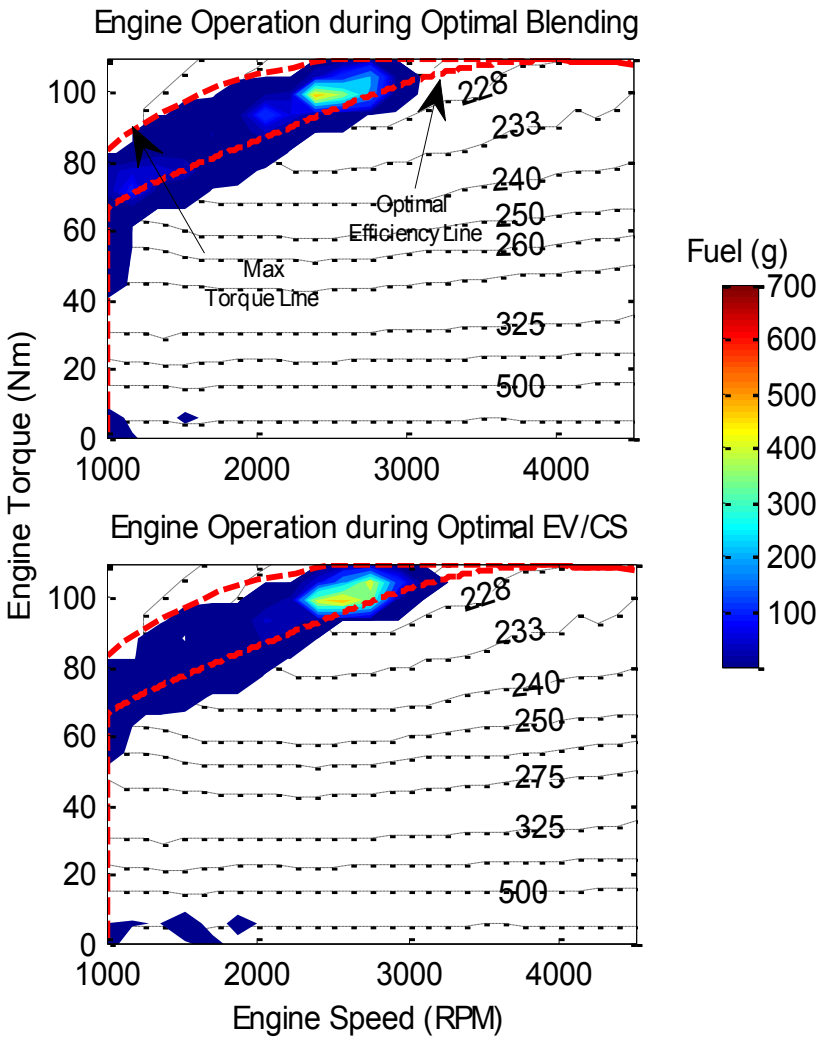

Figure 2.8 Engine Fuel usage shown on a BSFC map for Highway Cycle, $c_G = 1$ \$/gallon, $c_E = 10$c/kWh (Blending above, EV/CS below)

Observation #5: *The blending strategy is superior to the EV/CS strategy in terms of overall fuel and electricity cost when gasoline is cheaper than electricity per mile and the total driving distance is short to medium.* A "short" cycle, in this context, is one in which battery SOC does not reach 0.4 for EV/CS. This corresponds roughly to 25-30 miles (max) in trip length (refer to cycles #1 and #2 Fig. 2.6). A "medium" cycle is one which has a small portion (5-10 mi) of the trip after reaching an SOC of 0.4 for EV/CS (refer to cycles #3 and #4 Fig. 2.6). For the short cycles, EV/CS is unable to tap into combustion power, and propels the vehicle using electricity alone. Blending, on the other hand, is able to tap into

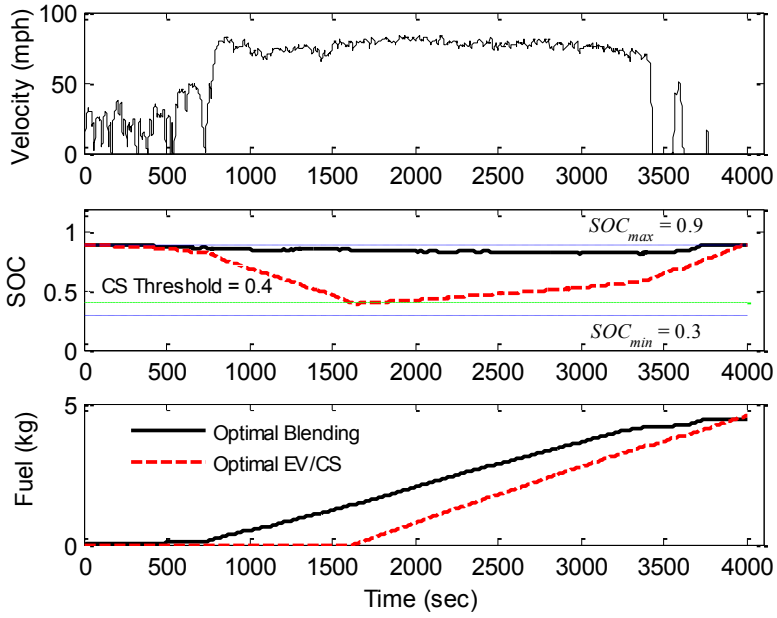

Figure 2.9 Comparison of Optimal Solutions for Minimizing Total Dollar Costs (Highway Cycle, $c_G = 1$ \$/gallon, $c_E = 10$c/kWh)

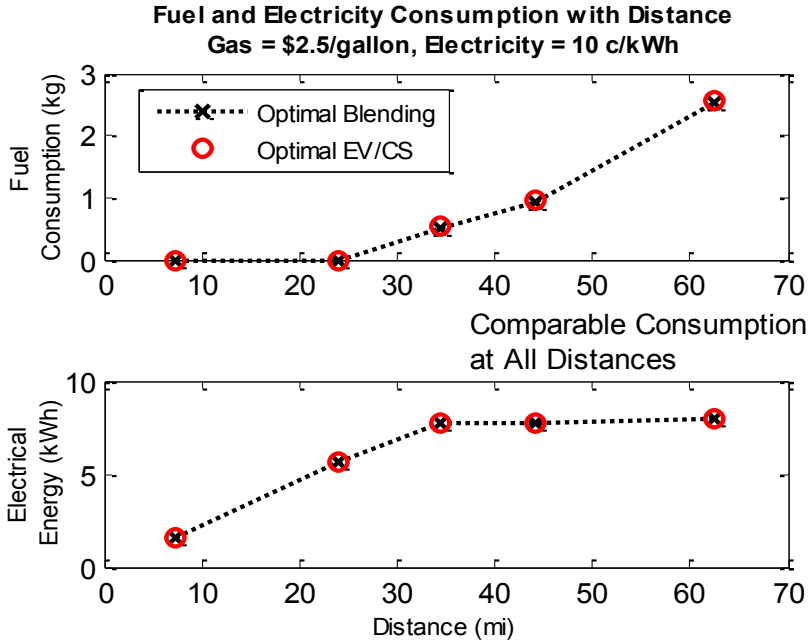

Figure 2.10 Fuel and Electricity Consumption graphed vs. Distance ($c_G = 2.5$ \$/gallon, $c_E = 10$c/kWh)

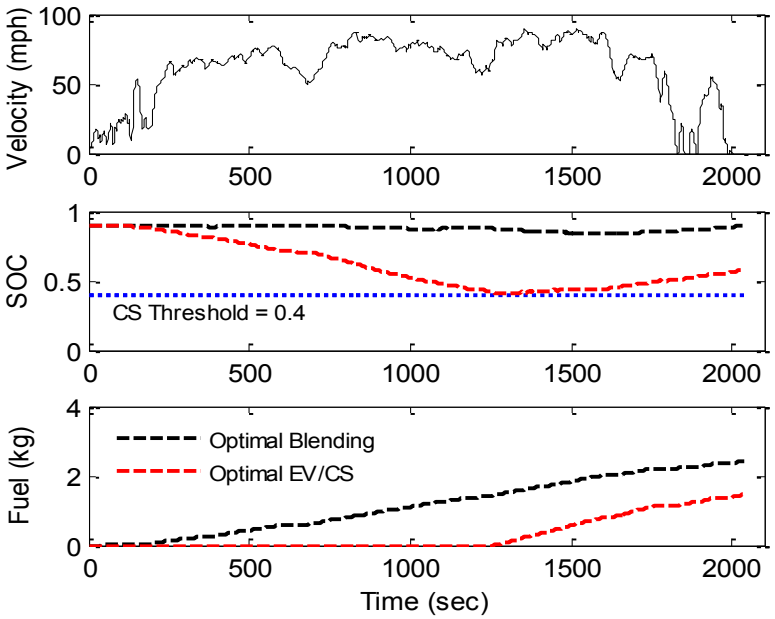

Figure 2.11 Comparison of Optimal Solutions for Minimizing Total Dollar Costs (Medium Cycle #1, $c_G = 1$ \$/gallon, $c_E = 10$c/kWh)

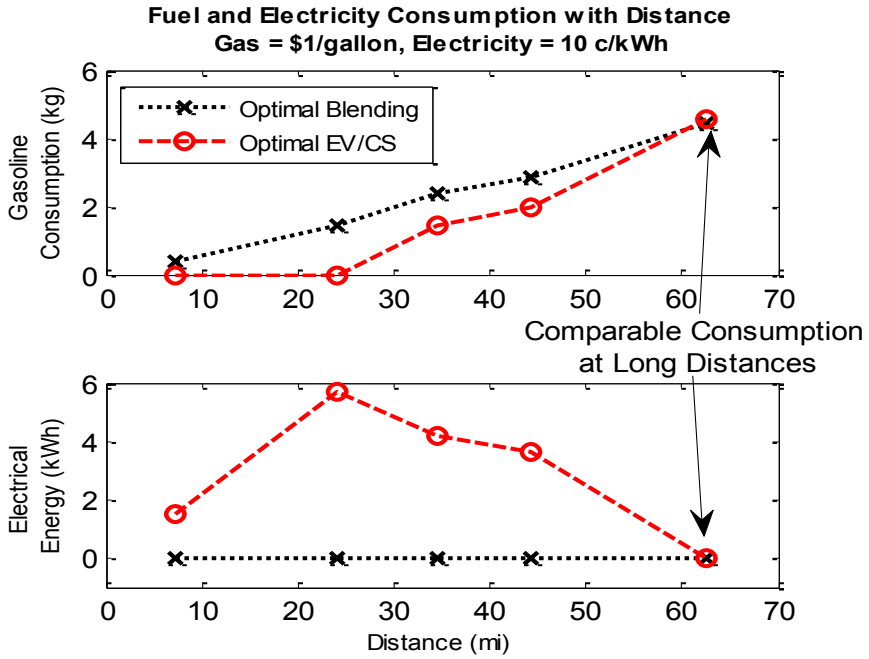

Figure 2.12 Fuel and Electricity Consumption graphed vs. Distance ($c_G = 1$ \$/gallon, $c_E = 10$c/kWh)

combustion power, thereby achieving lower overall trip energy costs. For medium-length trips, the EV/CS strategy is indeed able to tap into combustion power, but for a time duration that is insufficient for recharging the PHEV battery. Under such a scenario, the EV/CS strategy continues to consume more electricity than blending, thereby costing more overall. This is illustrated in Figs. 2.11 and 2.12. This is the only scenario in this optimization study where there is a significant difference in overall trip energy cost between blending and EV/CS.

Observation #6: *The blending strategy performs comparably to the EV/CS strategy in terms of overall fuel and electricity cost when gasoline is cheaper than electricity per mile for the chosen long trip*. Figure 2.9 illustrates this by showing that the total fuel and electricity costs for blending and EV/CS. These costs converge only for Cycle #5 (Fig. 2.12), whose length exceeds 60 miles, when gasoline is cheaper than electricity per mile. This result extends to all long trips irrespective of their driving nature (highway, urban etc.) based on the finding in [86]. In [86], we show that for a repeated urban drive cycle of approximately the same length as the long trip ($\tilde{6}2$ miles), the optimal EV/CS strategy performs the same as optimal blending due to the flexibility in engine operation in a series PHEV.

2.6 Summary

A fair comparison of two supervisory control strategies for PHEVs, namely Blending and EV/CS was performed using a deterministic dynamic programming (DDP) framework. The unique contributions of this work are twofold - 1) Resolving the challenges in the implementation of DDP for a series PHEV powertrain model and 2) The results, showing that there is no significant difference in the performance of the two popular control strategies for a series PHEV with minor exceptions (listed below). In addition, relevance of the findings is enhanced through the use of naturalistic drive cycles as inputs instead of commonly used federal test cycles.

For a series PHEV powertrain, due to the large size of their batteries capturing the battery's *SOC* dynamics through previously used DP implementations was computationally prohibitive. The factors for the computational intractability were the interpolations required to obtain the value function and the characterization of constraints through penalty functions. These issues were resolved through a DP implementation using a backward looking powertrain model and a finer state space gridding. The use of a backward looking powertrain model avoids the need for interpolations. The ability to evaluate constraints

before simulating the powertrain model avoid the need for penalty functions as only feasible state transitions are considered. The new DP implementation does not lose any optimality compared to previous formulations.

The following results were obtained from the DDP studies for a series PHEV: The performance of the optimal EV/CS control strategy in terms of combined fuel and electricity dollar costs is comparable to that of the optimal Blending control strategy except for cases when gasoline prices are low ($<$ \$1/gallon) and the trip lengths are short. Thus, under the assumption that gasoline is more expensive per mile than electricity, the EV/CS solution performs comparably to the blended solution for all driving distances. This result is in contrast with previous comparisons in the literature for a power-split PHEV, where results indicate that the EV/CS strategy performs worse than the Blended strategy. Differences in the results for the series PHEV were shown to be mainly due to the mechanical decoupling of the engine from the wheels allowing for flexible engine operation.

Chapter 3

Integrated Optimal Charging and Power Management of a PHEV

This chapter develops a dynamic programming based algorithm for the integrated optimization of charging and power management for a series PHEV powertrain. In chapter 2, the power management problem was solved. The DP implementation from chapter 2 will be extended to include optimal charging in this chapter by exploiting the boundary conditions between the charging and driving problems.

First, the literature and motivation for the development of this algorithm are discussed. The dynamic system model used to represent the PHEV powertrain during driving is briefly mentioned as it has been presented in detail in section 2.2. The modeling related to electric grid operation was developed by Kelly *et al.* in [90]. Hence, we will only discuss the relevant aspects of that model. Next, the DP based integrated optimization algorithm is presented. Then, the results showing the need for such an integrated framework and the tradeoffs between charging and fuel usage are presented. Finally, in section 3.5 we apply this algorithm to understand the CO_2 emissions impact of using PHEVs with a cleaner grid.

3.1 Literature and Motivation

This chapter examines the problems of optimizing the charging trajectory of a PHEV and optimally managing PHEV power when driving. We solve these two optimal control problems together, thereby accounting for their interdependence. Such combined optimization is essential because a PHEV, unlike a more traditional HEV, is expected to exchange significant amounts of energy with the electric grid. In doing so, PHEVs make it possible to replace some of the petroleum currently being used for propulsion with other sources of energy [1, 2]. To maximize this synergy, our overarching goal is to simultaneously optimize PHEV activity on the electric grid (i.e., charging) and on the road (*i.e.*, power management).

The literature motivates this work by highlighting several non-trivial tradeoffs between PHEV design/control on the one hand and power system optimization on the other. These tradeoffs often necessitate an integrated approach to optimal design and control in PHEVs and the power grid. For example, research by Bashash and Fathy reveals a tradeoff between one PHEV battery degradation mechanism (namely, anode-side resistive film formation) and total PHEV energy cost [38], based on the degradation map assumed by these authors. Mitigating this tradeoff involves charging the PHEV battery just enough to complete a given driving trip, immediately before the trip. Furthermore, Traut *et al.* show that a larger PHEV battery size does not necessarily imply lower lifecycle greenhouse gas (GHG) emissions [45]. Finally, the literature also explores the use of PHEVs for vehicle-to-grid (V2G) services such as provision of spinning reserves and regulation. These services can reduce GHG emissions [91], enable integration of intermittent renewable power sources, and provide cheaper reserves [3, 24]. Depending on the objectives and services that a PHEV provides to the grid, it may not be possible to charge the PHEVs battery optimally or fully [41, 44]. This affects on-road PHEV power management, thereby motivating the combined optimization of PHEV charging and power management.

The literature already presents significant research on optimal PHEV charging and power management, but the problems are considered separately. Optimal charging refers to the problem of finding a State-of-Charge (SOC) trajectory that minimizes some environmental or economic objective for a given PHEV over the span of a day [7, 9, 41]. The goal is typically to minimize the total dollar cost of electricity consumed by the PHEV, electric grid GHG emissions due to PHEV charging, or provide V2G services to the grid. Optimal power management refers to the problem of delivering power to a PHEVs wheels in the most effective manner. The most common minimization objectives in power management studies are gasoline consumption and dollar costs associated with a given trip [36, 86, 98]. Existing studies on optimal charging and optimal power management typically either assume or require the PHEV battery to be full at the onset of any given driving trip. Our work relaxes this assumption to enable a full exploration of tradeoffs and synergies between these two problems, for the first time.

Several optimal control methods have been applied to PHEV charging problems and power management problems. A review of these methods is presented in section 1.2.1. Assuming that grid operation, driving times and driving profiles are known for the day under consideration, we use a Deterministic Dynamic Programming (DDP) approach. This approach explicitly uses Bellmans principle for optimal control, and thus guarantees global optimality. The output of this process is a supervisory control trajectory that can be used to gain insights and extract rules for subsequent implementation [50, 51].

The main contributions of this paper are to develop a DDP-based framework for the above combined optimal control problem, and to analyze the dependencies between the optimal charging and power management of a PHEV through the resulting complete optimal solutions. The major challenges in this work are the integration of two problems with different dynamics and time scales together in a single optimal control framework, and the computational time required to obtain solutions. It is also necessary that this framework be capable of handling different constraints/scenarios (such as inclusion of renewable power sources on the grid and V2G services). One such scenario which examines the impact of CO_2 reduction in propulsion due to large amounts of wind power on the grid is presented in section 3.5.

3.2 Vehicle Powertrain and Grid Dispatch Models

The optimal control problem is solved to obtain optimal trajectories of the states and inputs related to PHEV charging and on-road power management. In this section, we present the system's states and inputs, and the constraints related to them. First, the PHEV powertrain model is briefly described. Then, the interaction between the electric grid and the PHEV battery is described in detail. Finally, the drive cycles and CO_2 traces over which the optimal control solutions are calculated are presented.

3.2.1 Vehicle Powertrain Model

The system dynamics describing the vehicle powertrain operation during driving is presented in detail in section 2.2. There are two takeaways that we wish to emphasize again. First, This powertrain model has 2 states: engine speed (ω_e) and battery state-of-charge (SOC), *i.e.* $z = \{\omega_e, SOC\}$ is the state variable whose optimal trajectory will be obtained. The two inputs used to control the model are the fuel flow rate to the engine ($\dot{m}_f$) and the torque demand from the generator (τ_g) *i.e.* $u = \{\dot{m}_f, \tau_g\}$. The constraints for this model are described in section 2.2.3. It should be noted that the dynamics and constraints for charging (presented in the next section 3.2.2) are different. Second, the model is implemented as a backward looking model (section 2.2.4) with a simulation time step of 2 seconds. The time step for the charging process is 60 seconds (1 minutes). These differences in the dynamics, constraints and time-steps pose a challenge in integrating the optimization of charging and power management of a PHEV.

3.2.2 Battery Charging and Grid Disptach Model

This section develops a different model intended for optimizing the way a single PHEV charges with grid electricity. The intent behind this model is twofold. First, the model captures the dynamics of battery charging, namely, Eq. 3.1.

$$I_b = \frac{V_{oc} - \sqrt{V_{oc}^2 - 4R_i P_b}}{2R_i} \tag{3.1a}$$

$$\frac{dSOC}{dt} = -\frac{I_b}{Q_{max}} \tag{3.1b}$$

This grid charging model has one state variable, $z = \{SOC\}$ and one input, $u = \{P_b\}$ in comparison with the 2 states and 2 inputs for the complete powertrain presented in the section above and 2.2. Second, the model allows us to quantify the grid CO_2 emissions associated with PHEV charging (*i.e.*, the emissions associated with generating the electricity supplied to the PHEV). To achieve this second goal, we employ an economic grid dispatch model presented by Kelly et al. in [90]. This dispatch model contains a list of power plants arranged in ascending order of generation costs ($/kWh). The model simulates grid dispatch for a given total power demand profile (obtained from the EPA eGrid database), and outputs the resulting dollar costs and CO_2 emissions associated with grid power generation. These CO_2 emissions reflect the upstream impacts and CO_2 produced at the power plant. The model is also capable of accommodating PHEV power demand in this simulation process.

Figure 3.1 illustrates a baseline scenario we use when optimizing the power management and charging of a given PHEV. The scenario focuses on the State of Michigan, and assumes that the total number of PHEVs charging from the grid at any given time is 15% of the total Michigan passenger vehicle fleet. This percentage translates to 1.25 million PHEVs charging from the grid at the maximum possible rate at all times during the day, based on the total number of passenger vehicles in Michigan in 2007 [92]. This very large number of PHEVs plugged into the grid corresponds to a PHEV market penetration level in the 20%-25% range. Assuming the total number of PHEVs charging with grid electricity at every instant in time to be constant provides a simple baseline scenario that can be easily refined by accounting for household travel data. Our goal, here, is to obtain baseline profiles of total grid power demand and grid CO_2 production per unit energy. The CO_2 rate is in the 550-850 g/kWh range, irrespective of the inclusion of PHEVs. This is because the underlying power plants are assumed to remain the same, hence resulting in the same range of average CO_2 . We use these profiles of CO_2 production per unit energy (described in next subsection) to optimize the charging and power management of a single PHEV for minimal

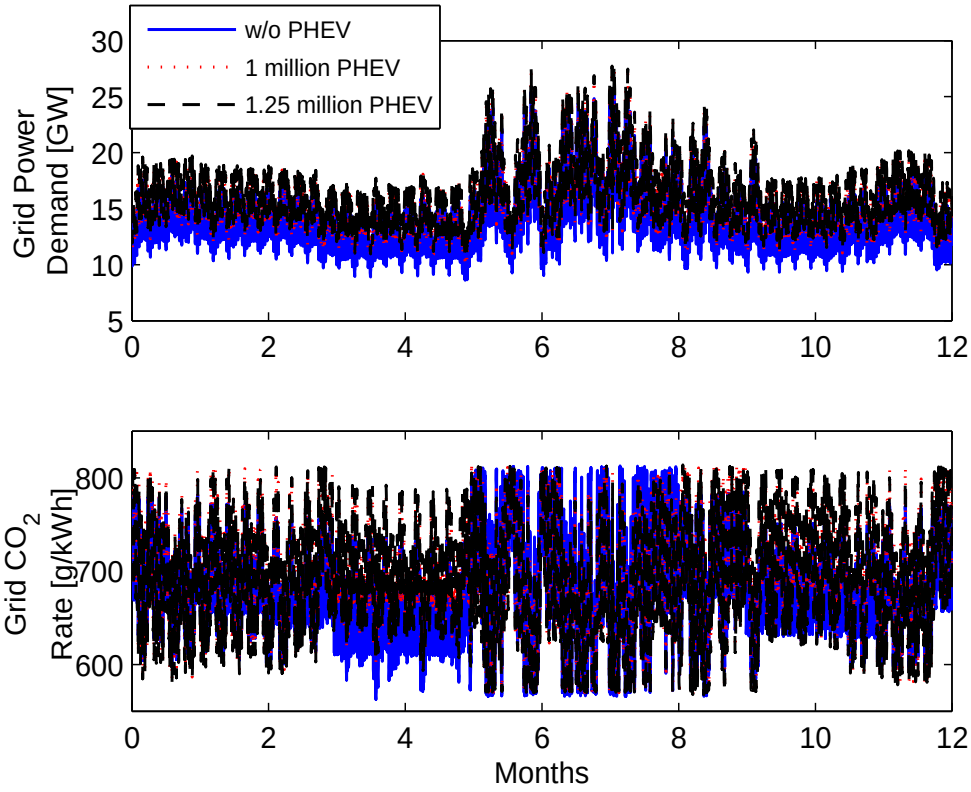

Figure 3.1 Grid Power Demand and CO_2 production for a Year under Different PHEV Penetration Scenarios

CO_2 emissions.

A different set of constraints affect the PHEV during grid charging than during on-road operation. The charging outlet considered is rated at 110 V and 15 A. Thus the charging power can be a maximum of 1.65 kW. Battery *SOC* is constrained to be between 0.3 and 0.9, as it was for PHEV on-road usage. The battery cannot discharge to the grid in the case studies considered herein. The constraints are represented in Eq. 3.2 below.

$$SOC_{min} \leq SOC \leq SOC_{max} \tag{3.2a}$$

$$0 \leq P_b \leq 1.65 \text{ kW} \tag{3.2b}$$

3.2.3 Drive Cycles and CO_2 Trajectories for Optimization

The objective in our optimal control problem is to minimize total CO_2 produced by a given PHEVs use of fuel and electricity. Three 24-hour CO_2 trajectories were chosen from the

CO_2 per unit energy data for an entire year (in Fig. 3.1). These three traces reflect days of high, medium and low CO_2 (Fig. 3.2) relative to the CO_2 traces for the entire year (Fig. 3.1), covering the entire range of CO_2 rate (550-850 g/kWh). We use these traces to account for the CO_2 corresponding to PHEV charging. Hourly grid demand data are used in the dispatch model [90]. Hence we assume, that the CO_2 production remains the same for each hour.

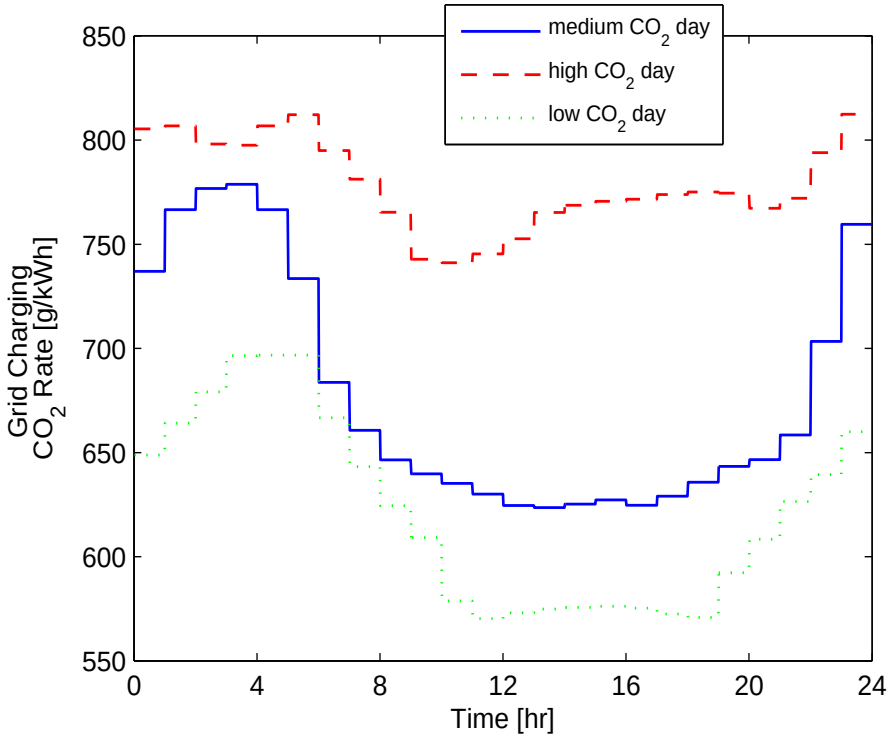

Figure 3.2 CO_2 traces used for optimization

We optimize PHEV charging and power management for a day where the PHEV performs two identical trips (23.9 miles long) in the morning and afternoon. Figure 3.3 shows the vehicle velocity for each trip as a function of travel distance (obtained from a naturalistic driving database collected at the University of Michigan Transportation Research Institute [89]). Furthermore, Fig. 3.4 shows the timing of the trips during the day. Daily driving distance and traffic conditions affect PHEV energy usage: a fact that has motivated researchers to optimize PHEV operation over large families of trips [36, 46]. This work, in comparison, focuses on developing a framework to show the interplay between optimal charging and power management. We illustrate this framework for the trip details in Figs. 3.3 - 3.4, but the framework is broadly applicable to any trip profile. The total daily driving distance of 47.8 miles necessitates either gasoline usage or multiple battery charging events during the

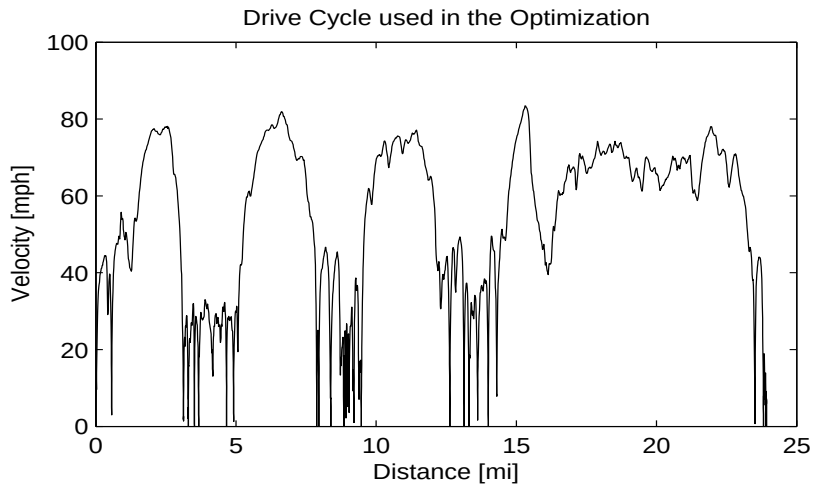

Figure 3.3 Drive Cycle Velocity graphed as a Function of Distance.

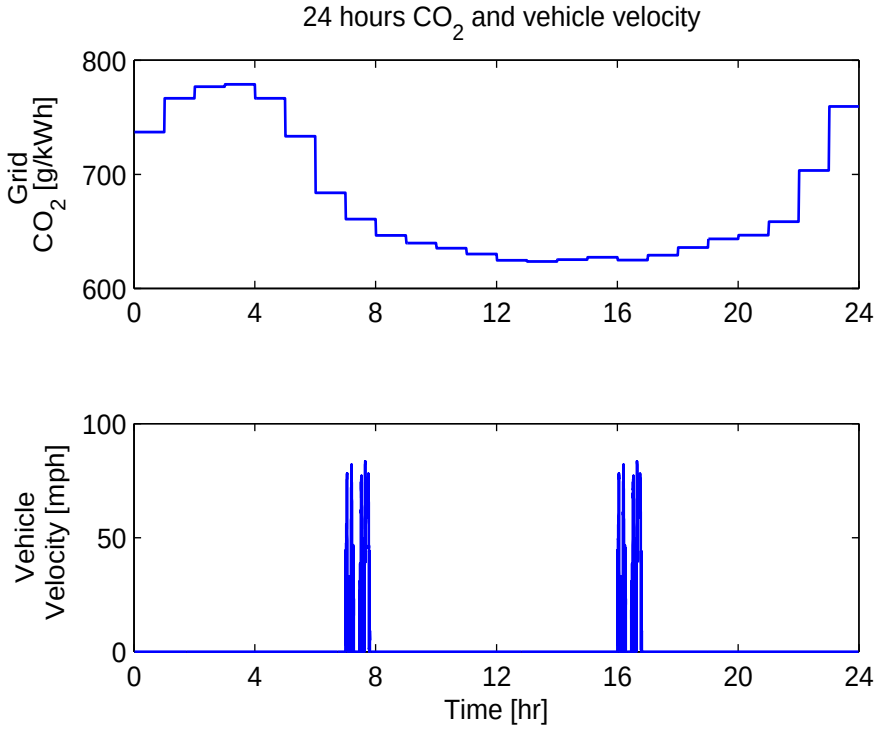

Figure 3.4 24 hour plot of Grid CO_2 Rate and Driving Trips. (The 24 hour period begins at 1AM, hence 8AM is the 7th hour in the graph above)

24 hour period. This helps demonstrate the use of our integrated optimization framework by elucidating some interesting tradeoffs between battery charging and fuel consumption.

3.3 Optimal Control Framework

The optimal control problem is formulated as follows:

$$\min_{(z(t),u(t))} J = \sum_{0}^{24} \left(\frac{CO_2}{gal} \dot{m}_f \Delta t_{dr} + \frac{CO_2}{kWh} P_b \Delta t_{ch} \right) \tag{3.3a}$$

$$\text{subject to} \quad \dot{z} = f(z(t), u(t), t) \tag{3.3b}$$

$$z \in Z_c \quad \textit{and} \quad u \in U_c \tag{3.3c}$$

where the optimization objective, J, is the total amount of CO_2 produced during a 24-hour period. This CO_2 is produced by both driving fuel usage (the first term in the expression for J) and grid charging (the second term). Gasoline consumption is ($\dot{m}_f$) gallons per time step during driving ($\Delta t_{dr} = 2$ sec). Battery charging power is given by Pb in kW and the charging time step is $\Delta t_{ch} = 60$. It is important to note that the dynamics and constraints given in the above equations are different depending on whether the PHEV is driving or charging. These differences in the dynamics and constraints are explained in the previous section 3.2.2 in more detail. The states and inputs of the system are z and u respectively, and they are governed by the system dynamics (sections 2.2.2 and 3.2.2). The admissible ranges of z and u are Z_c and U_c respectively. The constraints on the states (set Z_c) and on the inputs (set U_c) are described in sections 2.2.3 and 3.2.2. In the remainder of this section, the salient features of the DP implementation (from section 2.3.1) are reviewed. Then, the integration of the two problems into a single optimal control algorithm is presented.

3.3.1 Dynamic Programming Implementation

The Bellman equation is written as Eq. 3.4, which is the DP algorithm used for optimal control in this work.

$$V(k, x^i(k)) = \min_{X(k+1, x^i(k))} \left[c(x^i(k), x^j(k+1)) + V(k+1, x^j(k+1)) \right] \tag{3.4}$$

where $c(x^i(k), x^j(k+1))$ is the cost of transitioning from state x^i at time k to x^j at time $k+1$ and $V(k, x^i(k))$ is the optimal cost to go from state x^i at time k to the final time. The state space is divided into a finite number of states at every time step that belong to the set $X(k) = \{x^1(k), x^2(k), \ldots, x^i(k), x^j(k), \ldots x^N(k)\}$. Equation 3.4 can be read as the optimal

cost to go from state x^i at time k is equal to the cost of transitioning from state x^i at time k to state x^j at time $k+1$ plus the optimal cost to go from x^j at time $k+1$ to the final time T_f, minimized over all possible transitions to feasible reachable states in $X(k+1)$ (*i.e.* $X(k+1,x^i(k))$). This equation is evaluated starting from final time T_f, where the cost to go function at the final time $\mathrm{V}(T_f,X(T_f))$ is initialized for all states. Using Eq. 3.4, for every state at time step T_f-1, we obtain the optimal cost to go for every state at T_f-1 as $\mathrm{V}(T_f-1,X(T_f-1))$. This process is repeated till the initial time where $\mathrm{V}(1,X(1))$ is obtained. $\mathrm{V}(1,X(1))$ gives the optimal cost to go from every state at initial time and is used to find the optimal initial states and the consequent optimal trajectories depending on the choice of the initial states.

Use of the backward looking model with the DP algorithm shown in Eq. 3.4 has the following advantages compared to previous approaches in the literature [36, 79, 84]. First, the algorithm setup does not need interpolations as only transitions to states in $X(k+1)$ are considered. Second, when considering the set $X(k+1)$ of all possible future states, the battery charge/discharge power limits and other such constraints on the states are used to limit the set of allowable future states (to the set $X(k+1,x^i(k))$). This drastically reduces the number of powertrain simulations. It also overcomes accuracy issues (discussed in [84, 34]) regarding implementing the constraints using penalty methods. These two key advantages make the DP problem computationally feasible in our case. A more detailed discussion of this algorithm and its advantages in presented in section 2.3.1. Next, we discuss the integrated framework necessary to address charging and power management in a single framework.

3.3.2 Integrated Optimization Framework

The two optimal control problems - of charging and power management, have the same objective (*i.e.* to reduce CO_2 emissions), but the system dynamics, constraints and the time steps involved are different. During on-road operation of the PHEV, the system has two states $z=\{\omega_e,SOC\}$ and two inputs $u=\{\dot{m}_f,\tau_g\}$, that have to be optimally determined. During charging, the system has one state $z=\{SOC\}$ and one input, $u=\{P_b\}$, that have to be optimally determined. Fig. 3.5 illustrates the charging and driving events throughout the day. It is obvious from Fig. 3.5 that the trajectory/actions taken during one event affects the optimal actions to be undertaken during the other events.

To tackle these differences, but still use the Bellman equation 3.4 effectively, ensuring optimality, a complete optimal framework is used. This framework proceeds backwards in time, starting at the end of the 24 hour period under consideration (see Fig 3.5). The

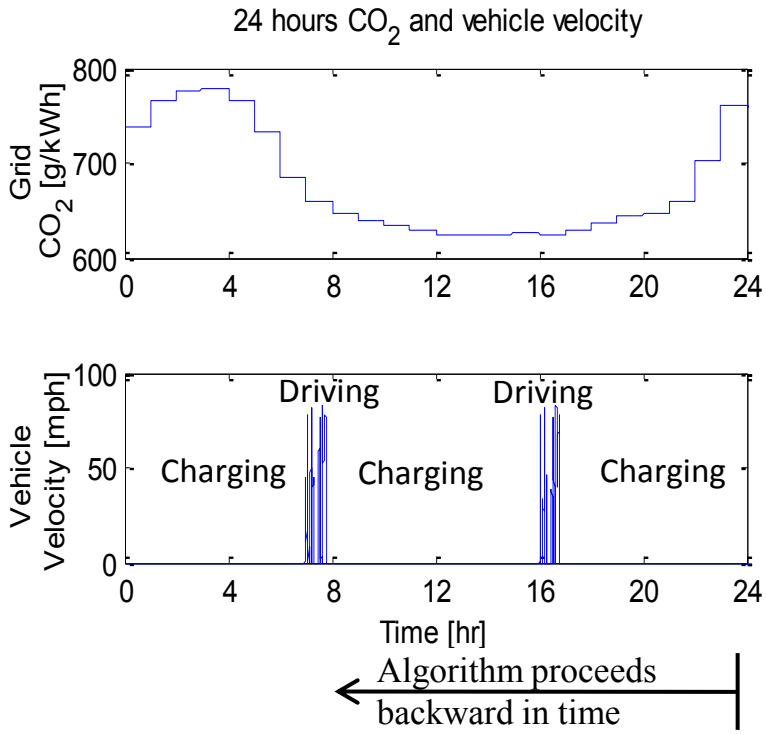

Figure 3.5 24 hour plot of Grid CO_2 Rate and Driving Trips

following steps (and Fig. 3.6) explain the method used:

- *Step 1*- Optimal charging is the problem under consideration at the final time step, so the value function is initialized for every discretized value of *SOC* only.
- *Step 2*- Equation 3.4 is then applied at every time step proceeding backwards in time until the end of the second driving trip. Here the dynamics and constraints related to charging are applied.
- *Step 3*- At this time step the value function is modified from a 1D array (V_1) with entries for each discretization of *SOC* only to a 2D array (V_2) with entries for each discretization of *SOC* and ω_e. This is done by concatenating or repeating the same value function for every discretization of ω_e. Essentially, it means that the optimal cost-to-go is immaterial of the engine speed at the final driving time step.
- *Step 4*- Equation 3.4 is then applied at every time step proceeding backwards in time until the beginning of the second driving trip with ($V = V_2$). Here the dynamics and constraints related to driving are applied.

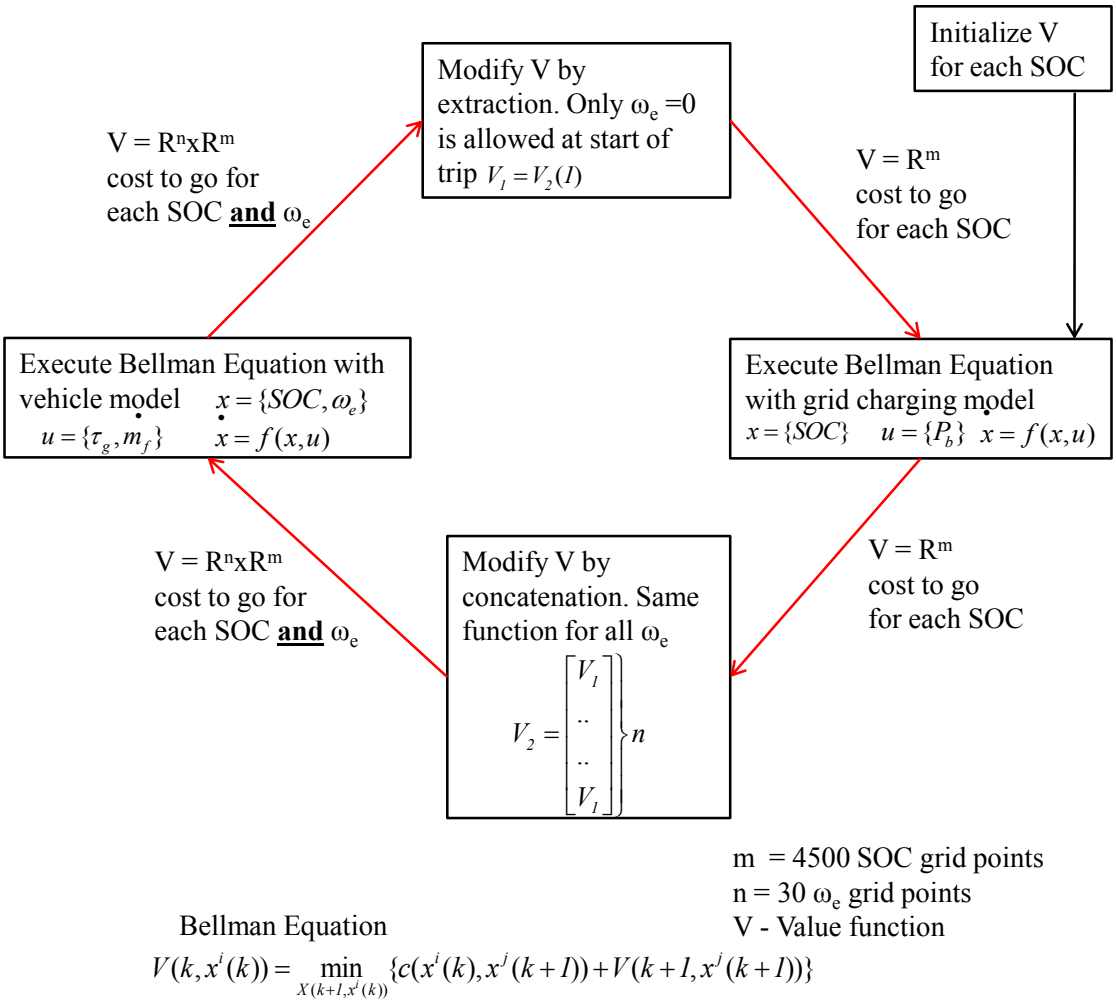

Figure 3.6 Framework for the Integrated Optimization for Charging and Driving

- *Step 5*- At this time step the value function is modified back from a 2D array (V_2) to a 1D array (V_1) by using the value function entries associated with only the zero engine speed state as that is the only allowable engine speed at the start of a driving trip. Essentially, this means that only a zero engine speed state is allowed at the first driving time step.
- *Step 6*- Follow steps 2 through 5 until the beginning of the first driving trip.
- *Step 7*- Follow step 2 until the initial time step to get the value function (optimal cost-to-go) for all SOC discretizations.

Essentially the loop in Fig. 3.6 is followed twice starting with the initialization block. In

steps 3 and 5 where the Value function is converted from a 1D array to a 2D array and back respectively, we are utilizing the constraints on the states (ω_e and SOC) at the boundaries of the charging and driving problems to continue using the Bellman equation throughout.

In this framework, SOC is a state variable that is common to both the system's dynamics and this approach ensures its continuity. Since battery usage should not be unduly rewarded, we impose an additional constraint that the initial and final SOC has to be same. During step 2, the system dynamics have one state and input with constraints related to grid charging, while during step 4 the system dynamics and constraints are those related to PHEV on-road usage. This framework is computationally feasible due to the use of a backward looking model and the interpretation of the Bellman equation as presented in Eq. 3.4 and section 2.3.1. This framework can also be used for solving a generic double optimal control problem, which are linked through a state variable (which is SOC in our problem). Furthermore, it can be extended to linked multiple optimal control problems with well defined transition of states from one problem to the other.

3.4 Results

The framework presented in the previous section is used to obtain optimal state and control input trajectories for a 24 hour period. The 24 hour period begins at 1 AM. Hence, zero on the time scale in all the graphs indicate 1 AM. The two driving trips being at 8 AM and 5 PM. These are the 7th and 16th hour of the 24 hour period respectively. Since the initial and final SOC have to be the same to ensure no undue advantage of using electricity, for each optimization *case*, the optimal trajectories are obtained for initial and final SOC of 0.3 through 0.9 in increments of 0.1 (seven runs). Three optimization cases are examined, for the three CO_2 cases of high, medium and low (Fig. 3.2). It is important to note, while analyzing the results, that these CO_2 trajectories are obtained on different days from the Michigan grid mix, which is coal intensive. The CO_2 impact of gasoline combustion is 8.78 kg/gal [93]. This value does not include the upstream impacts of manufacturing the gasoline.

3.4.1 Tradeoffs between Charging and Fuel Consumption

Optimal trajectories of SOC, grid charging rate and cumulative fuel consumption for the three cases of high, low and medium CO_2 rates are graphed in Figs. 3.7, 3.8 and 3.9 respectively. The initial and final SOC for the 24 hour period is chosen as 0.7 in these graphs. For

the day with high grid CO_2 rate, we see that it is optimal to extensively use engine fuel while driving and even charge up the battery while driving. There is almost no charging from the grid. Figure 3.8 shows a case of the day where the grid mix results in low CO_2. The optimal solution, in this case, is to charge as much as possible before a driving trip and use all the electricity while driving. Battery usage while driving is observed by the rapid drops in *SOC* beginning from the 7th and the 16th hour when the driving trips occur. While these two solutions might seem trivial, it is necessary to remember that using a dynamic model of the PHEV, the engine efficiency is not constant over the trip. Thus, these two seemingly trivial solutions are not easy to surmise *a priori*. In this case of a medium CO_2 day, the optimal control solution does not charge the battery before the first driving trip as the CO_2 production rate from the grid before the first trip is higher than the rest of the day. This results in a small amount of engine fuel usage during the first driving trip. Due to the low CO_2 in the middle of the day, we see that the battery is completely charged up before the second driving trip, resulting in all electric driving and no engine usage. This solution is not as simple as the high and low CO_2 cases and shows the advantage of considering a complete optimal approach to PHEV charging and power management.

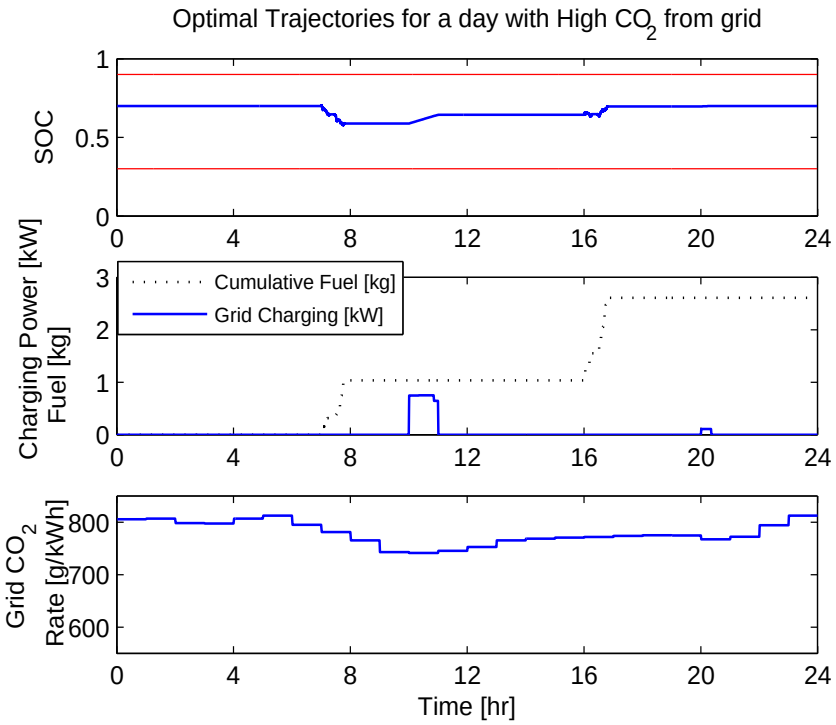

Figure 3.7 Optimal trajectories for a day with high CO_2 from the grid

Other than emphasizing the optimality of a combined charging and power management

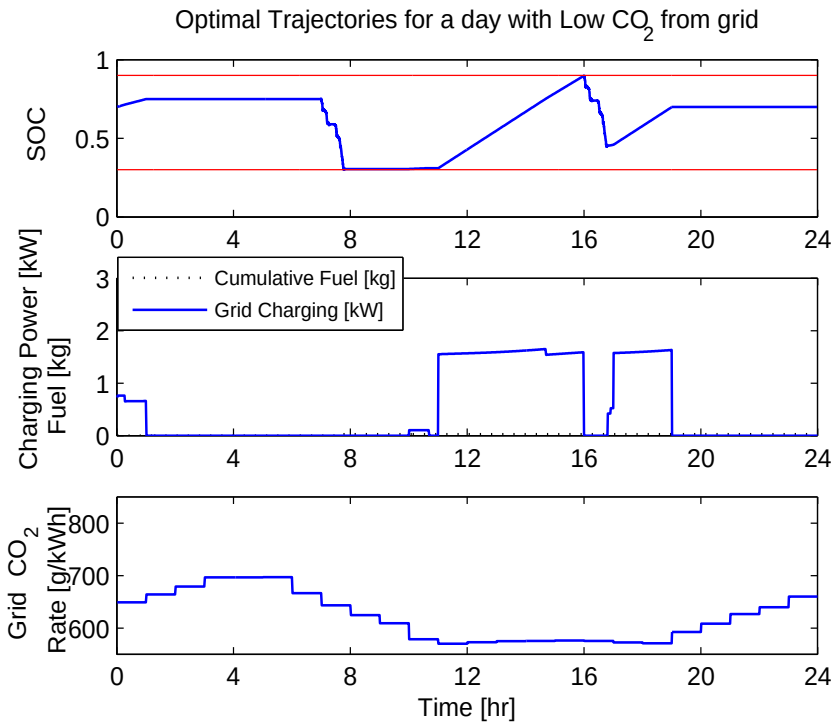

Figure 3.8 Optimal trajectories for a day with low CO_2 from the grid

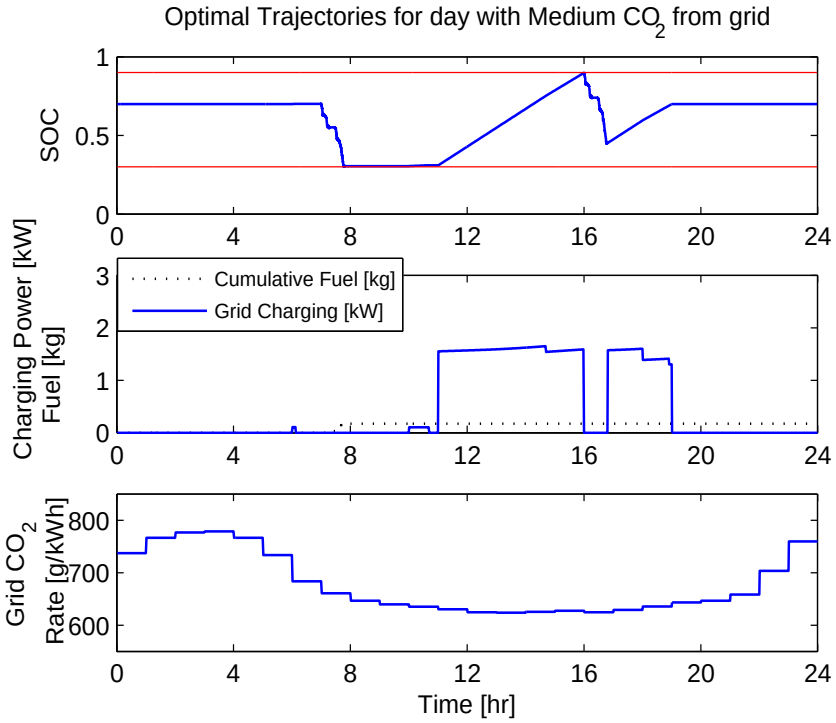

Figure 3.9 Optimal trajectories for a day with medium CO_2 from the grid

approach, there are additional interesting features that these graphs reveal. First, since CO_2 is the objective, the CO_2 produced per unit energy by the two power sources (engine fuel and electric grid) are the deciding factors in the tradeoffs involved. Second, these CO_2 numbers are a function of the grid mix, driving behavior (distance, velocities and trip times) and the engine efficiency map, which are all chosen to be fixed values in these examples. Hence it is necessary to optimize the control stochastically over all these variations or to obtain control rules for different grid mixes, driving behaviors and engine operating efficiencies to be implemented in a PHEV.

3.4.2 Constrained Charging

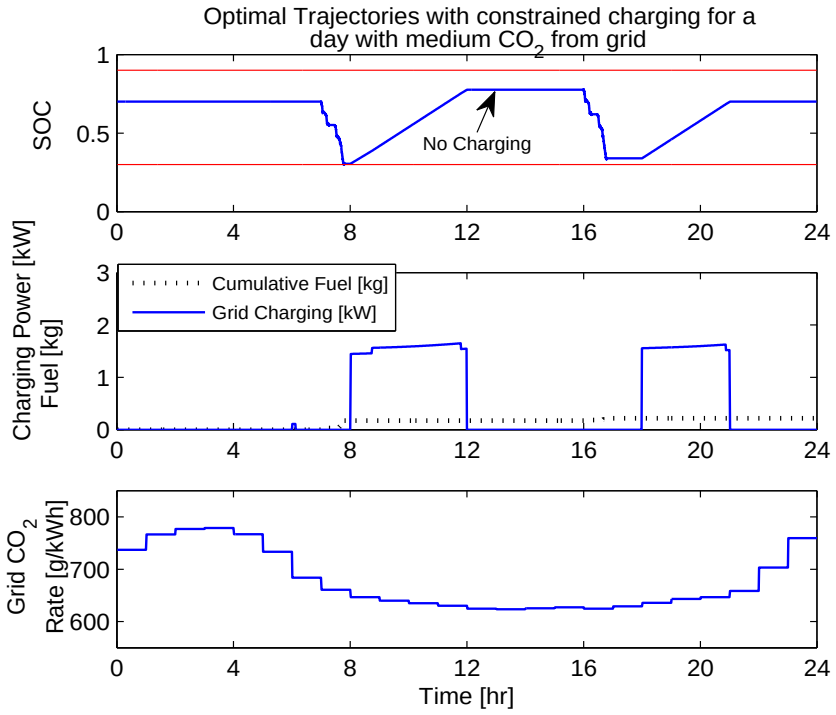

Figure 3.10 Optimal trajectories with no-charging constraint at peak load (hours 12-18) for a day with medium CO_2 from the grid

Finally, due to the low CO_2 per unit energy during the day time (hours 12 to 18), significant amounts of PHEV charging takes place at these times (in Fig. 3.8 and 3.9). These are peak hours for grid demand. It is not beneficial for grid stability, longevity and costs, to charge the battery during peak load [1, 2, 3]. During the peak hours, due to a larger fraction of the grid power being satisfied by natural gas, the CO_2 per unit energy is lower. Thus it would make an interesting problem to trade-off some indicator of grid load (such

as electricity price) to avoid exacerbating the peak (this serves as motivation for the work in Chapter 4). Imposing a constraint on not charging during these time periods would be another strategy. Using the framework (Fig. 3.6), a constraint of no charging during peak load (hours 12-18) is implemented for the medium CO_2 day.

Figure 3.10 shows the results and two important observations are noted. First, the no charging constraint results in lower amount of battery charging before the second trip, resulting in a small amount of extra fuel usage during this trip. Thus the charging constraint affects the power management strategy. Second, battery charging occurs at an earlier time when the grid produces higher CO_2 per unit energy. The resulting CO_2 for the 24 hour period with this no-charging constraint is 7.72 kg, as compared to 7.64 kg without the constraint. The constrained solution avoids peak-charging with only a 1% increase in daily CO_2. Even though this tradeoff is highly dependent on the assumptions (about driving and the electric grid), the framework is powerful enough to expose the need for a combined approach to charging and power management.

3.4.3 Impacts of Initial *SOC*

Another interesting aspect of this optimization framework comes from the constraint that the initial and final *SOC* in the 24 hour period considered must be the same. Figure 3.11 shows three optimal *SOC* and cumulative CO_2 trajectories for different initial *SOC* at 1 AM (initial time step) for the medium CO_2 grid mix. The total CO_2 produced in the case for 0.3,0.7 and 0.9 initial *SOC* are 8.02 kg, 7.64 kg and 7.61 kg respectively. The optimal trajectory with 0.3 as initial *SOC* does not fully charge the battery before the first driving trip because of high grid CO_2 during that time. This results in some fuel usage during the first trip and consequently in CO_2 production during that trip. While the 0.7 and 0.9 cases have sufficient battery energy due to previous evening's charging and hence produce little or no CO_2 during the driving trip. In all the cases, substantial charging occurs before the second trip resulting in CO_2 production on the grid. These trajectories show that it is not always the best solution to charge the battery fully before a driving trip. For the initial $SOC = 0.3$ case, if we imagine that due to some unforeseen reason the consumer could not charge the battery in the evening (hours 18-22), then it is not optimal from a CO_2 perspective to charge the PHEV overnight completely. Rather, it is optimal to drive the first trip on gas and charge the battery thereafter. This non-intuitive solution is possible to obtain only due to the consideration of both the charging and power management solution together.

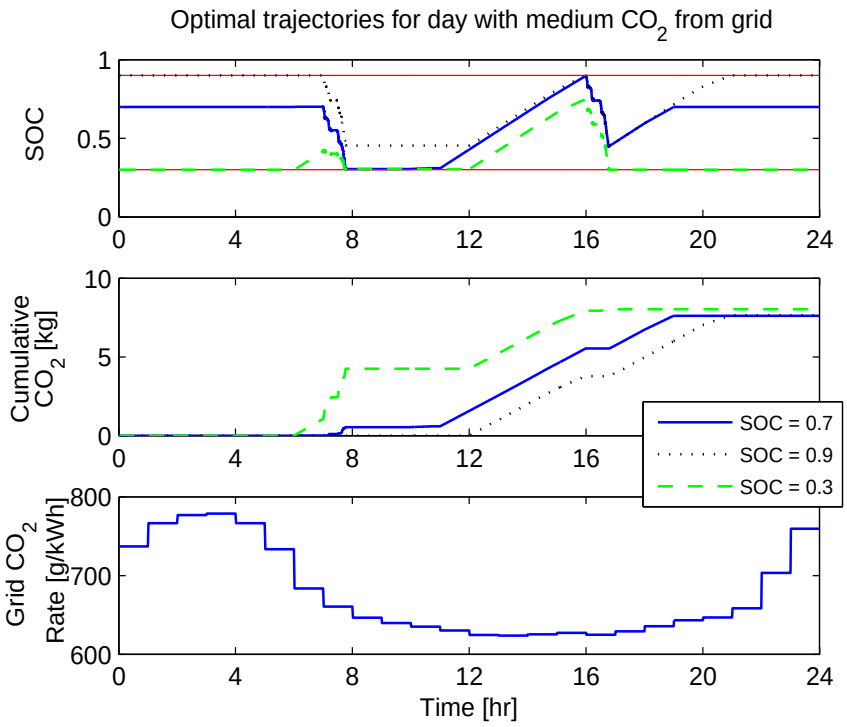

Figure 3.11 Optimal trajectories for a day with medium CO_2 from the grid for different initial *SOC*

3.5 Impacts of Wind Penetration

This section investigates the reduction in total CO_2 emissions resulting from PHEV charging on the grid with significant wind penetration. We use a rigorous optimal control framework to quantify this CO_2 reduction from transportation. Recent forecasts suggest that the electric grid will include a significant amount of renewable power sources [2, 52]. A PHEV is considered a key enabler in clean transportation through charging from a cleaner grid. Studies suggest significant reduction of CO_2 emissions resulting from a grid with higher penetration of renewable resources [3, 94]. In this paper we analyze in detail the CO_2 emissions impact of using PHEVs with a cleaner grid.

3.5.1 Motivation and Scope

There is an obvious CO_2 emissions benefit of charging a PHEV from a grid with more renewable sources and using this energy for transportation. However there are two major challenges to be addressed. First, the intermittent renewable power sources will require more storage and regulation on the grid. Using PHEV batteries for storage and regulation has been previously studied [42, 43, 95, 96]. Secondly, achieving maximum synergy requires

optimized charging and driving of a PHEV considering total emissions [43, 96]. In this work we will address the second challenge by using a global optimal control approach for fair comparison of cases rather than simplistic approaches in preliminary studies [96].

Previous studies regarding grid integration of PHEVs assume PHEV population numbers and complete control over all PHEV batteries when not being used on the road [42, 95]. These studies are extremely relevant to understand the total load and controllability aspects of the load. However, we wish to study the impacts of charging from a cleaner grid on PHEV power-management, and quantify the CO_2 benefits that a synergistic PHEV-grid connection can produce at the consumer (individual PHEV) level. Thus, our studies focus on a single PHEV's 24 hour charging opportunities. In other words, this study focuses on the optimal control strategies that should be implemented in a PHEV, or to be followed by a consumer, for that individual PHEV owner to have the least CO_2 impact.

We developed an Integrated Charging and Power Management Framework in section 3.3.2 of this chapter. This integrated optimal control algorithm considers the dependence between the charging and power management problem, thereby providing a complete optimal solution. The algorithm also makes it possible to quantify the reduction in CO_2 emissions due to any changes in either the driving behavior or grid mixes. The remainder of this section will discuss the wind power data used for our studies and the results quantifying the CO_2 reduction in PHEV operation due to significant penetration of wind power.

3.5.2 Wind Power Data

The wind power data used in our studies are obtained from the Eastern Wind Integration and Transmission Study (EWITS) [97]. AWS-Truewind created this dataset with assistance from NREL/DOE. This data consists of three years (2004-2006) of 10-minute time step wind speeds. The study evaluated *potential* sites for wind power development and *forecasted* wind power output at sites with high potential. In our work, projected wind power from offshore wind in the state of Michigan is used. A total of 210 sites were chosen in this study. Each site had a maximum rating of 2 MW, or a total of 4.2 GW installed wind capacity is considered in this study.

Due to significant variability in wind speeds over time and space, it is not practical to implement optimal charging and power management trajectories for one specific chosen wind power trace. Figure 3.12 shows a graph of wind power output, which is summed up over all offshore locations (210 sites), and averaged over all days of the year for the years 2004-2006. The datasets show that the wind output has significant temporal variability, but averaging over all days of the year produces identical 24-hour wind traces for each of the 3

years. We call these the Yearly Averaged Traces. In our study, we only use 2004 data, and will focus on that particular yearly averaged trace.

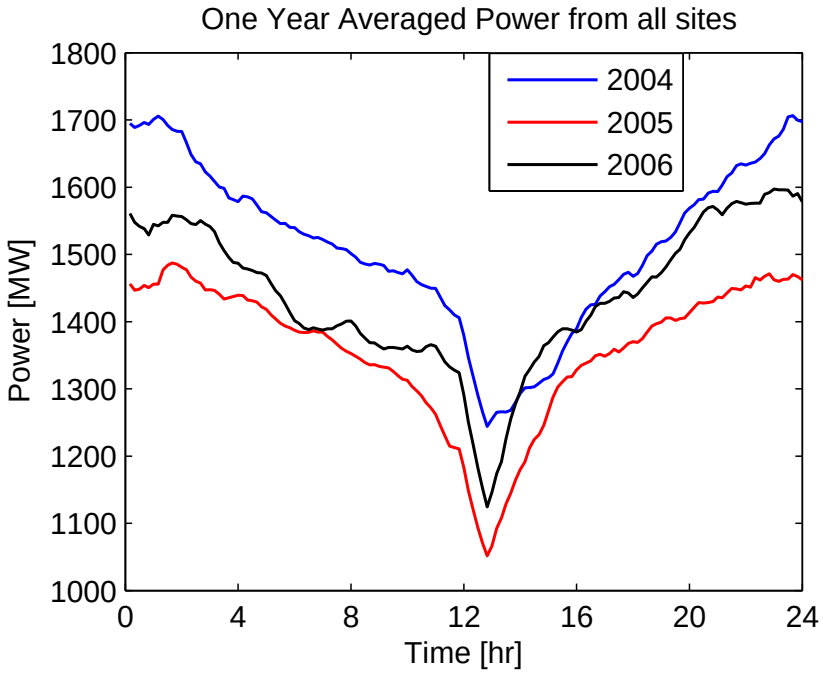

Figure 3.12 Wind Power trace summed over all sites and averaged over a Year (Yearly Averaged Traces).

To assess the performance of an average optimal solution on different days, three days with different levels of wind power are considered. A day with 85 percentile wind energy content was selected as a ”high wind” day. The ”medium day” represents 50 percentile wind energy content and the ”low day” is chosen as a day with 15 percentile wind energy content as shown in 3.14. Figure 3.13 shows the wind traces corresponding to these days along with the yearly averaged trace. The actual amount of power and energy supplied by wind power to satisfy the grid demand is shown in Figure 3.15. It is observed that on the high wind day, up to 18% of the grid energy is from wind, compared to only 4% on the low wind day. Figure 3.15 also shows that even on the day with lowest wind, at some point during the day, wind power supplied close to 15% of the demand. Hence all these scenarios describe wind penetration levels that are currently not observed in the Michigan grid. Finally, Figure 3.16 shows the CO_2 traces resulting from the different amounts of wind supplied during a particular day. These traces impact the optimization algorithm's decision to charge from the grid as it might be beneficial to charge from the grid at different times depending on the grid mix. The process of including wind power data is depicted pictorially in Fig. 3.17.

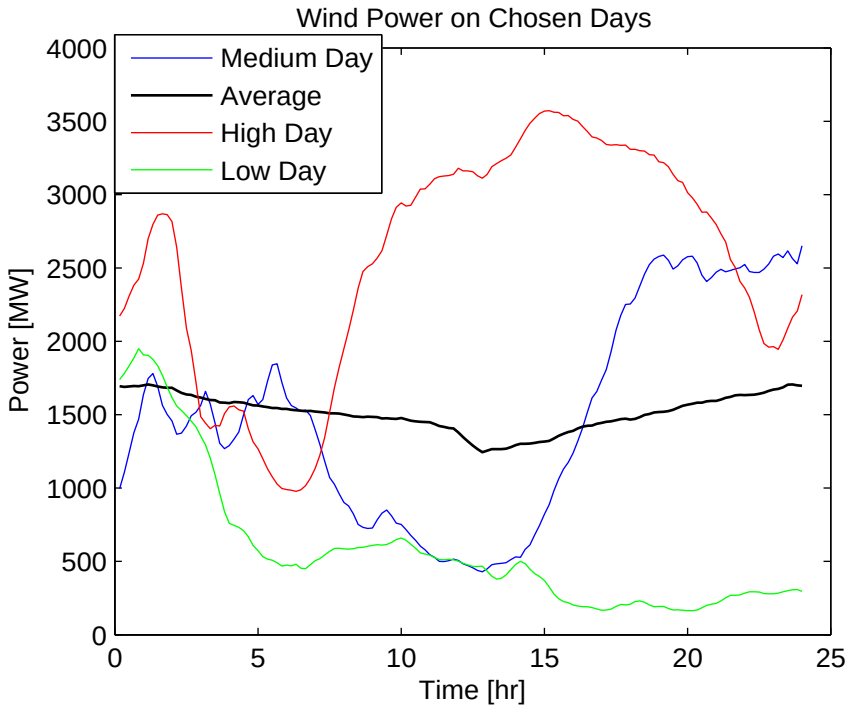

Figure 3.13 Wind Power traces on different days compared to the Yearly Averaged Trace.

3.5.3 Optimization Conditions

The optimal control problem is the same as formulated by Eq. 3.3, with the objective being minimization of total CO_2 emissions. This optimization is performed for different CO_2 conditions related to different grid mixes (Fig. 3.16), for initial *SOC* conditions ranging from 0.3 to 0.9 in steps of 0.1. The driving pattern is the same as described previously in section 3.2.3. A drive cycle of 23.9 miles is repeated at 8 AM and 5 PM.

The optimization algorithm as presented in section 3.3.2 above is used in all the cases. This demonstration shows one possible use of the integrated optimization framework. Again it is necessary to note that we wish to understand the optimal tradeoffs and obtain insight. Thus we optimize several cases rather than obtaining an optimal *stochastic* solution. Thus these results are specific to the assumptions on wind power, grid mix and driving behavior. Hence we present a qualitative analysis of interesting trends rather than focusing on the numbers.

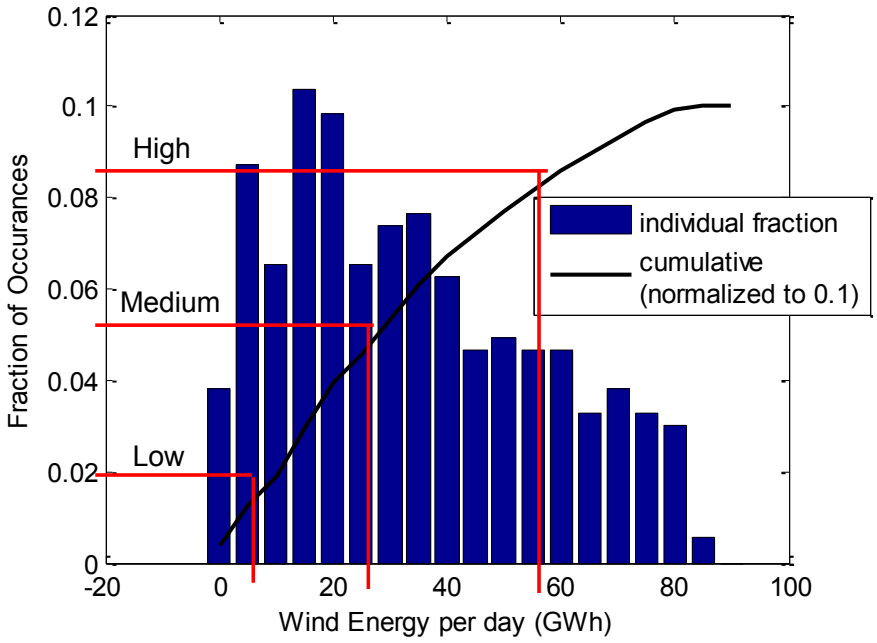

Figure 3.14 Daily Wind Energy Histogram for a year, indicating days of high, low and medium wind power.

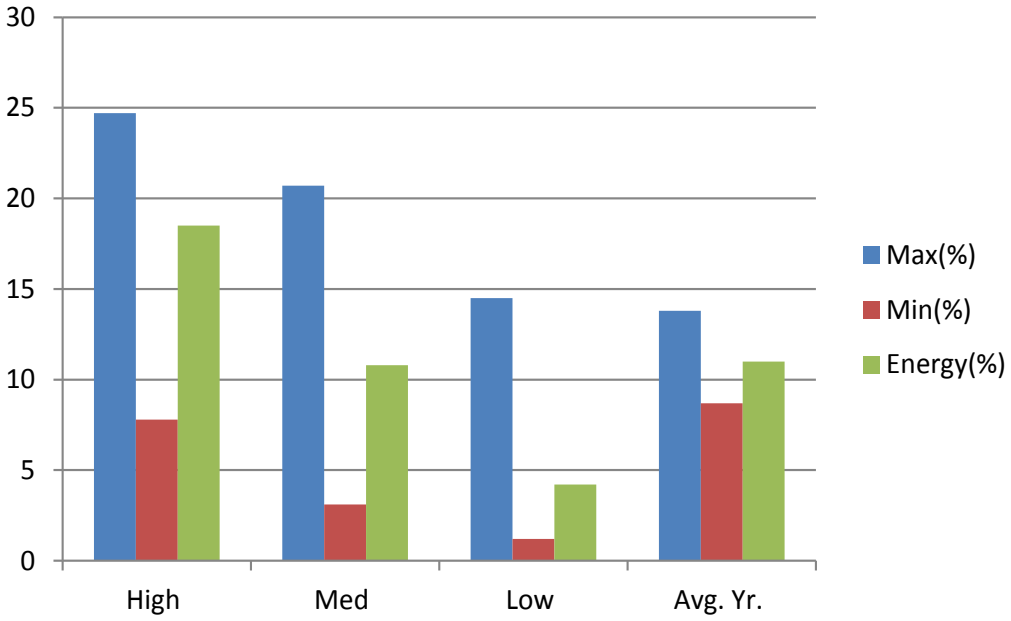

Figure 3.15 Amount of Power and Energy Supplied by Wind in Different Cases to Satisfy Grid Power Demand

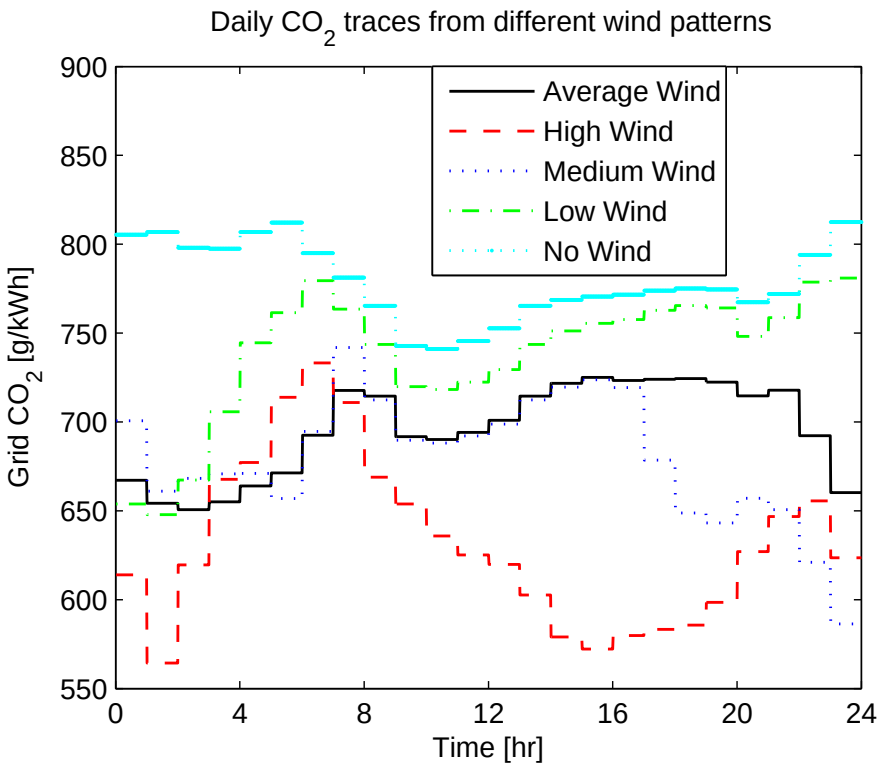

Figure 3.16 CO_2 traces Produced by a Grid Mix with Different Amounts of Wind

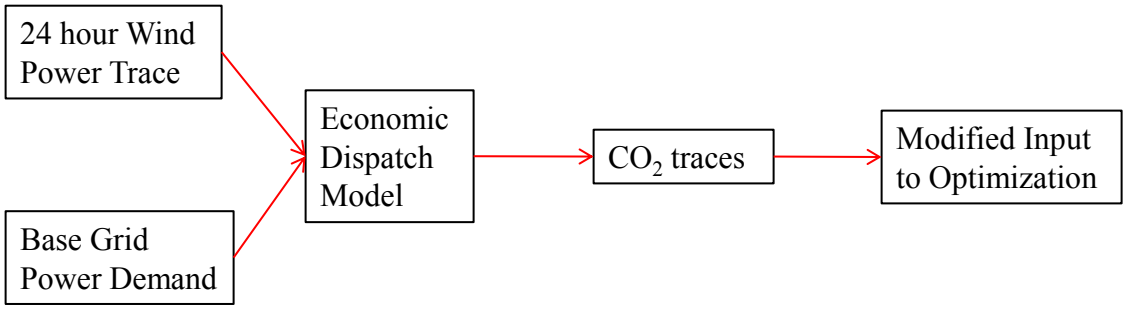

Figure 3.17 CO_2 traces Produced by a Grid Mix with Different Amounts of Wind

3.5.4 Results

The results we present will be the optimal trajectories for an individual PHEV which interacts with the grid and follows the driving patterns as described in section 3.2.3. The results are highly sensitive to the driving requirements and the grid mix. However, our goal is to analyze each optimal solution in detail and learn from these 'best case' scenarios. The following are the highlights of the results:

- Total CO_2 emissions decrease due to inclusion of wind power (even in the case of

lowest wind power).

- Due to our integrated charging and power management algorithm, we capture the optimal benefits offered by wind power on the grid. It is shown that the optimal trajectories vary significantly depending on the wind penetration.
- We quantify the loss of optimality resulting from wind variability in Fig. 3.20 by providing a comparison of the 'yearly average' optimal solution to the other solutions.

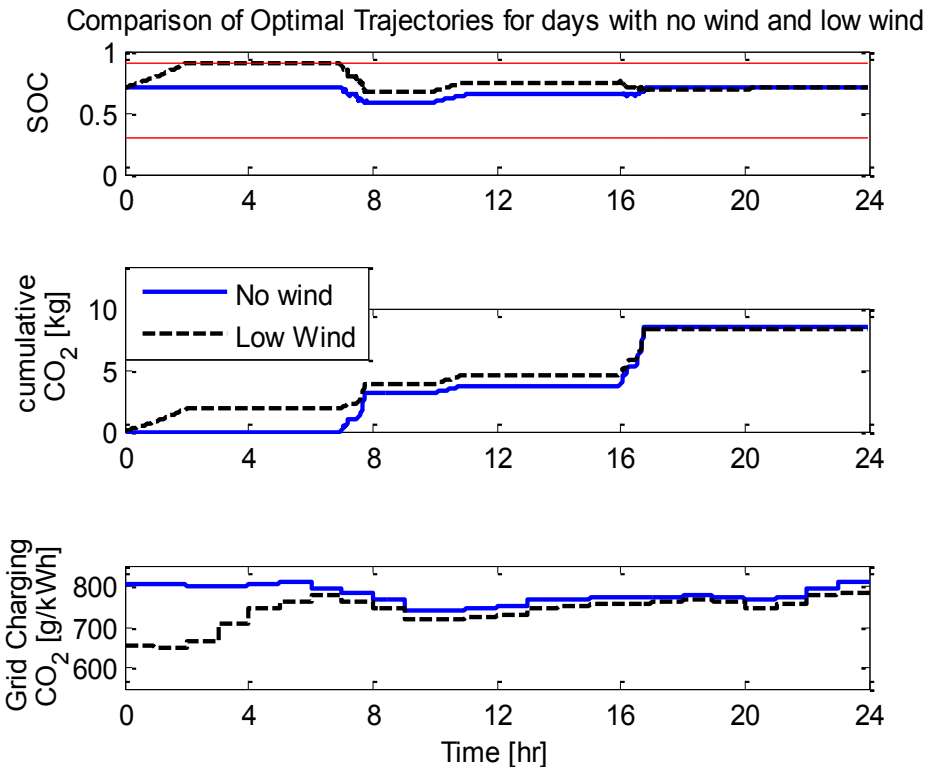

Figure 3.18 Optimal Trajectories for Days with No and Low Wind

Next, we explain each of these results in more detail. It is obvious that adding large quantities of wind will result in reduced CO_2 per unit energy produced on the grid. It is less straightforward to understand the impact of increased wind power on reduction in CO_2 produced from transportation. Total CO_2 emissions decrease due to inclusion of wind power (even in the case of lowest wind power). First, we compare two cases, one without any wind power on the grid and the other with a low amount of wind power on the grid (low amount of wind power refers to the low day as described in section 3.5.2). Figure 3.18 presents the resulting CO_2 produced over 24 hours due to the PHEV's transportation needs in the two cases. The observations from this figure are that there is a small reduction in CO_2

(2%) due to inclusion of wind power (in this case of lowest wind power) and the optimal *SOC* trajectories in the two cases are different. The difference is observed in the first few hours, when the CO_2 output of the grid is lower due to wind. For the low day, there is an insignificant amount of wind for the rest of the day. Thus even though a higher amount of grid energy is used for driving in the case with low wind (and a higher amount of gasoline used in the case with no wind), the amount of CO_2 produced differs only by 2%.

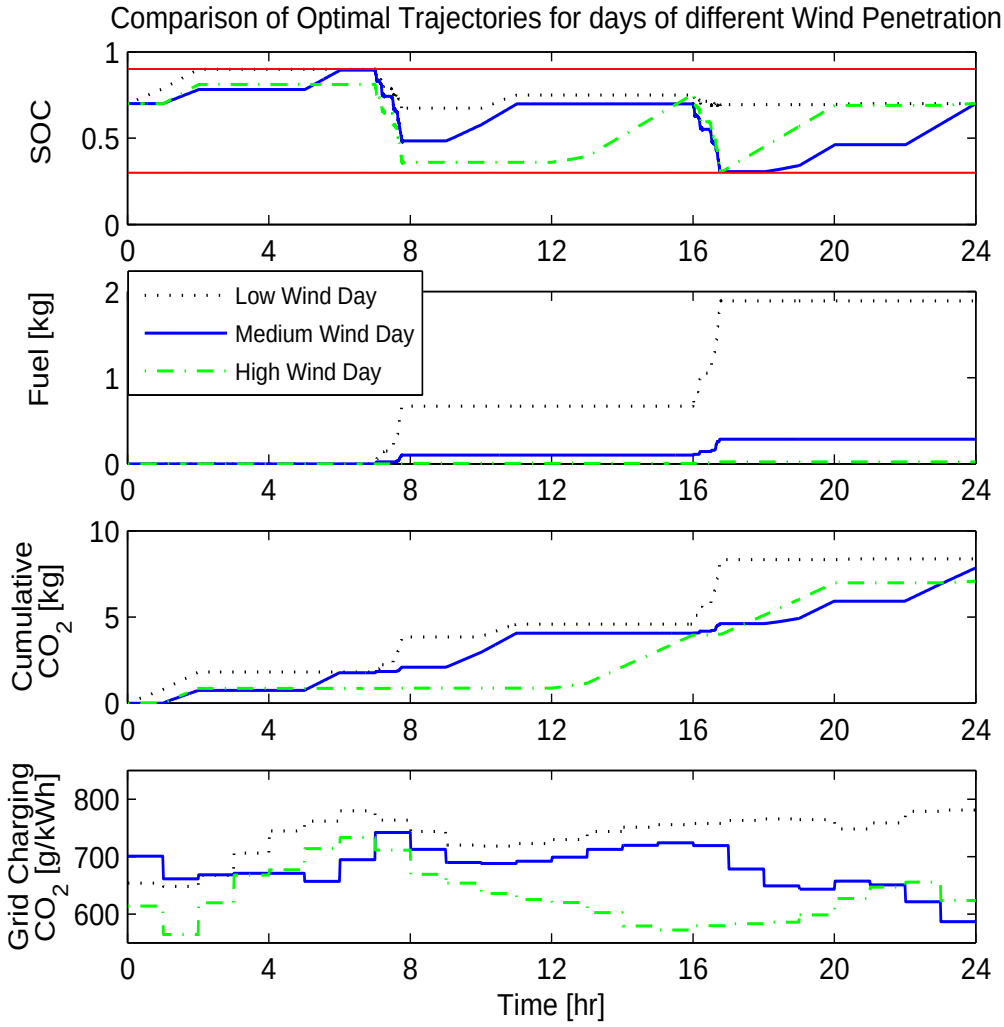

Figure 3.19 Optimal Trajectories for Days of High, Low and Medium Wind

A comparison of optimal trajectories for the three days with different levels of wind penetration was performed. Fig. 3.19 shows the difference in optimal trajectories related to the three days with different amounts of wind. The differences are due to - *i*) the tradeoffs between the CO_2 produced by gasoline fuel and electricity and *ii*) due to varying amounts of

wind throughout the day, resulting in different CO_2 from the grid at different times. Thanks to a combined approach, we can capture these differences. For example, in the medium wind case, we observe that higher grid CO_2 (due to low wind) during hours 10-16 results in the optimal solution using some gasoline for the second trip rather than charging before the second trip. Such tradeoffs between gasoline usage and charging are seen in all the cases depending on the CO_2 produced by the chosen grid mix.

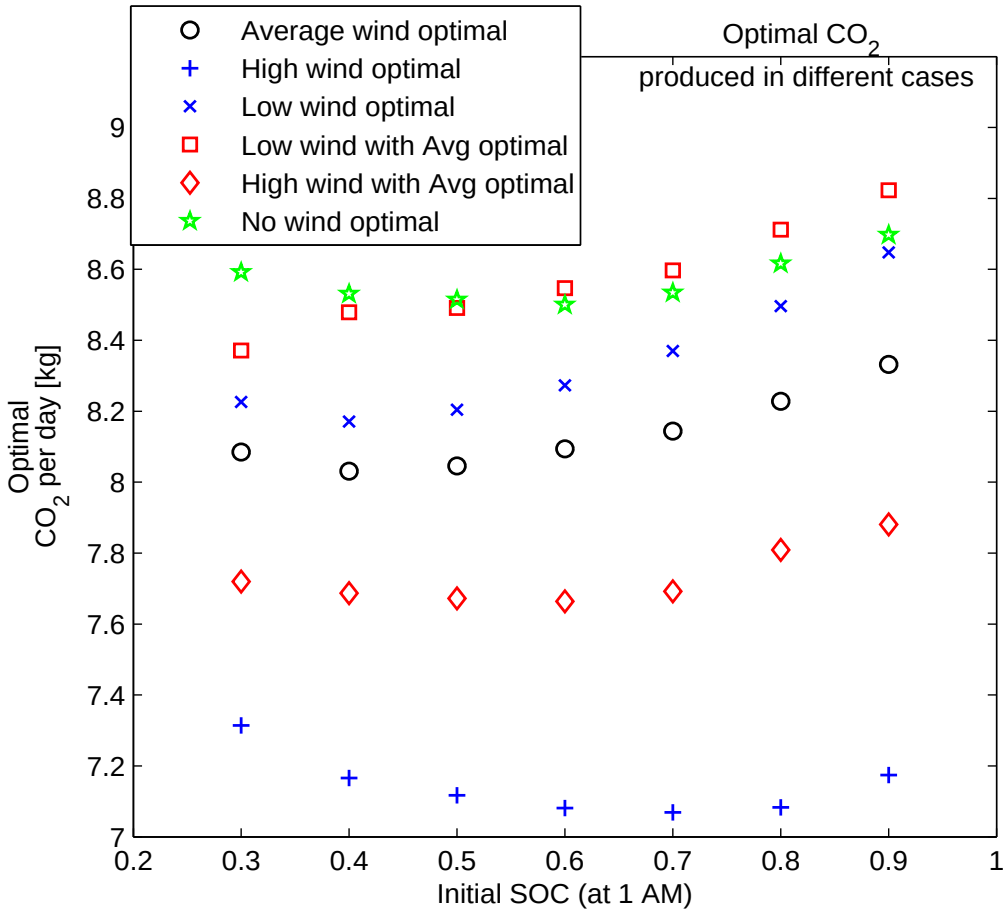

Figure 3.20 Comparison of loss of optimality

As mentioned in section 3.5.2 on wind data, it is not practical to implement optimal solutions for every single day due to wind variability. So we obtain an optimal solution for the yearly average wind case (which is fairly consistent as shown in Fig. 3.12). Comparing this average performance to the optimal solutions on the days with high, low and medium wind, we quantify the loss of optimality resulting from wind variability in Fig. 3.20. In particular, there is a maximum loss of 10% amongst the cases considered. Looking at the variation in wind power in Fig. 3.13 and in the wind penetration in Fig. 3.15, it can

be observed that despite such variations, the final CO_2 loss (of optimality) as compared to applying the average-best control solution is 10% in the worst case. This is due to the narrower range of variations in the resulting CO_2 produced by the grid in all the cases, as seen in Fig. 3.16. Quantifying the penalty stemming from variability of wind energy is a unique finding of this study. This showcases the opportunities to develop control rules for different grid mixes and eventually obtain stochastic optimal results.

3.6 Summary

A complete optimal framework which considers the dependence between optimal charging and power management is introduced. It is computationally feasible due to a DP implementation using backward looking system dynamics model. The steps of the framework are explained and applied to 24 hour driving and grid mix scenarios. Three different cases with days of high, low and medium CO_2 are studied along with two naturalistic driving trips.

The results show that it is necessary to consider a combined approach to optimally charge and drive a PHEV. Depending on the objective and constraints, it is shown that it is not always optimal to fully charge the battery before every driving trip as assumed in the literature. This framework is also capable of exploring tradeoffs that might result from usage of a PHEV for grid related services or restricted charging.

This optimal control approach of considering combined charging and power management of a PHEV with a DP algorithm was also used to study the synergistic interaction of the PHEV with a cleaner grid (more wind). Three different cases of varying amounts of wind power on the electric grid were considered. The results show that an integrated approach is capable of extracting the optimal CO_2 reduction benefit wind power depending on the chosen wind power trace. Since it is not practical to implement optimal solutions for every single day due to wind variability, a comparison of loss of optimality resulting from applying average optimal solutions on the high and low wind days is also presented.

Chapter 4

Multi-Objective Dynamic Programming for Optimal Control of a PHEV

This chapter presents a computationally attractive Multi-Objective Dynamic Programming (MODP) algorithm. The algorithm is applied to obtain the optimal supervisory control for PHEVs to minimize two objectives - total CO_2 emissions and operational dollar costs to an individual PHEV owner. First, the literature and the motivation for this work is discussed in detail. Then the optimization conditions chosen for this study are presented. The vehicle powertrain and grid dispatch models used in this study have been presented in detail in chapters 2 and 3. Next, the multi-objective dynamic programming algorithm is presented. Finally, the results show the optimal Pareto front with a good spread ranging from one extremal point to the other. The results also reveal interesting insights for the tradeoffs that can be achieved in minimizing the CO_2 emissions and cost objectives for the underlying grid mix and driving conditions assumed.

4.1 Literature and Motivation

This chapter develops an optimal control algorithm to address multiple objectives and obtain the Pareto set directly, without any prior weighting factors. The algorithm is applied to obtain the optimal PHEV supervisory control considering two objectives; total CO_2 emissions and dollar costs to the consumer. A PHEV, unlike an HEV, is expected to exchange significant amounts of energy with the electric grid. Through this interconnection, PHEVs can create significant opportunities for CO_2 emissions reduction, reduction of operational costs to utilities and consumers and provide several vehicle to grid (V2G) services such as frequency regulation [2, 3]. To best utilize a PHEV for these multiple purposes, it is necessary to obtain optimal control solutions considering multiple objectives. Thus, our overarching goal in this chapter is to develop a multi-objective control optimization framework and apply it to obtain optimal PHEV supervisory control solutions.

Previous research in optimal PHEV and HEV supervisory control have mostly considered a single objective. The objectives considered include fuel consumption [29, 98], emissions [99, 100], dollar costs [36, 86] battery health [101] and drivability [33]. In [33, 99], authors consider emissions or drivability as constraints while optimizing objectives such as fuel economy. Though this approach allows for consideration of multiple objectives, the solutions are optimal only with respect to one objective, while satisfying a constraint on the other objective. The optimization methods used include Equivalent Consumption Minimization Strategy (ECMS) [98], Intelligent rule based control [29], Dynamic Programming (DP) [36, 86, 100], Evolutionary Algorithms (EA) [9, 38]. The dynamic programming approach explicitly uses Bellmans principle for optimal control, and thus guarantees global optimality. The output of this process is a supervisory control trajectory that can be used to gain important physical insights and extract implementable rules for subsequent online power management [50, 51]. This motivates us to apply optimal control using DP.

To consider multiple objectives in supervisory control optimization, two approaches have been adopted previously. One is using Multi Objective Evolutionary Algorithms (MOEA) [57, 58]. Since EAs work with populations of points in each iteration, a number of Pareto-optimal solutions may be captured in an efficient manner using non-domination operators [59, 60]. However, the supervisory control has to be parameterized in order to use such algorithms due to their static nature. This parameterization results in a loss of optimality because the optimal control actions are dynamic in nature. The second approach is to combine multiple objectives into a single objective through a weighting scheme, and use the optimal control methods mentioned in section 1.2.1. Though this approach has produced results showing the tradeoffs between the objectives successfully, it has the following drawbacks. First, the choice of weights determines the outcomes and these weights are subjectively chosen. Second, in order to obtain the complete Pareto front, the optimization has to be repeated several times. Finally, this approach is not conducive to obtain the non-convex regions of the Pareto front [61].

Multi-Objective Dynamic Programming (MODP) extends the Bellman's equation to consider multiple objectives through a non-domination operator [102]. MODP obtains the optimal Pareto surface directly while retaining the dynamic nature of the optimality. However, it is computationally expensive in terms of both time and memory requirements. The major cause for these computational issues is that MODP requires the calculation of a non-dominated surface at every time step for every state discretization. Algorithms have been proposed to improve computational time [103, 104]. Such algorithms require convexity assumptions to hold true and cannot be easily applied to a complex nonlinear system such as a PHEV powertrain.

There are two major contributions in this chapter. First, we integrate ideas from MOEA with MODP to capture Pareto-optimal solutions with lower computational time and memory requirements. Thus retaining the dynamic nature of optimality from MODP, while obtaining a uniformly spread Pareto surface in a computationally feasible manner. Second, this algorithm is applied to obtain the optimal charging and power management solutions for a series PHEV powertrain to minimize the total CO_2 emissions and dollar costs incurred by a consumer. The results demonstrate the non trivial tradeoffs between the objectives and provide insight in designing the optimal supervisory control. Furthermore, the algorithm can be used for multi-objective optimal control of other systems.

4.2 Optimization Conditions

The objective in our optimal control problem is to minimize total CO_2 produced and dollar costs incurred by a given PHEVs use of fuel and electricity. The PHEV powertrain model ODEs and its backward looking implementation are presented in section 2.2.4. The charging of the PHEV battery from the grid and the grid dispatch model are discussed in section 3.2.2.

For this study, the PHEV performs two identical trips (23.9 miles long) in the morning and afternoon. Fig. 4.1 shows the vehicle velocity for each trip as a function of travel distance. The total daily driving distance of 47.8 miles necessitates either gasoline usage or multiple battery charging events during the day, thereby elucidating some interesting tradeoffs between battery charging and fuel consumption.

The CO_2 shown in the first subplot of Fig. 4.2 is obtained by using the grid dispatch

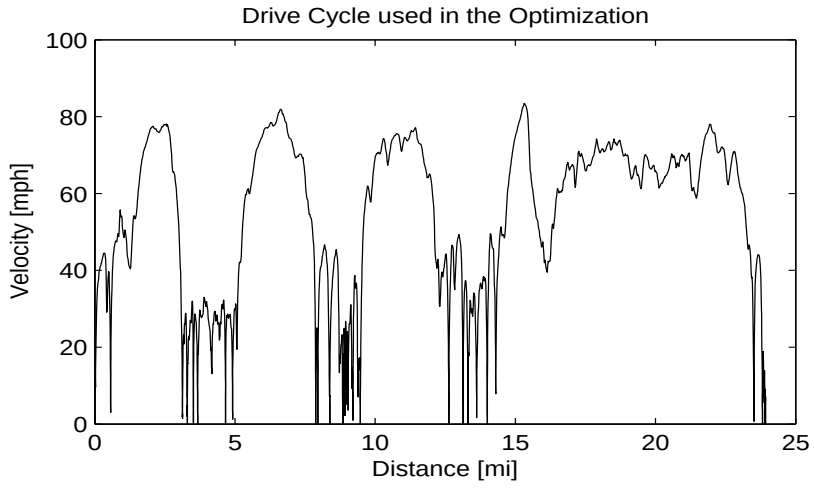

Figure 4.1 Drive Cycle Velocity graphed as a Function of Distance.

model. The cost trace in Fig. 4.2 is obtained through a different method.

- *CO_2 trace*: This particular trace was chosen as it closely represent a medium level of CO_2 from the Michigan grid. The medium level of CO_2 is in reference to the year-long CO_2 production on the Michigan grid (see [90] and section 3.2.2). Since the grid dispatch changes hourly, these traces change hourly.
- *Cost trace*: The grid dispatch model cannot accurately predict the costs as the cost-structure adopted by different utilities is proprietary, and changes drastically with the inclusion of newer electricity sources [90]. Hence we use the Midwest ISO data on the cost of buying electric power to the utilities [105]. These electricity costs are in the range of 0.3-3 cents/kWh based on the grid power demands. The electricity prices faced by consumers in the Midwest at different times of the day (again based on grid demand) ranges from 5-25 cents/kWh [106]. Thus we multiply the electricity cost trace as given by the Midwest ISO by 10. This increase in the cost as faced by the consumer includes transmission and distribution costs, other operational costs and profit margins of the utilities. The resulting cost trace is plotted along with the CO_2 trace in Fig. 4.2.

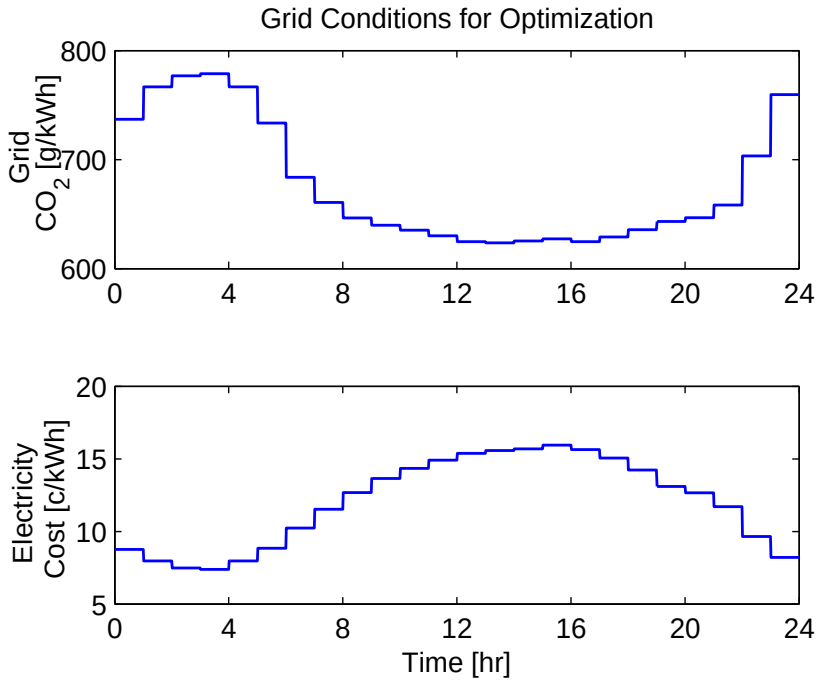

Figure 4.2 Electricity Cost and CO_2.

Daily driving distance and traffic conditions affect PHEV energy usage: a fact that has motivated researchers to optimize PHEV operation over large families of trips [36, 88]. Similarly, the grid mix varies both temporally and spatially [3, 19, 90], resulting in different amounts of CO_2 and costs. This work, in comparison, focuses on developing of an optimization framework capable of handling multiple objectives in an elegant manner. We illustrate this framework for the trip and grid mix details in Fig. 4.3, but the framework is broadly applicable to any trip profile, grid mix and set of objectives.

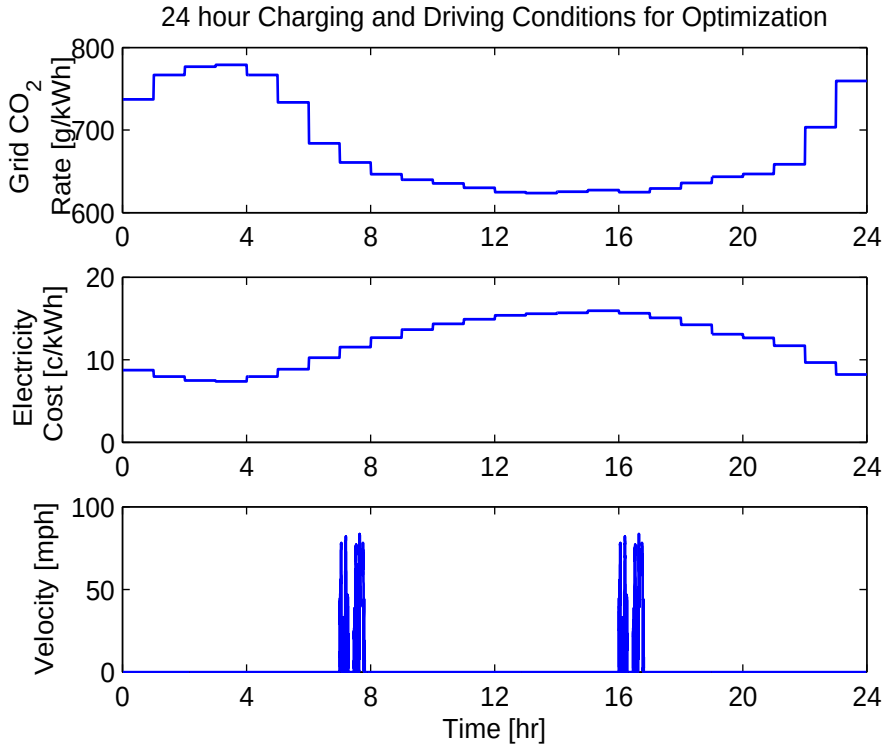

Figure 4.3 Driving events, Grid CO_2 and Costs over the 24 hour Optimization Horizon.

4.3 Multi-Objective Control Optimization

The optimization problem is formulated as follows

$$\min_{(z(t),u(t))} J = \left\{ \begin{array}{l} \sum_{0}^{24} \left(\frac{CO_2}{gal} \dot{m}_f \Delta t_{dr} + \frac{CO_2}{kWh} P_b \Delta t_{ch} \right) \\ \sum_{0}^{24} \left(\frac{\$}{gal} \dot{m}_f \Delta t_{dr} + \frac{\$}{kWh} P_b \Delta t_{ch} \right) \end{array} \right\} \tag{4.1a}$$

$$\text{subject to} \quad \dot{z} = f(z(t), u(t), t) \tag{4.1b}$$

$$z \in Z_c \quad \textit{and} \quad u \in U_c \tag{4.1c}$$

The optimization objective, J, is the total amount of CO_2 produced and the total operational dollar costs during a 24-hour period. Gasoline consumption is $\dot{m}_f$ gallons per time step during driving ($\Delta t_{dr} = 2$ sec). Battery charging power is given by P_b in kW and the charging time step is $\Delta t_{ch} = 60$ sec. The price of gasoline is chosen as \$3/gallon and the CO_2 rate is 8.78 kg/gallon. The cost and emissions of electricity are described in the previous subsection. The constraints on the states and inputs (i.e. the sets Z_c and U_c) are described in detail in the previous chapter (section 3.2.2).

Note that there are two components to each of the costs. One component is from fuel usage while the other is from electricity usage. In order to obtain a total optimal solution, we have to integrate the process of optimal charging and optimal power management into a single framework. This is not a trivial problem as the system dynamics and constraints differ significantly during the two processes. In [107] and chapter 3, we present a dynamic programming based algorithm that integrates the two optimal control problems. This is achieved by exploiting the constraints at the boundaries of the two problems and provides a complete optimal control solution over the driving and charging events. The results presented in [107] also show the need for the consideration of the two problems under a single framework. Next, the MODP algorithm is presented.

4.3.1 Multi Objective Dynamic Programming Algorithm

To state the algorithm briefly, the Value function is initialized in step 1. All possible future paths are calculated in step 2. Step 3 obtains the non-dominated paths. The set of possible non-dominated paths is filtered down to a manageable size by using the concept of crowding distance in step 4.

The following algorithm was implemented for MODP (framework presented in Fig. 4.4. Note that upper case letters indicate sets and italicized letters indicate elements of a set.

- *Step 1*- Initialize an Optimal Cost-to-go (or Value function) V(Z_d,t_f,C) at the final

time step t_f, over all states defined by the discretization $Z_d = \{z^1, z^2, \ldots, z^i, z^j, \ldots, z^N\}$, where N is the number of state discretizations. The set of objectives is given by C (in our case C = $\{CO_2, \$\}$). Thus $V(z^i, t_f, C)$ is a vector in $\mathbb{R}^2$ for each state point z^i at time step t_f.

- *Step 2*- For each state z^i in Z_d, at time step $k \in [1, t_f - 1]$, calculate the set of all value function vectors (V') by evaluating Eq. 4.2 over all possible future state transitions $z^j(k+1)$ given by the set Z_c from Eq. 4.1c.

$$V'(z^i(k), k, z^j(k+1), C) = c(z^i(k), k, z^j(k+1)) + V'(z^j(k+1), k+1, C) \tag{4.2}$$

  In our problem we have two objectives, so $V'(z^i(k), k, z^j(k+1), C)$ is a vector in $\mathbb{R}^2$. The costs of transitioning from z^i at time step k to z^j at time step $k+1$ is given by the vector c. Thus V'($z^i(k)$,k,C) is the set given by $V'(z^i(k), k, C) = \{\, y : y = V'(z^i(k), k, z^j(k+1), C),\ \forall z^j \in Z_c \}$

- *Step 3*- For each state z^i in Z_d, at every time step k, evaluate the set of non-dominated value functions (V^{ND}) by checking the following conditions for all elements of V'. For elements y^r, $y^s \in V'$, y^r is said to dominate y^s, *iff* $y^r(n) \leq y^r(s)$ for all n objectives and the inequality is strict for some n.

- *Step 4*- Sort the elements in V^{ND} according to any one objective. Evaluate the crowding distance for all elements in V^{ND} as defined and demonstrated in [60]. Select a threshold number of points (which is 20 in our case) with the highest crowding distances to effectively represent the Pareto surface given by V.

Repeat steps 2 to 4 from time step t_f -1 to the initial time step = 1 using the set V from step 4. At time step = 1, the set V represents the optimal Pareto front at all state points. A flowchart for the algorithm is presented in Fig. 4.4.

All the above steps except step 4 are part of previous MODP formulations [102]. Without step 4 the number of elements in the set V^{ND} and consequently in V increase exponentially with every time step. A theoretical discussion on such phenomenon can be found in [103]. The use of a crowding distance metric keeps the number of elements in the set V^{ND} fixed at every time step (to a chosen threshold). This results in feasible computational time and memory requirements. For the conditions described in section 4.2, the algorithm solved for the optimal Pareto front in three days while generating more than 10 GB of data.

Several distance metrics have been previously used to obtain representative Pareto

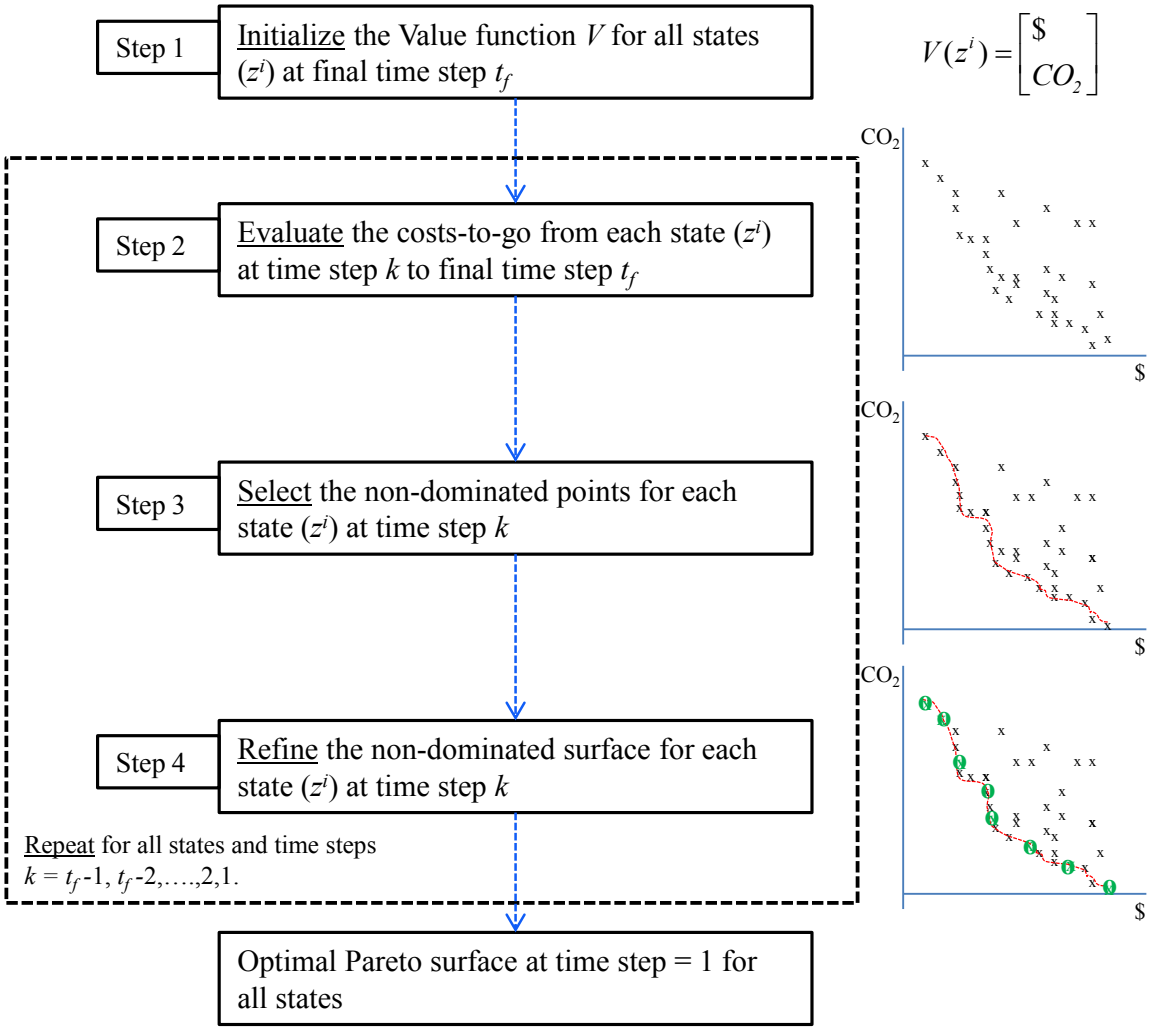

Figure 4.4 Flowchart describing the MODP Algorithm.

surfaces with lower computational costs [59, 60]. Crowding distance as defined and demonstrated in [60] has the following advantages. First, it preserves diversity or the Pareto surface has a uniform spread. This can be observed in the Pareto surface presented in the results section. Second, it can be calculated faster than sorting the non dominated elements (step 3 in the algorithm), thereby adding a negligible computational effort to the entire algorithm.

4.4 Optimization Results

The above optimization algorithm (section 4.3.1) is applied to optimize the supervisory control for PHEV charging and on-road power management under the conditions presented in section 4.2. The initial and final *SOC* are restricted to be the same (= 0.6). The following four observations are gathered from the results.

First, the Pareto front reflecting the tradeoffs between achieving minimum CO_2 and minimum operating costs for a single PHEV has a good spread (Fig. 4.5). Since the crowding distance metric gives importance to retaining the extreme points of the Pareto front, we can see that the extreme points are captured. This is of vital importance because it signifies that filtering of the non-dominated surface retains optimality. The two extreme points (represented by square markers) are obtained by single objective optimization.

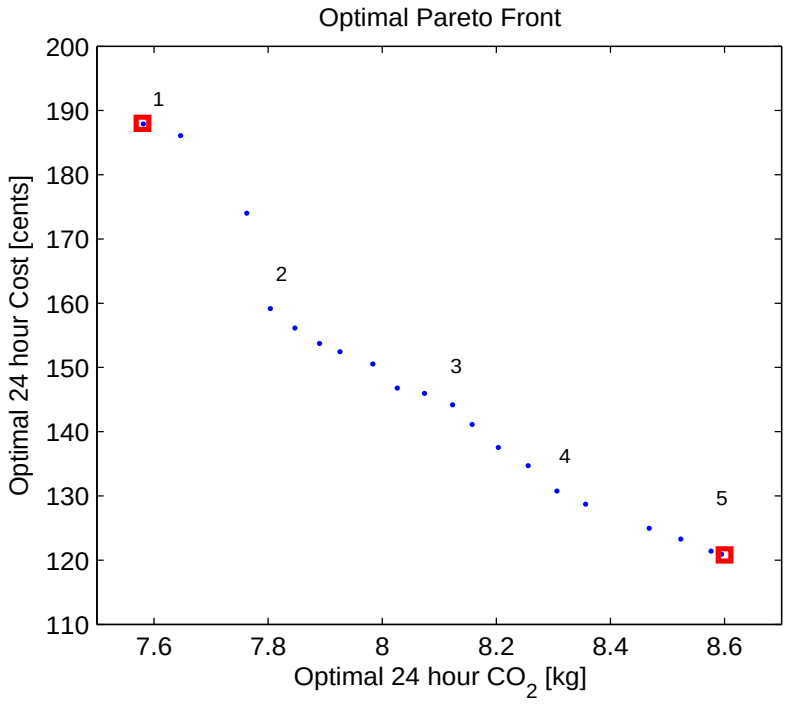

Figure 4.5 Optimal Pareto Front.

Second, for the chosen grid and driving conditions, we can infer at least two interesting tradeoffs. 1) If a consumers goal is cost centric, by choosing point 4 instead of point 5 for optimal PHEV operation, we will be increasing the operating costs by 11.4% while reducing the CO_2 by only 4%. 2) If our goal is CO_2 centric, then the Pareto front shows that we can obtain a 15.2% reduction in costs with only a 2.9% increase in CO_2 by choosing point 2 instead of point 1. Again, these results are only of qualitative importance because they are for the specific grid mix and driving behavior assumed. Depending on the underlying

conditions the tradeoffs will change and our framework (section 4.3.1) can expose such tradeoffs.

Third, in Fig. 4.5, the regions between points 1 and 2 and around point 3 show that the algorithm captures the non-convex regions of the Pareto front. Multi objective optimization problems considered as single objective optimization problems with linear weighting cannot capture these points [61].

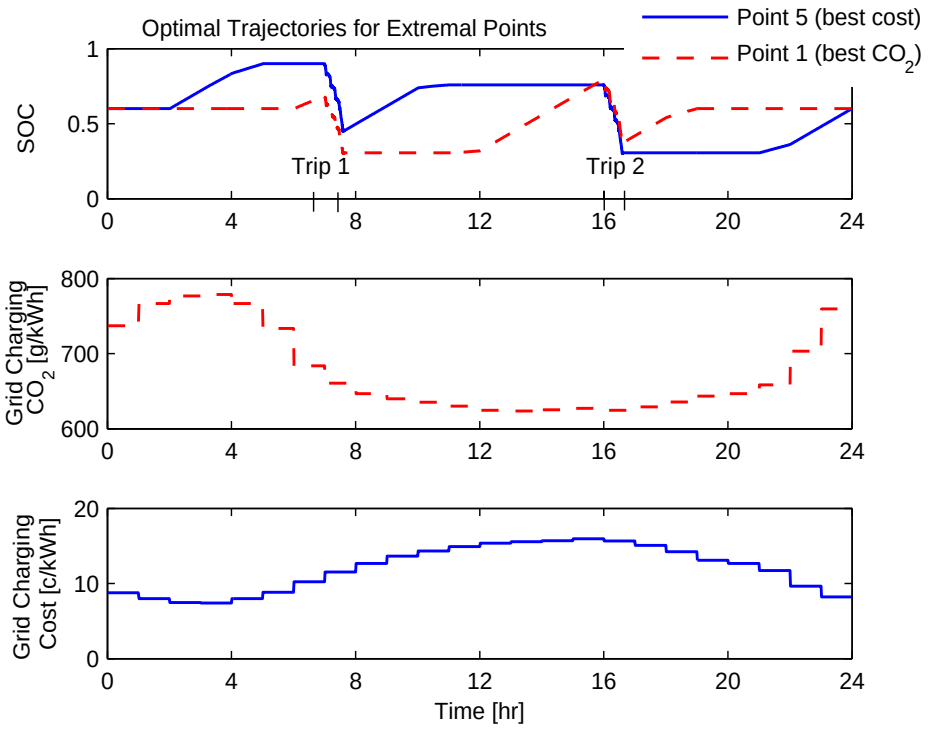

Figure 4.6 Comparison of Optimal Trajectories (for points 1 and 5).

Finally, by studying the optimal trajectories corresponding to the extremal points in Fig. 4.6, we observe that the optimal trajectories correspond to the best cost and CO_2 cases. This again verifies that the Pareto front has a good spread. Fig. 4.7 compares the optimal trajectories corresponding to points 1 and 2 (from Fig. 4.5). Applying methods presented in [100], or intuitively, we can obtain implementable rules for optimal control depending on the acceptable tradeoffs. For example, by setting a threshold of 683 g/kWh and charging below this threshold with no other restrictions approximately produces the results corresponding to point 2. This results in significant cost reduction for a small increase in CO_2 emissions.

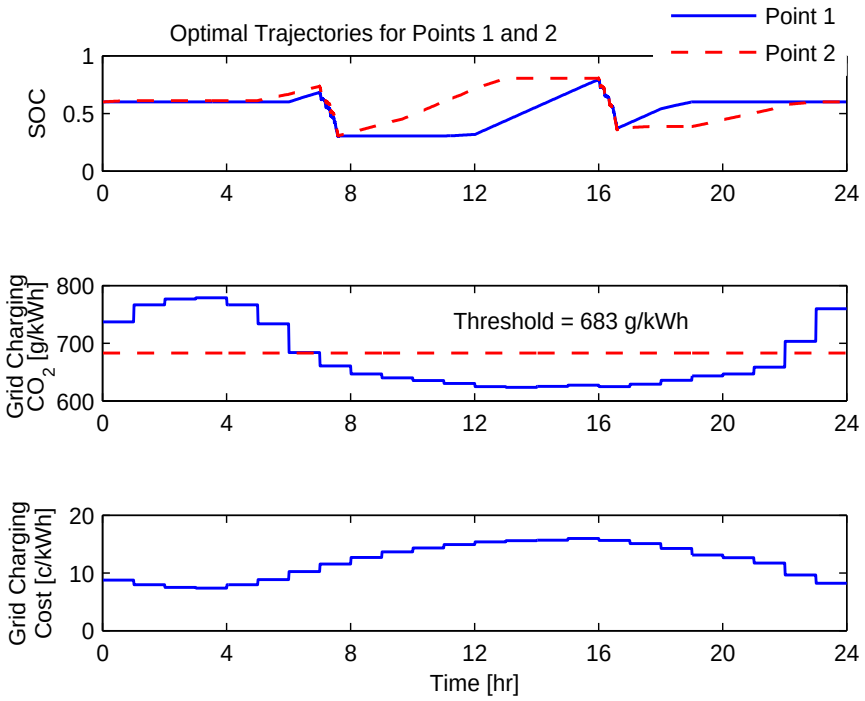

Figure 4.7 Comparison of Optimal Trajectories (for points 1 and 5).

4.5 Summary

The development of a computationally attractive MODP framework which utilizes the concept of crowding distance from MOEA to efficiently characterize the Pareto front is explained. Crowding distance is used as a metric to retain fewer number of points to represent the Pareto front at every state discretization and every time step. This results in only a linear increase in memory and time requirements with the number of time steps as compared to and exponential increase in previous approaches. Thus, the refinement of the Pareto front significantly reduces the computational time and memory requirements making the problem feasible. However, this refinement still obtains a uniformly spread Pareto front that spans the entire range of the objective space thereby retaining sufficient optimal features of the Pareto front.

This algorithm is applied to obtain the optimal supervisory control for a PHEV to minimize two objectives - CO_2 emissions and operational dollar costs to an individual PHEV owner. The algorithm generates an optimal Pareto front with good spread ranging from one extremal point to the other. For the grid mix and driving behavior assumed, we exposed tradeoffs related to both the objectives. It is shown that the tradeoffs are almost linear for

a cost centric goal, whereas the tradeoffs for a CO_2 centric goal show that allowing for a small increase in CO_2 can result in a more amplified reduction in operational dollar costs.

Chapter 5

Computationally Efficient Combined Plant Design and Controller Optimization

This chapter presents a novel approach to the optimization of a dynamic systems design and control. Solving these two problems by considering their dependence on each other results in a system level optimum. We propose a novel approach that uses a previously-derived coupling measure to quantify the impact of plant design variables on optimal control cost. This proposed approach has two key advantages. First, because the coupling term quantifies the gradient of the control optimization objective with respect to plant design variables, the approach ensures combined plant/control optimality. Second, because the coupling term equals the integral of optimal control co-states multiplied by static gradient terms that can be computed a priori, the proposed approach is computationally attractive.

The literature and motivation for this research is presented first. Then, the general equations concerning the design and control optimization problems are introduced. The optimality conditions are derived and discussed with particular attention to the meaning and calculation of the coupling term. An example problem of integrated structure/control optimization of a beam under vibrations is proposed and solved by using two methods, one which uses the coupling measure and the other without using the coupling measure. The results of the combined plant and controller optimization problem obtained by the two methods are compared and the numerical relevance of the coupling measure is discussed.

5.1 Literature and Motivation

This chapter presents a novel approach for optimizing the design (i.e., plant) and control of a dynamic system simultaneously. The approach rigorously guarantees combined optimality, and is also more computationally efficient than traditional simultaneous optimization. Solv-

ing the plant design and control optimization problems simultaneously or in a combined fashion 1) guarantees complete dynamic system optimality [63, 64, 65, 66] and 2) considers the dependence of the controller design problem on the plant design [63, 67, 68, 69, 70]. The computational cost of simultaneous plant/control optimization can be quite prohibitive [71, 72, 73]. Hence, there is need for an efficient yet rigorous computational plant/control optimization framework. In this paper, such a framework is developed. Its use is demonstrated by applying it to a problem of beam mass reduction (plant design optimization) and vibration attenuation (control optimization).

Solving the plant design and control optimization problems together guarantees complete dynamic system optimality [63, 108] and helps attain synergistic results which cannot be always achieved by solving them separately [64]. If the two optimization problems depend on each other, then we call the system "coupled". In coupled systems the differences in the system design and performance obtained from combined optimization vs. sequential optimization is more pronounced [108, 109]. It is also shown that in some cases the plant design and the control optimization problems may be conflicting [64]. This means that an optimal plant design may be expensive (or hard) to control. Complete dynamic system optimality is also essential to ensure a fair comparison of the performance of two or more systems [110]. Finally, an understanding of the dependence of the controller design problem on the plant design can help decide the need for a combined approach vs. a sequential approach [111]. It is with the above considerations in mind that Soong and Cimellaro emphasize integrated control/structural systems as an important research topic in their article on future directions of research on structural control [65].

Several solution strategies have been outlined for effectively solving combined design and control optimization problems [108, 112]. These strategies can be broadly divided into Simultaneous and Nested strategies. In the simultaneous strategies the two optimization problems are considered together hence guaranteeing system level optimality by intrinsically considering the dependence between the two optimization problems . The main challenge in implementing the simultaneous solution strategy is reconciling the dynamic nature of the control optimization problem with static nature of the design optimization problem [66, 113]. This challenge is resolved by parameterizing the controller (or obtaining surrogate models based on optimal control solutions) and considering these parametrized variables along with the design variables in a single optimization [29, 66, 113]. Thus simultaneous strategies are computationally attractive [66, 108] but lose some optimality due to the paramterization of some dynamic characteristics. Nested optimization strategies consider the two optimization problems separately in an iterative fashion incorporating the result of design optimization problem on the control optimization problem and vice versa in the next iteration [112, 114].

Nested solution strategies have been used due to the freedom it provides with regard to choosing the structure of the controller [112], but this generally adds to the computational cost in comparison with simultaneous methods described above.

Concurrently sensitivities, jacobians, or gradients that capture the dependence of the optimal controller on the plant design have been used in solution strategies to further support and strengthen these methods [63, 70]. These measures have the following attractions - 1) They give a perspective on the coupling between the plant design and optimal control problems to choose the starting design for the problem, 2) can be used to tune optimization parameters such as weighting of the design and control optimization objectives and 3) to choose an appropriate optimization algorithm that can be executed effectively [63, 70]. Peters *et al.* discuss the definitions and applicability of different measures of coupling in [70]. The two coupling measures discussed in [70] are bi-directional coupling and unidirectional coupling. Bi-directional coupling considers the dependence of the design problem and the control problem on each other [115], whereas unidirectional coupling only considers the dependence of the optimal control problem on plant design [76].This is a reasonable assumption for system optimization problems that can be partitioned such that the coupling is unilateral. We use the unidirectional coupling term derived in [76] in setting up our computationally efficient combined optimization framework.

Computational costs related to combined optimization methods are generally higher than those for sequential optimization methods. This is due to the need for a higher number of optimal control evaluations and larger design space for the combined optimization. The cost of computing sensitivities or Jacobians capturing the impact of plant design on control performance can also be a computational challenge as mentioned in [71, 73]. In [72], authors use evolutionary algorithms for simultaneous plant design-controller optimization of a two link planar manipulator and explain that gradient based (local) optimization techniques cannot be used for this complex non-linear optimization problem. Systems exhibiting non-smooth behavior need to be solved using algorithms that find the global optimal [71, 73]. These global optimization methods such as evolutionary algorithms are computationally intensive mainly due to an increased number of function evaluations. Due to these reasons, the computational cost of combined plant and control optimization can be quite prohibitive.

In summary, combined optimization methods can yield systems that achieve synergistic plants and controllers, and satisfy combined plant/control optimality but computational costs might not favor the use of such methods. Motivated by this problem, we use a previously derived coupling term [76] in the following ways. First, because this coupling term quantifies the sensitivity of the optimal control objective with respect to plant design variables, it can be used as a Jacobian within the plant design problem in a way that guarantees combined

optimality. Second, because the coupling term is given by the integral of optimal control co-states multiplied by a static gradient function that can be computed a priori, such use of the coupling term as a sensitivity function for plant optimization is computationally attractive. Specifically, these insights provide a framework that makes it possible to optimize a system's plant for ease of control, thereby guaranteeing combined plant/control optimality within a tractable computational setting. The unique contribution of this chapter to the literature is the development of this framework, and its demonstration within the context of an optimal beam design and vibration attenuation problem. Preliminary work and results regarding the development of this framework is presented in [74].

5.2 Problem Definition

There are two optimization problems to be solved: a plant design optimization problem and a controller optimization problem. First, we define the plant and controller optimization problems separately. Then, the combined plant and controller optimization problem is defined. The plant design optimization problem is typically expressed as a static optimization problem as in Eq. 5.1.

$$\min_{x_p} F_p \text{ subject to } \quad h_p(x_p) = 0 \text{ and } g_p(x_p) \leq 0 \tag{5.1}$$

The goal of the plant optimization problem is to minimize a plant objective (F_p) by varying a design vector (x_p) subject to equality and inequality constraints h_p and g_p respectively. The control optimization problem is commonly formulated as a dynamic optimization problem given in Eq. 5.2

$$\begin{aligned} &\min_{z(t),u(t),T} \left(\Phi(z(T),T) + \int_0^T (L(z(t),u(t),t)dt \right) \text{ subject to} \\ &\dot{z} = f(z(t),u(t),t), \eta(u(t),t) \leq 0, \Psi(z(T),T) = 0, z(t_0) = z_0 \end{aligned} \tag{5.2}$$

This formulation of the continuous-time optimal control problem neglects disturbances and sensor noise and assumes all states to be measured directly for simplicity. Extensions of the above formulation to combined plant/observer/controller optimization problems are presented in [76]. In Eq. 5.2, the objective is to minimize a weighted sum of a final state objective function (Φ) and the time integral of a functional (L). This weighted sum reflects two common goals in controller design, namely, minimal steady state error and acceptable transient behavior. Optimization variables include the control input trajectory, $u(t)$, the state

trajectory, $z(t)$, and the terminal time, T. Optimization constraints are the plant's open-loop state equations (f), limitations on control actuation (η), possible constraints on the final state or final time (Ψ), and initial conditions (z_0).

The two problems presented above are combined by a linear weighting of their objectives. The constraints and optimization variables of the combined problem are the union of the constraints and optimization variables of the two problems respectively. In [61], several multi-objective optimization weighting methods are described. From these, we adopt linear weighting for simplicity. This paper accounts for the influence of plant design on controller objective and constraints, but neglects the influence of controller design on plant constraints for simplicity. This is accounted for in Eq. 5.3 by the presence of the design vector (x_p) in the system dynamics and control actuation constraints. While this formulation limits the generality of our analysis somewhat, we are still able to address a large number of practical combined plant and controller optimization problems where controller design does not affect the set of feasible plants. Based on these assumptions, the following combined plant and controller optimization problem is considered:

$$\begin{aligned} \min_{x_p,z,u,T} & \left\{ w_p F_p + w_c \left(\Phi(z(T),T) + \int_0^T (L(z(t),u(t),t)dt \right) \right\} \\ \text{subject to } & h_p(x_p) = 0, g_p(x_p) \leq 0, \dot{z} = f(z(t),u(t),t,x_p), \\ & \eta(u(t),t,x_p) \leq 0, \Psi(z(T),T) = 0, z(t_0) = z_0 \end{aligned} \tag{5.3}$$

5.3 Optimality Conditions

Suppose that the objective function and constraints in Eq. 5.3 are all continuous and differentiable with respect to the combined optimization variables $(x_p, z(t), u(t), T)$. First order necessary combined optimality conditions, or "system" optimality conditions are derived in [76] using calculus of variations for the problem in Eq. 5.3. We also present a derivation of the optimality conditions in Appendix C. The resulting optimality conditions are as follows

$$\begin{aligned} & h_p(x_p^*) = 0, g_p(x_p^*) \leq 0, \dot{z}^* = f(z^*(t),u^*(t),t,x_p^*), \\ & \eta(u^*(t),t,x_p^*) \leq 0, \Psi(z^*(T^*),T^*) = 0, z^*(t_0) = z_0 \end{aligned} \tag{5.4}$$

$$\begin{aligned}\alpha^* \neq 0, \beta^* \geq 0, \beta^{*T} g_p(x_p^*) = 0, \lambda^*(t) \neq 0 \\ \mu^*(t) \geq 0, \mu^*(t)\eta(u^*(t), t, x_p^*) = 0, \nu^* = 0\end{aligned} \tag{5.5}$$

$$\left[\frac{dF_p}{dx_p} + \frac{dh_p^T}{dx_p}\alpha + \frac{dg_p^T}{dx_p}\beta + \frac{w_c}{w_p}\int_0^T \left(\frac{\partial f^T}{\partial x_p}\lambda + \frac{\partial \eta^T}{\partial x_p}\mu\right) dt\right]^* = 0 \tag{5.6}$$

$$H = L + f^T\lambda, \left[\frac{\partial H}{\partial z} + \dot{\lambda}\right]^* = 0, \left[\frac{\partial H}{\partial u} + \frac{\partial \eta^T}{\partial u}\mu\right]^* = 0 \tag{5.7}$$

$$\left[\frac{\partial \Phi}{\partial z} + \frac{\partial \Psi}{\partial z}\nu - \lambda\right]_{t=T}^* = 0 \tag{5.8}$$

We name these conditions the *Leitmann conditions* in acknowledgement of the fact that an early version of these conditions appears in the pioneering text on the calculus of variations by George Leitmann. In these conditions, the * superscript denotes optimality. Equations 5.4 represent constraint satisfaction at the optimum, which is an obvious necessity for the desired optimum. Equations 5.5 are transversality conditions associated with penalizing constraint violations. Equations (5.6-5.8) are the stationarity conditions that the objective and the constraints have to satisfy at the optimum. The left hand sides of Eqs. 5.6-5.8 are the variations of the augmented combined design and control objective with respect to the optimization variables $(x_p, z(t), u(t), T)$, where the augmented objective considers the constraints through Lagrange multipliers $(\alpha, \beta, \lambda(t), \mu(t), \nu)$. Equations (5.7) represent a general control optimization problem, which is solved with the final condition given by Eq. 5.8.

In [76], it is observed that Eq. (5.6) is very similar to the KKT stationarity conditions. This is because Eq. (5.6) represents the variation of the augmented Lagrangian with respect to the design vector (x_p). The difference between KKT conditions and Eq. (5.6) is the last term in the equation. This term is a result of the dependence of the controller optimization problem on the design vector (x_p). Hence this term is denoted by Fathy in [76] and [63] as the coupling term (Γ):

$$\Gamma = \frac{w_c}{w_p}\int_0^T \left(\frac{\partial f^T}{\partial x_p}\lambda^* + \frac{\partial \eta^T}{\partial x_p}\mu^*\right) dt \tag{5.9}$$

It should be observed that the control objective is dependent on the design vector (x_p)

through the constraints (f) and (η). Hence it is suggested in [76] that the coupling term can also be mathematically represented as Eq. (5.10) below. We prove this equality of the coupling term defined by Eqs. 5.9,5.10 in Appendix D.

$$\begin{aligned} \Gamma &= \frac{w_c}{w_p}\frac{dF_c^*}{dx_p}, \text{ where} \\ F_c^* &= \Phi(z^*(T),T) + \int_0^T (L(z^*(t),u^*(t),t)dt \end{aligned} \tag{5.10}$$

It should be noted in Eq. 5.10 that the coupling term is related to the gradient of the *optimal* control objective (F_c^*) and not F_c. In the results section we will show that the two expressions for the coupling term, given by Eq. 5.9 and Eq. 5.10 are also numerically equal. Thus the coupling term quantifies the coupling between the plant and controller optimization problems by considering the influence of plant design on the optimal attainable control objective.

5.4 Optimization Framework

Figure 5.1 is a flowchart explaining how Eqs. 5.4-5.9 are used in a combined system optimization framework. Numerically, to obtain the combined optimal solution, Eqs. 5.7,5.8 are solved to obtain an optimal controller for a given design, and then the resulting co-state trajectories are substituted in Eq. 5.6 to obtain the gradient of the combined objective, which is then used to obtain the next design based on the optimization algorithm being used. The above method is repeated for the next design till the gradient given by the LHS of Eq. 5.6 is close enough to zero, or the change in design variables is within an allowed tolerance. This is very similar to previous nested optimization algorithms employed in [108, 111]. The difference between our nested optimization and the previous formulations is that in the design chosen for the next iteration, in [111], authors consider the sensitivity of the closed loop eigenvalues to the structural design, and in [108], authors do not use any sensitivity information while our proposed framework considers the sensitivity of the optimal attainable control objective to the design. This sensitivity is encapsulated in the above formulation through the coupling term, Eqs. 5.9,5.10.

Another difference compared to previously used computational methods is explained here. Previous nested or simultaneous combined design and control optimization approaches used the gradient calculated in Eq. 5.6 of the form $\left(\frac{dF_p}{dx_p} + \frac{dh_p^T}{dx_p}\alpha + \frac{dg_p^T}{dx_p}\beta + \frac{w_c}{w_p}\frac{dF_c^*}{dx_p}\right)$. In the

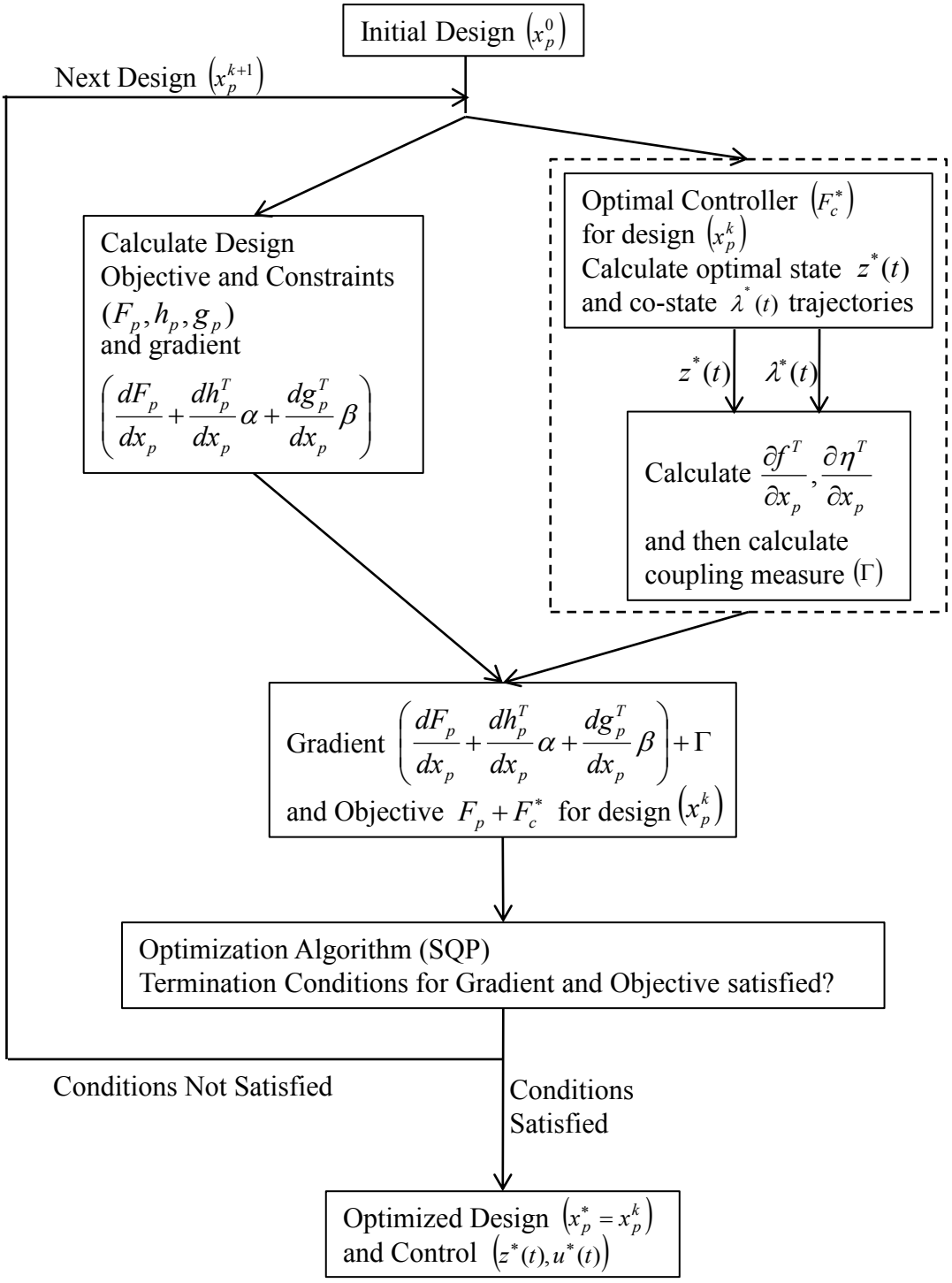

Figure 5.1 Optimization Framework Flowchart

calculation of this gradient, the calculation of $\frac{w_c}{w_p}\frac{dF_c^*}{dx_p}$ requires the solution of the optimal controller problem. It should be noted that to calculate $\frac{w_c}{w_p}\frac{dF_c^*}{dx_p}$ the number of times the optimal control problem has to be solved is dependent on the dimension of the design vector (x_p), i.e. the number of design variables. If n is the dimension of the design vector (x_p), the optimal control problem has to be solved *at least* $n+1$ times to obtain the derivative $\frac{w_c}{w_p}\frac{dF_c^*}{dx_p}$. This can be computationally very expensive depending on the time taken to solve the optimal control problem. In the optimality conditions given by Eq. 5.6, we use the coupling term defined in Eq. 5.9, which is equal to $\frac{w_c}{w_p}\frac{dF_c^*}{dx_p}$. In Eq. 5.9, the coupling term is calculated as an integral and needs the solution of the optimal control problem for only one design. In the results section, we show that this computational advantage of solving the optimal control problem only once instead of $n+1$ times does indeed translate to a reduced number of function calls required to obtain the gradient at each design. This results in a reduced number of total function calls in the combined optimization and reduced computational time.

5.5 Beam Design and Control Problem

The coupling between the plant and controller optimization problems is particularly manifest in vibration control applications as shown in [64, 65, 113]. In [64], Smith *et al.* show that an optimal combination of passive (design) and active (control) vibration attenuation obtained by combined design and control optimization performs better than the optimal combination of passive and active vibration attenuation obtained by a sequential design optimization and then control optimization. For this reason we choose the problem of structural design of a cantilever beam and its controller. The plant optimization problem aims to obtain a structure with the minimum total mass of the beam. The controller optimization problem is posed as an LQR problem. The beam is modeled as a finite collection of N nodes. The Euler-Bernoulli beam vibration equations are obtained for each node and they are represented in state space form. The states ($z(t)$) of the structure are the displacement and velocity of each node. The width of each node is a design variable, keeping the thickness (th) and length (dx) of all the nodes the same. Thus the design vector (x_p) is the vector of widths of each node ($\mathbf{w}$). The control input ($u(t)$) is a moment applied at the fixed end of the cantilever. The beam is viewed as a linkage which is desired to be rotated by a certain angle. Once this desired angular position is reached the beam has a certain velocity at this final position. The control problem is to bring the beam to rest given this initial angular velocity. Figure 5.2 shows the cantilever beam, the moment input applied to it at the fixed end, a diagram of a

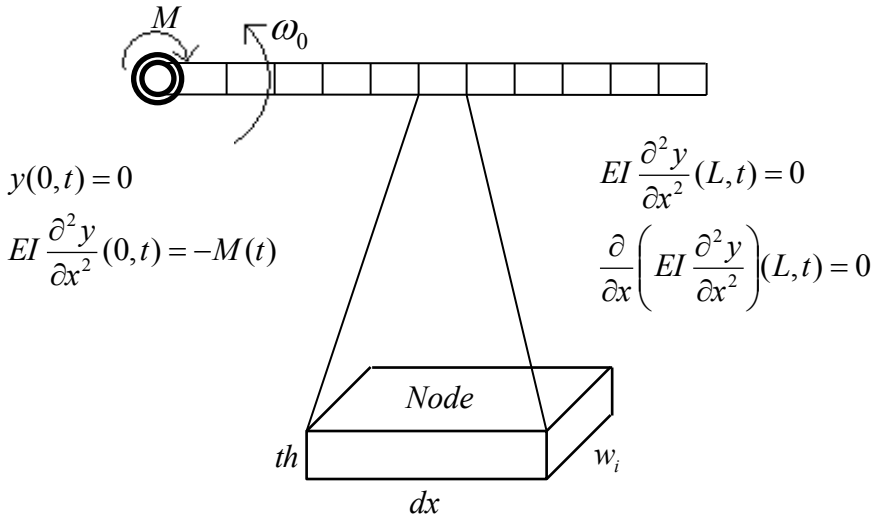

Figure 5.2 Diagram of the beam, an example node, the initial conditions and boundary conditions.

node and the boundary conditions used in this problem.

With these definitions of the variables we write the design optimization problem as:

$$\min_{\mathbf{w}} \sum_{i=1}^{N} m_i \text{ subject to } \mathbf{w_{min}} \leq \mathbf{w_i} \leq \mathbf{w_{max}} \quad \forall i \tag{5.11}$$

where $m_i = \rho(th)(dx)(w_i)$ is the mass of node i. $\mathbf{w_{min}}$ and $\mathbf{w_{max}}$ are the minimum and maximum allowable width respectively of a node. ρ is the density of the material. The control optimization problem for the beam is formulated as follows:

$$\begin{aligned} &\min_{(z(t),u(t))} \int_0^T \left(z^T Q z + u^T R u\right) dt \text{ subject to} \\ &\dot{z} = f(z,u) = \mathbf{A}z + \mathbf{B}u, z(0) = z_0 \end{aligned} \tag{5.12}$$

The initial conditions for this problem are z_0. The cantilever beam has an initial angular velocity as explained previously. This angular velocity is equivalent to each node having a linear velocity whose value depends on the distance of the node from the fixed point. The vector (z_0) assigns this initial linear velocity to each node. Using the above definitions of

the design and controller optimization problems, the combined optimization problem is:

$$\begin{aligned} &\min_{(x_p,z(t),u(t))} \left\{ \sum_{i=1}^{N} m_i + W_c \left(\int_0^T \left(z^T Q z + u^T R u \right) dt \right) \right\} \\ &\text{subject to } \mathbf{w_{min}} \leq \mathbf{w_i} \leq \mathbf{w_{max}} \ \forall i, \text{ and} \\ &\dot{z} = f(z,u,\mathbf{w}) = \mathbf{A}(\mathbf{w})z + \mathbf{B}(\mathbf{w})u, z(0) = z_0 \end{aligned} \tag{5.13}$$

For the problem in Eq. 5.13, the optimality conditions for the cantilever beam design and control problem can be obtained similar to those given in Eqs. 5.4-5.8. The terms in Eq. 5.9 for the coupling measure Γ are obtained using the following expressions Eq. 5.14, in which the matrix differentials are analytically derived

$$\frac{\partial f^T}{\partial x_p} = \left[\frac{\partial \mathbf{A}}{\partial \mathbf{w}} z(t) + \frac{\partial \mathbf{B}}{\partial \mathbf{w}} u(t) \right]^T, \frac{\partial \eta^T}{\partial x_p} = 0 \tag{5.14}$$

Equations 5.7,5.8 are the differential equations for the optimal state ($z^*(t)$) and optimal co-state ($\lambda^*(t)$) trajectories, depending on the values of the Q and R matrices. The differential equations are solved with the boundary condition $\lambda^*(T) = 0$. These calculations were performed in MATLAB using the *lqr* command. The solutions for the optimal state, co-state and control trajectories from *lqr* are substituted in the expressions calculated in Eq. 5.14, which are in turn used to calculate the coupling term (Γ). The combined gradient, which is the LHS in Eq. 5.6 is then calculated as it is easy to analytically obtain the derivative of the plant objective and plant constraints with respect to the design vector (x_p) in this problem.

5.6 Results and Discussion

5.6.1 Equality of Coupling Term and Control Gradient

The coupling terms given by Eqs. 5.9,5.10 are shown to be equal in Appendix D. Before performing combined design and control optimization we numerically verify this equality of the coupling term and the gradient of the optimal attainable control. Figure 5.3 shows a plot of the coupling terms calculated by Eq. 5.9 and by Eq. 5.10 and it is observed that the coupling term is indeed numerically equal to the gradient of the optimal attainable control as a function of the design variables (which are the widths of the nodes). The maximum difference between the two calculations of the coupling term is less than 1.2%. These differences occur due to the numerical procedures used to calculate the coupling term and

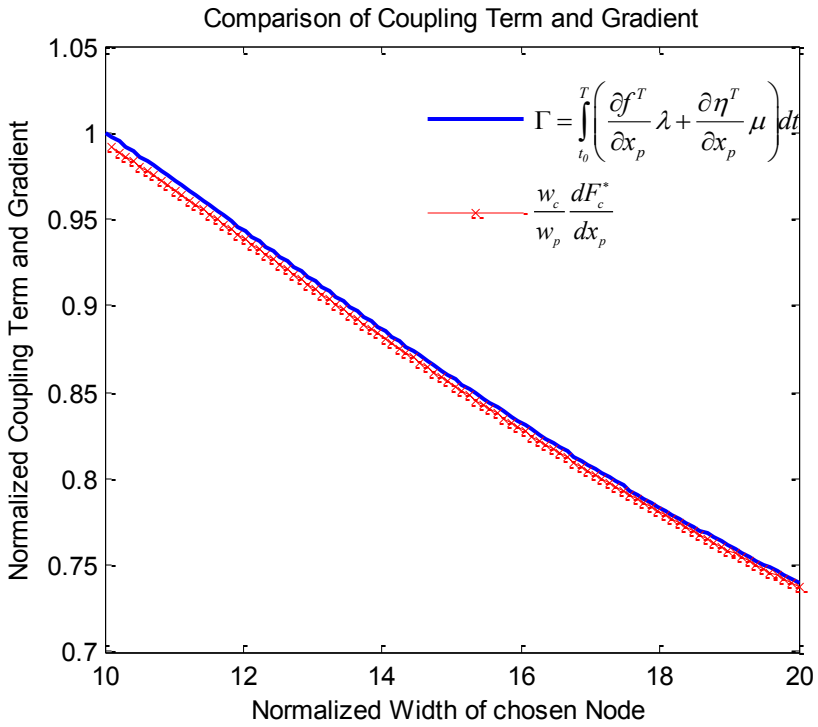

Figure 5.3 Coupling Term as calculated by Eq. 5.9 and Eq. 5.10

the gradient. The coupling term is calculated by substituting the values of the terms in Eq. 5.14, the terms themselves being analytically derived. On the other hand, the gradient is calculated using a fixed-step backward Euler finite difference scheme. The two expressions (from Eq. 5.9 and Eq. 5.10) are thus considered equal and the coupling term will be used to provide gradient information in the optimization framework as explained in section 5.4.

The combined design and control optimization problem in Eq. 5.13 is solved using *fmincon* in MATLAB for two cases. In the first case, the coupling term is not calculated, and hence the optimization algorithm numerically calculates gradient from the expression $\left(\frac{dF_p}{dx_p} + \frac{dh_p^T}{dx_p} \alpha + \frac{dg_p^T}{dx_p} \beta + \frac{w_c}{w_p} \frac{dF_c^*}{dx_p} \right)$. This is accomplished by evaluating the objective and constraints at different designs close to the design where the gradient is required and applying the Euler forward difference scheme. In the second case, the gradient is calculated as mentioned in the previous section using the coupling term Γ (from Eq. 5.9, and then supplied to the optimization routine as shown in the optimization framework (Figure 5.1). Since we use a gradient-based optimization algorithm in this study, the choice of the initial design influences the number of function evaluations required to reach the optimum. In both the cases of our problem, the initial designs are chosen to be the same. The initial design is

chosen to be the design which results in the lowest beam mass (or the optimal plant design because minimizing mass is the objective of plant design). The two cases were solved for different numbers of nodes representing the beam, which correspond to different numbers of design variables. The number of nodes or design variables chosen and the number of function calls required to obtain an optimal solution in all the cases is shown in Table 5.1.

5.6.2 Computational Efficiency Improvement

Table 5.1 Number of Function Evaluations in the Optimization

Number of Nodes (N)	with gradient information	without gradient information
5	19	60
7	19	72
10	21	132
12	23	169
15	25	210

From Table 5.1 we notice that when the gradient information is provided by calculating the coupling term the number of function calls required to obtain an optimal solution is less than in the cases where the gradient is calculated by a finite difference scheme. This is due to the extra function evaluations needed by the finite difference scheme to calculate the gradient compared to the cases when the gradient is supplied by calculating the coupling term. We observe in Table 5.1 that the difference in the number of function calls increases as the number of nodes increase. The number of nodes (N) is equal to the dimension of the design vector, which is the vector of the widths of each node. The difference in the number of function evaluations is smaller when the dimensions of the design vector are lower because of 1) The number of function evaluations required to obtain the gradient at the beginning of each iteration is lower, 2) The number of function calls needed to obtain the step size at each iteration does not depend on the dimension of the design vector as it is a scalar problem, thus masking the smaller gain in reduced number of function calls for lower dimensions. Figure 5.4 shows how the optimization improves the normalized objective function with the number of function calls for the case $N = 7$ nodes. It can be seen that the objective is minimized to the same value with less than a third of the function calls when the coupling term is used to provide gradient information in the optimization.

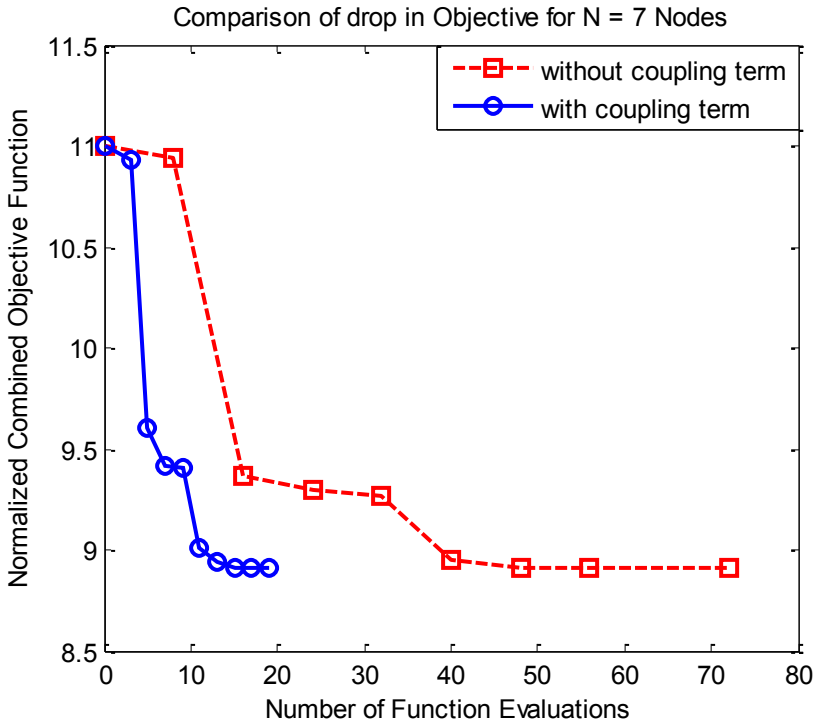

Figure 5.4 Comparison of Drop in Objective with Function Calls

5.6.3 Combined Optimal Solutions

To analyze the results of the combined design and control optimization we look at solution for the case when $N = 10$ nodes were used to model the beam. This means that the optimization has 10 design variables which are the widths of each of the nodes. Figure 5.5 shows the optimal configuration of the beam obtained by combined design and control optimization. We observe that the width of the beam is not uniform meaning the optimal value of the design variables which represent the width of the beam are unequal. These results are similar to the uneven optimal beam width and uneven optimal plate thickness results obtained by Pil *et al.* in [71] and by Zhu *et al.* in [112] respectively. This uneven lumping of mass along the length of the beam represents a compromise between the passive and active vibration control policies. Figure 5.6 shows the width of the beam for the case of a sequential optimization solution.

In the sequential optimization the plant design optimization problem is solved to obtain the plant with the lowest design objective and then the control optimization problem minimizes the LQR objective for this optimal plant design. Since the plant design objective is to reduce the total mass of the structure, if we were to solve the design optimization

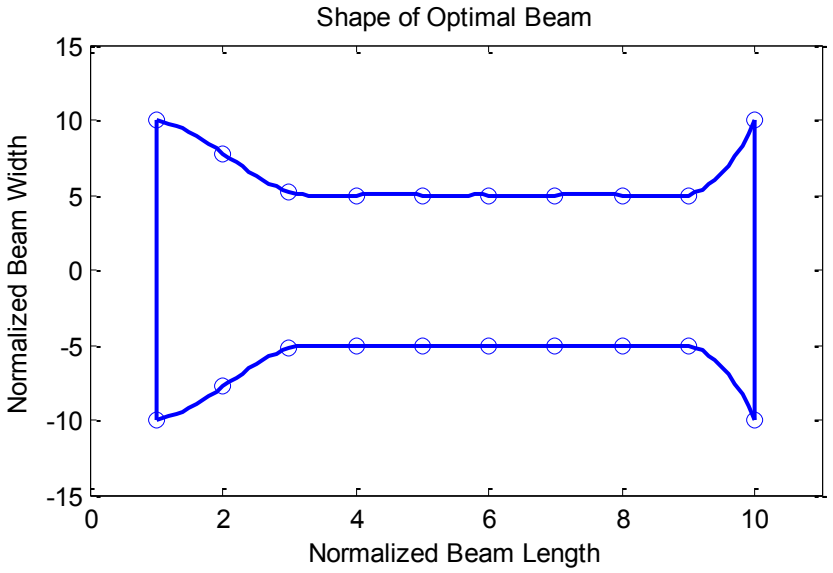

Figure 5.5 Optimal Beam: Width Variation with Beam Length

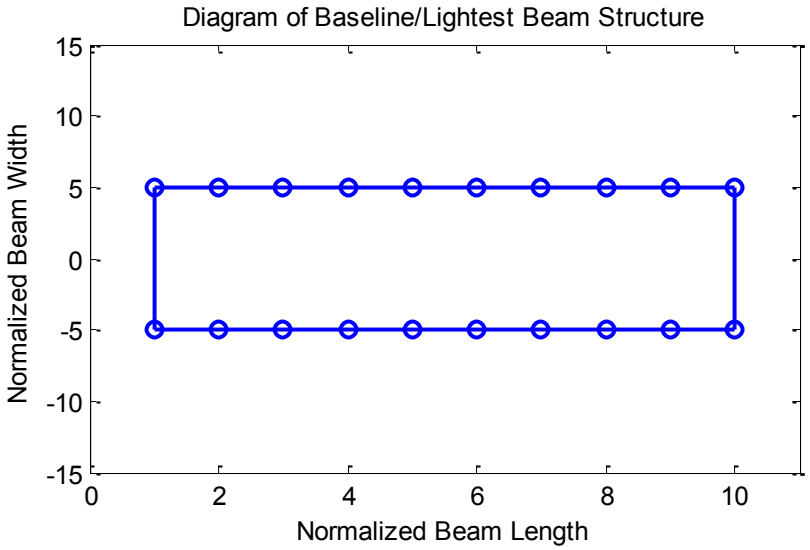

Figure 5.6 Lightest Beam: Width Variation with Beam Length

problem separately, then the solution is trivial. The solution would be to have the minimum possible width in all the nodes ($w_i = \mathbf{w_{min}}$). In our case the value of $\mathbf{w_{min}}$ is 10 units and $\mathbf{w_{max}}$ is 20 units. So the solution of the design problem would mean that the beam has a uniform width of 10 units as shown in Figure 5.6. From Fig. 5.5, we observe that this is not the case at the combined design and control optimum, where the optimal beam width is a maximum of 20 units and a minimum of 10 units. An improvement in the combined

objective function for the combined optimization case over the sequential optimization case is observed. The normalized combined design and control objective given by Eq. 5.13 for the sequential optimization case is 11 and that for the combined optimization case is 9.96 indicating a 9.45% improvement. The differences in the plant designs shown in Figs. 5.5 and 5.6 and the resulting improvement in the objective function shows the need for and the impact of combined design and control optimization.

The need for combined design and control optimization can also be inferred by the value of the coupling term at the sequentially optimal plant design. If the norm of the coupling term evaluated at the sequentially optimal plant design is non-zero, then the controller design problem is dependent on the plant design variables at the sequential design optimum. For example, in this problem where $||\Gamma||_2 = 0.144$ (this is the value of the L_2-norm of the coupling term which is normalized with respect to the value of the objective function at the optimal plant design solution). Thus the coupling term which measures the dependence of the controller design problem on the plant design variables or gives an ease of control measure that can be used to judge the need for a combined design and control optimization framework. Theoretically, if the coupling term has all its components as zero at the sequential design optimum solution, or equivalently has the smallest possible value for the norm, i.e $||\Gamma||_2 = 0$, then the design and control optimization problems are decoupled and can be sequentially solved to satisfy system level optimality. Numerically, we might see that the value of the components of the coupling term might be small (close to zero), but its closeness to zero must be judged depending on the problem and the accuracies desired in the problem. Fathy discusses other cases of decoupling in [63] but the above discussion shows that we can use the coupling measure Γ to judge the need for solving the combined design and control optimization problem vs. sequentially solving the two problems.

5.7 Summary

We introduced a notion of coupling between the plant design and controller optimization problems by considering the dependence of the control optimization problem on the design variables. A computationally efficient framework for combined design and control optimization using this coupling term was proposed and demonstrated. Using this framework we performed combined optimization of beam mass reduction and vibration attenuation. These results were compared to the results of the sequential optimization strategy to show the need for a combined optimization framework and the corresponding improvement in the objective while reducing the computational time.

We showed, both analytically (in Appendix D) and numerically (in Fig. 5.3) that the coupling term derived in [76] represents the gradient of the optimal attainable control. The coupling term was then used to obtain the gradient information for the optimization problem and in the process offered the following advantages: 1) The coupling term captured the dependence of the controller performance on the design variables providing a simple way to introduce the dependence of the controller on the design variables during the design optimization iterations, 2) The calculation of the coupling term eliminates the need to calculate the gradient of the optimal control objective as the two are numerically equal, thus resulting in a reduced number of function calls and hence reduced computational time. The results for the optimization showed a significant reduction in the number of function calls. This improvement in the reduction of the number of function calls increases with the increase in the number of design variables.

Checking the value of the coupling measure at different points in the design space we have demonstrated an understanding of the interdependence between the design and control problems. This was shown by the non-zero value of the coupling term at the optimal plant design. This understanding can be used to choose the initial design for the problem, to tune the optimization parameters such as weighting of the design and control optimization problems, and most importantly to decide on the need for sequential vs. combined design and control optimization approach.

It should be noted that in the above analysis we made sure that the necessary derivatives exist by ensuring the continuity and the differentiability of the system model. The equations shown above and the procedure for optimization are valid for non linear systems as well. Using an LQR controller we could easily solve Eq. 5.7 and Eq. 5.8, but for non linear systems the optimal control problem might have to be solved using other optimal control approaches (e.g., Dynamic Programming). These approaches are in general computationally expensive. Hence, our demonstration of using the coupling term to reduce the number of times the optimal control problem is solved is extremely useful. For the example optimization problem chosen in this paper, a gradient based optimization algorithm (SQP) was used. Thus the gradient could be directly used for optimization. Gradient information can also be useful for non-gradient based optimization methods such as Genetic Algorithms to improve their efficiency as demonstrated by Lee *et al.* in [73] . Since a combined design and control optimization framework has to solve the control optimization problem for every design iteration irrespective of the algorithm used, the gradient information can be obtained as the coupling term with little or no extra computation after the control optimization problem is solved for that iteration as demonstrated in this paper. Thus without incurring large computational costs one can obtain gradient information which can be used to improve the

efficiency of non-gradient based algorithms as well, emphasizing the reach and contribution of this work.

Chapter 6

Combined Design and Control Optimization of a PHEV

This chapter presents the application of the computationally efficient combined design and control optimization algorithm developed in chapter 5 for the optimal design and control of a PHEV powertrain. The major challenges resolved in this chapter are to calculate the coupling term considering the nonlinear dynamics and costs related to the PHEV powertrain. The calculation of the coupling term requires analyzing the dependence of the system dynamics and control constraints on the battery size and the calculation of the optimal co-states. We present the insights that the coupling term offers, and then use these observations to obtain the combined optimal battery size. Finally, The optimal battery size and its dependence on different assumptions are discussed.

The remainder of this chapter is structured as follows. First, we discuss the relevant literature and motivate the work in this chapter. Next, the design impacts of battery sizing are presented. Then the combined optimization problem for the PHEV powertrain is formulated. To solve this problem, the framework developed in the previous chapter is utilized. The calculation of the coupling term, which is an essential ingredient in this framework is elucidated as that an important contribution of this work. Finally, the results report the insights obtained from the calculation of the coupling term and the combined optimal battery sizes.

6.1 Literature and Motivation

This chapter presents the application of a combined design and control optimization method for PHEV component sizing and optimal supervisory control. Optimal battery size and the optimal supervisory control actions are the results obtained. Due to their ability to charge from the grid and store significant amounts of electrical energy in their batteries, PHEV battery sizing significantly affects their charging and on-road power management decisions

[2, 4, 5, 6]. At the same time, to obtain the optimal battery size it is necessary to understand how this battery would be used/controlled [116, 118]. For example, a 16kWh battery is capable of providing sufficient energy for two 20 mile trips in all-electric mode. This all-electric performance can also be achieved by a smaller battery with multiple charging events throughout the day. In addition to these considerations, batteries are expensive and their sizing is an important concern for consumer acceptance of PHEVs [25, 62]. Thus, to obtain a system level optimal design while considering optimal controller performance, we employ a combined optimization approach in this chapter.

Previous optimization research for hybrid powertrains has mostly addressed optimal control and optimal design separately. Optimal supervisory control of PHEVs relates to their optimal charging on the grid [9, 38, 39], or on-road power management [27, 36, 79]. Optimal design studies have investigated different PHEV configurations [117], battery sizing [6, 118], engine and motor sizing [5, 120, 118]. In [5, 6, 81], authors expose some dependencies between the design and control problems through battery sizing studies. In [6], authors show that smarter power management algorithms can reduce vehicle energy consumption and hence reduce battery energy capacity requirements. In [118], authors demonstrate that a battery size capable of 25-50 miles all-electric driving has a lower life-cycle emissions impact than a larger battery. A similar finding is also reported by Kelly *et al.* in [119]. Furthermore, the need for a combined battery sizing and control optimization approach is strongly suggested in [5, 6, 116, 118].

Several combined design and control optimization methods have been previously developed. Many of these methods are demonstrated with applications in structural design and vibration control [67, 68, 69, 70, 71, 72, 112]. There are basically two optimization approaches, which can be further classified. The first is a simultaneous approach where the controller is parameterized and optimized along with the design [66, 108, 113]. This parameterization results in a loss of optimality but renders the problem computationally attractive. The parameters describing the controller can be obtained in several ways, by defining rules [108, 113] or by optimizing the control at different designs and generating a surrogate design dependent control function [66]. The second combined optimization approach is called a nested approach where the plant design and control optimization problems are solved separately. In this approach the dependence between the two problems is assessed by iteratively solving for the design and the control [71, 72], or by calculating a sensitivity term that quantifies this dependence [70, 76]. The nested approach is computationally intensive due to the need for multiple control optimization evaluations at points in the design space [71, 72], but it is rigorous as there are no restricting assumptions on the controller structure.

Combined design and control optimization methods have been previously applied to

powertrain design and control in [45, 66, 77, 110, 118]. Most studies apply the simultaneous approach. In [29, 118], authors include threshold parameters that represent control rules along with the design variables in the optimization. In [66], authors obtain stochastic optimal power management solutions for a several fuel-cell hybrid designs. They develop a surrogate model representing the optimal controller as a function of the design and optimize the plant design. It should be noted that system level optimal designs are necessary for a fair comparison of different system's performances. Baumann *et al.* use a combined approach to compare the performance of Fuel Cell Battery, Fuel Cell Ultracapacitor, and Fuel Cell Battery Ultracapacitor powertrains. Finally, in [77], authors apply an iterative procedure where the design and control problems are solved alternatively. The results show improvement in the powertrain design even though this procedure is repeated only for two iterations. It is observed that a full-scale nested procedure, even though it guarantees combined optimality has not been applied to powertrain design. The main reasons being the computational complexity of the powertrain models and the time and memory requirements for a nested optimization approach.

Summarizing the above discussion on previous work to define the research challenges for this chapter: First, due to the significant dependence of the control actions on the battery size in a PHEV we need to adopt a combined design and control approach. Second, this optimization approach has to be computationally efficient. The need for computational efficiency arises from the complexity of both the optimization algorithm and the powertrain model itself. The PHEV powertrain model has been simplified in [121] (to a convex model) in order to apply tools from convex optimization which are computationally efficient. In this chapter we wish to focus on improving the optimization algorithm and demonstrate its application to the complex powertrain model.

Such an efficient algorithm was developed in [74, 63] and explained in detail in chapter 5. The associated framework and the computational benefits are demonstrated for a beam mass reduction and vibration attenuation problem. In this beam design problem, the system dynamics are linear with quadratic control costs. Though this algorithm is faster than previous combined optimization methods, it requires the calculation of co-states. These co-states are used to quantify the sensitivity of the optimal control problem to a given design. The unique contributions in this chapter of the dissertation are: 1) the calculation of the sensitivity of the optimal control problem to a given design for the complex PHEV powertrain model and 2) optimal battery designs obtained by incorporating this sensitivity of the optimal control to the battery size.

6.2 Models and Design Impacts

In this section we briefly mention the models that describe PHEV on-road operation and charging from the grid. The design impacts of battery sizing for a PHEV are discussed. These design impacts will be included in the optimization approach as explained in section 6.4.

6.2.1 Models

The models describing PHEV component operation and their interconnections are described as ODEs of the form.

$$\dot{z} = f(z,u) \tag{6.1}$$

These ODEs and the details of the maps describing component efficiencies are presented in section 2.2.2 of chapter 2. This model is discretized and implemented in the backward looking form (as presented in appendix A). The states of this system are $z = \{\omega_e, SOC\}$ and the inputs are $u = \{\dot{m}_f, \tau_g\}$. It should be noted that the efficiency maps are highly non-linear (Figs. 2.2, 2.3, 2.4, 2.5) and the dynamics of the engine speed state are discontinuous. This is because the engine speed has a zero state when the engine is off and an idle speed to maximum speed range when the engine is on. Since the engine dynamics are not affected by battery sizing, the discontinuity of the engine speed state does not pose any numerical problems.

The charging model describing PHEV activity on the grid has one state $z = \{SOC\}$ and one input $u = \{P_b\}$. The CO_2 emissions and cost per unit energy of the electric energy is directly proportional to the charging power input (P_b). A detailed description of the grid dispatch model used and the associated charging model is presented in section 3.2.2 of chapter 3.

6.2.2 Design Impacts of Battery Sizing

Since our design variable is the battery size, it is necessary to quantify the costs associated with the battery size. These impacts of battery sizing will be included in the optimization as explained in section 6.4 below.

Due to the rising popularity of Li-ion batteries for both vehicle and non-vehicle applications, there has been a considerable amount of research to make these batteries cheaper

and lighter. Several cost targets and estimates are presented in [122, 123, 124]. The cost estimates range from $200/kWh to $1000/kWh depending on the time scale and assumptions made. In addition, there are significant uncertainties related to gasoline prices as well as electricity prices in the future. Thus we do not consider any battery sizing studies for optimal cost, instead we evaluate optimal battery sizes for minimum life-cycle CO_2 emissions. However, the approach presented in section 6.4 can be applied to optimal cost studies in the future.

The CO_2 impacts associated with a certain battery's life are categorized into CO_2 from materials and manufacturing, use and recycling phases. Note that we are only concerned with CO_2 emissions and not other greenhouse gases. The use phase CO_2 emissions are evaluated using our optimal control algorithm as demonstrated in chapter 3. In [122, 123], authors talk about materials, manufacturing and recycling phase CO_2 emissions. The amount of CO_2 resulting from the manufacturing phase ranges from 90-120 kg/kWh, as reported in [122, 123] depending on the materials used and the manufacturing processes. Accounting for recycling of the battery materials can bring this CO_2 impact down to 75-90 kg/kWh [122]. In [45, 118, 125], authors use a value of 120 kg of CO_2/kWh for the impact of battery design. Another important consideration to assess the design impacts is the total miles or the number of days that this battery will be used for. We will look at two cases of a battery that will be used for 100000 and 200000 miles. The design impact is quantified by Eq. 6.2 below

$$\frac{dF_p}{dx_p} = 90 \text{ kg/kWh} \tag{6.2}$$

The constraints on the design stem from its need to satisfy on-road power demand and achieve a certain performance. In order to satisfy a variety of power demands associated with different driving behaviors, we simulate the powertrain model (section 2.2.2) for cycles in the naturalistic drive cycle database [89]. To satisfy these road power demands at zero grade and in all electric operation at an *SOC* of 0.4, we need a minimum battery size of 11.29 kWh. This battery size also satisfies the following performance requirements (discussed in [126]): 1) all electric 0-60 mph in 12 seconds or less and 2) 6.5 % grade at 55 mph for 1200 seconds. A maximum battery size of 17.29 kWh is subjectively chosen and can be changed if this constraint is active. The battery size is normalized by 13.29 kWh. Hence, the design variable value $x_p = 1$ is equivalent to a battery size of 13.29 kWh. The design constraints described above restrict the normalized battery size to $x_p \in [0.85, 1.35]$.

6.3 Optimization Problem

Our goal in this section is to describe the optimization problem and the procedure used to solve it. We make the assumption that the same driving pattern is repeated through the life of the battery. Hence we minimize the CO_2 impacts of PHEV operation (*i.e.* charging and driving) over a 24 hour period with 47.8 miles of driving and scale this impact to reflect 100000 or 200000 miles of driving. The total CO_2 impact is assessed by adding the PHEV design impacts (*i.e.* CO_2 associated with manufacturing a certain battery size).

6.3.1 Problem Formulation

The optimization problem is defined as follows

$$\min_{z(t),u(t),x_p} J = \left\{ CO_2(x_p) + \sum_{0}^{T_{EOL}} \left(\frac{CO_2}{gal} \dot{m}_f \Delta t_{dr} + \frac{CO_2}{kWh} P_b \Delta t_{ch} \right) \right\} \tag{6.3a}$$

$$\text{design constraints:} \quad x_p \in [0.85, 1.35] \text{ or } [11.29 \text{ kWh}, 17.29 \text{ kWh}] \tag{6.3b}$$

$$\text{control constraints:} \quad f_{\omega_e} : \dot{\omega}_e = f_{\omega_e}\left(\omega_e, \dot{m}_f, \tau_g\right) \tag{6.3c}$$

$$f_{SOC} : \dot{SOC} = f_{SOC}\left(SOC, \tau_g\right) \tag{6.3d}$$

$$\eta_1 : SOC_{min} \leq SOC \leq SOC_{max} \tag{6.3e}$$

$$\eta_2 : SOC(0) = SOC(24) = 0.7 \tag{6.3f}$$

$$\eta_3 : P_{c,max}(SOC) \leq P_b \leq P_{d,max}(SOC) \tag{6.3g}$$

$$\eta_4 : \omega_{e,min} \leq \omega_e \leq \omega_{e,max} \tag{6.3h}$$

$$\eta_5 : -\dot{\omega}_{e,min} \leq \dot{\omega}_e \leq \dot{\omega}_{e,max} \tag{6.3i}$$

$$\eta_6 : 0 \leq \dot{m}_f \leq m_f, \dot{m}ax(\omega_e) \tag{6.3j}$$

$$\eta_7 : 0 \leq \tau_e \leq \tau_{e,max}(\omega_e) \tag{6.3k}$$

$$\eta_8 : 0 \leq \tau_g \leq \tau_{g,max}(\omega_g) \tag{6.3l}$$

In the objective function there are three terms. The first term signifies the CO_2 impact of the battery design per day. This CO_2 impact is discussed in the previous section 6.2.2. The second and third terms of the objective are the CO_2 produced from gasoline usage and grid charging respectively. This is the CO_2 produced till the End Of Life (EOL) of the PHEV battery (till T_{EOL}). The design constraints are discussed in the previous section 6.2.2. The

control constraints are the system dynamics, and the constraints described in sections 2.2.3 and 3.2.2. It should be noted that other than the *SOC* dynamics (Eq. 6.3d) the only control constraints that are affected by battery sizing are the battery charge and discharge constraints given by Eq. 6.3g.

6.4 Optimization Algorithm

The optimization algorithm has been presented in section 5.4 of the previous chapter and this framework is shown in again in Fig. 6.1. This algorithm has two main features: 1) computational efficiency due to the use of the coupling term as explained in section 5.4 and 2) it guarantees combined optimality by considering the dependence between the optimal control and plant design problems through the coupling term. Appendix C derives the optimality conditions and Appendix D shows that the coupling term defined in Eq. 6.4 below is equal to the gradient of the optimal attainable control objective. Thus, the calculation of the coupling term is central to the evaluation of the combined optimal solution as highlighted by red box #1 in Fig. 6.1. Another important aspect of the optimization algorithm (as highlighted by the other red box #2 in Fig. 6.1 is the utilization of this coupling term to obtain the optimal solution. Next, we elaborate on these two essential steps in the algorithm.

6.4.1 Calculation of the Coupling Term

The coupling term is defined as follows (previously defined in Eq. 5.9):

$$\Gamma = \int_0^{T_{EOL}} \left(\frac{\partial f^T}{\partial x_p} \lambda^* + \frac{\partial \eta^T}{\partial x_p} \mu^* \right) dt \tag{6.4}$$

In Eq. 6.4, $\frac{\partial f^T}{\partial x_p}$ is the gradient or the sensitivity of the system dynamics with respect to the battery size (x_p). The gradient or the sensitivity of the control constraints (*i.e.* $\eta_1 - \eta_8$ in Eq. 6.3) to the battery size is given by $\frac{\partial \eta^T}{\partial x_p}$. It should be observed that the control objective (given in Eq. 6.5a below) is implicitly dependent on the design vector (x_p) through the constraints (f) and (η). In Eq. 6.4, * denotes the optimal control trajectories or solutions. The co-states associated with the system dynamics constraints are λ, and the co-states associated with the control constraints are μ. The optimal co-states reflect the price of the constraints (or their restrictiveness) as explained in [127, 128]. Thus the coupling term reflects some dependence of the optimal control solution on the design variable. In Appendix D, we prove that the coupling term is indeed equal to the gradient of the optimal attainable control

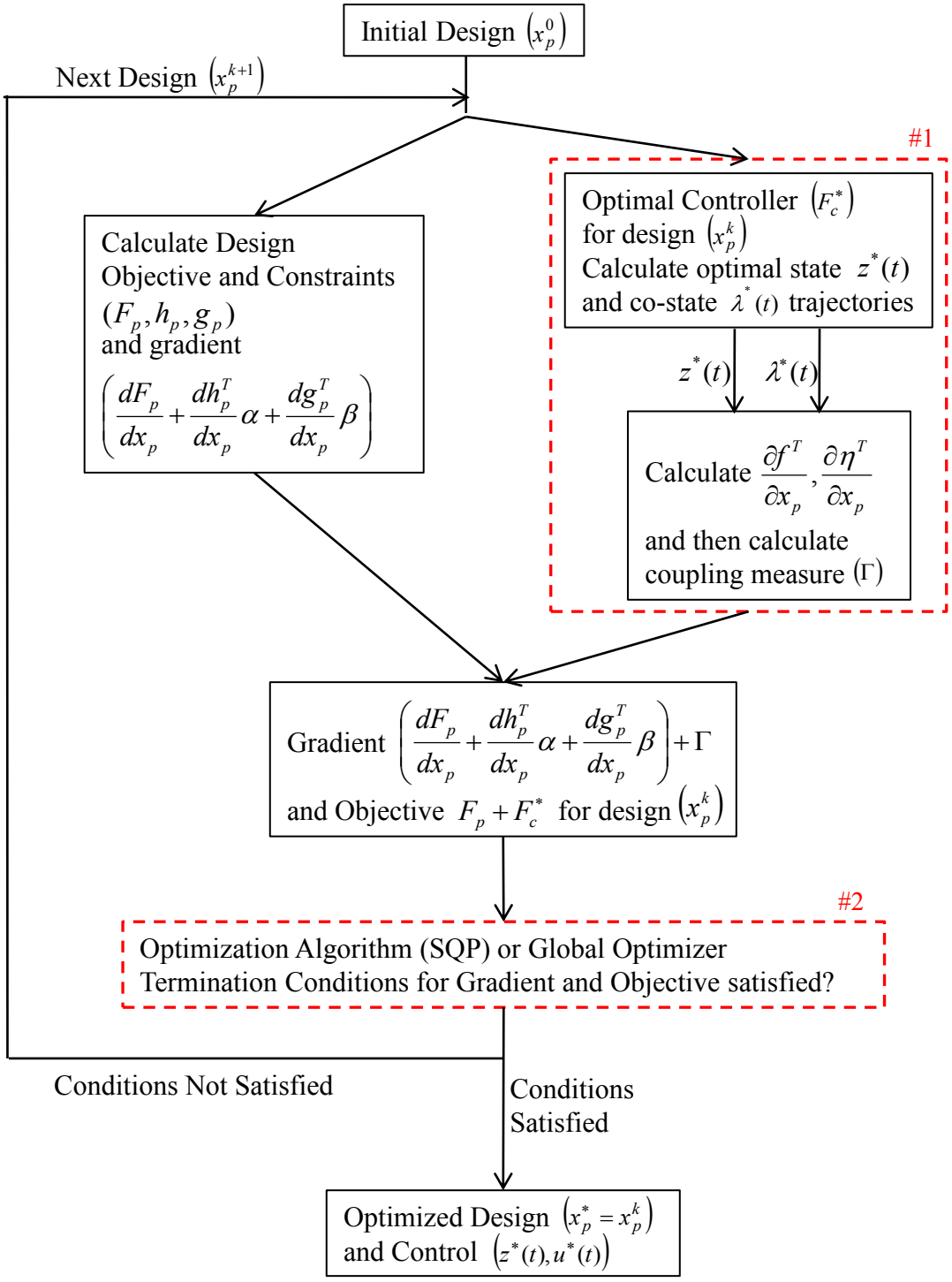

Figure 6.1 Optimization Framework Flowchart

objective (Eq. 6.5b). Note that this equality is true at the *optimal* control solution and not everywhere in the control space. Thus there is a need to solve the optimal control problem as defined by the objective in Eq. 6.5a below and the constraints in Eq. 6.3c - 6.3l above.

$$F_c^* = \sum_0^{T_{EOL}} \left(\frac{CO_2}{gal} \dot{m}_f{}^* \Delta t_{dr} + \frac{CO_2}{kWh} P_b{}^* \Delta t_{ch} \right) \tag{6.5a}$$

$$\Gamma = \frac{dF_c^*}{dx_p} \tag{6.5b}$$

In section 3.3 of chapter 3, we present an optimal control algorithm that obtains the optimal state and input trajectories for charging and power management of a PHEV, for given driving behavior and grid mix conditions. The resulting optimal trajectories are shown in section 3.4 of chapter 3. Thus, we have to obtain the co-states and the gradients for a given optimal control solution in order to calculate the coupling term.

Calculation of Gradients

The gradient associated with the dynamics $\frac{\partial f^T}{\partial x_p}$ is a two dimensional vector (in $\mathbb{R}^2$) with each entry representing the gradient of the dynamics of each of the states with respect to the battery size. The engine dynamics (Eq. 2.9 of chapter 2) are not dependent on the battery size. Thus we have

$$\frac{\partial f_{\omega_e}}{\partial x_p} = 0 \tag{6.6}$$

The *SOC* dynamics (Eq. 6.7 below) are dependent on the battery size through 1) the obvious dependence of battery energy capacity on the battery size (Eq. 6.8a), 2) dependence of the internal resistance on the battery size (Eq. 6.8b) and 3) the dependence of wheel power demands on the battery size through its mass (Eq. 6.8c). In Eqs. 6.7 and 6.8, x_p is the normalized battery size. The bar on the variables denotes the values of the variables at x_p = 1. In Eq. 6.8c, m_b and m_v are the mass of the battery and the vehicle respectively at the normalized battery size x_p = 1 (which is 13.29 kWh).

$$I_b = \frac{V_{oc} - \sqrt{V_{oc}^2 - 4R_i(x_p)P_b(x_p)}}{2R_i(x_p)} \tag{6.7a}$$

$$f_{SOC} : \frac{dSOC}{dt} = -\frac{I_b}{Q_{max}(x_p)} \tag{6.7b}$$

$$Q_{max}(x_p) = x_p \bar{Q}_{max} \tag{6.8a}$$

$$R_i(x_p) = \frac{\bar{R}_i}{x_p} \tag{6.8b}$$

$$\frac{\partial P_b}{\partial x_p} = \frac{\partial P_m}{\partial x_p} = \frac{m_b}{m_v}\bar{P}_m \tag{6.8c}$$

Differentiating the dynamics in Eq. 6.7 with respect to the normalized battery size and considering the dependencies above, we obtain,

$$\begin{aligned}\frac{\partial f_{SOC}}{\partial x_p} &= -\frac{\partial I}{\partial x_p}\frac{1}{\bar{Q}_{max}} + \frac{I}{Q_{max}^2}\frac{\partial Q_{max}}{\partial x_p} \\ &= -\frac{\partial I}{\partial x_p}\frac{1}{\bar{Q}_{max}} + \frac{I}{Q_{max}^2}\bar{Q}_{max} \end{aligned} \tag{6.9a}$$

$$\frac{\partial I}{\partial x_p} = \bar{v} - \frac{2x_p\bar{v}^2 - \frac{P_b}{\bar{R}_i} - \frac{\partial P_b}{\partial x_p}}{2\sqrt{x_p^2\bar{v}^2 - \frac{x_p P_b}{\bar{R}_i}}} \tag{6.9b}$$

$$\text{where} \quad \bar{v} = \frac{V_{oc}}{2\bar{R}_i} \text{ and } \frac{\partial P_b}{\partial x_p} = \frac{m_b}{m_v}\bar{P}_m$$

To obtain the gradient of the control constraints, we observe that the constraints on the engine and the generator variables are not dependent on the battery size. The *SOC* is a normalized variable that quantifies the amount of charge in a battery. It is a state variable which is not dependent on the battery size, even though its dynamics are dependent on the battery size. Thus the only constraint that is affected by the change in battery size is the battery discharge/charge power limit constraint (η_3 in Eq. 6.3). Thus, the following equations represent the gradient of the constraints

$$\frac{\partial \eta_i}{\partial x_p} = 0 \quad \text{for} \quad i = 1,2,\ldots,8 \quad \& \quad i \neq 3 \tag{6.10a}$$

$$\frac{\partial \eta_{3c}}{\partial x_p} = \bar{P}_{c,max}(SOC) - \frac{\partial P_b}{\partial x_p} \quad \text{and} \quad \frac{\partial \eta_{3d}}{\partial x_p} = \frac{\partial P_b}{\partial x_p} - \bar{P}_{d,max}(SOC) \tag{6.10b}$$

where $\frac{\partial P_b}{\partial x_p}$ is calculated as shown in Eq. 6.8c.

Calculation of Co-states

The co-state associated with the system dynamics is λ and the co-states associated with the control constraints are denoted μ. We observe that only the co-states associated with non-zero gradients of the dynamics and control constraints need to be calculated in order to obtain the coupling term. For example, since $\frac{\partial f_{\omega_e}}{\partial x_p} = 0 \implies \frac{\partial f_{\omega_e}}{\partial x_p}\lambda^*_{\omega_e} = 0$. Thus we need to calculate only three co-states: λ_{SOC}, μ_{3c}, μ_{3d} associated with the *SOC* dynamics and the charge and discharge constraints respectively. λ_{SOC} is calculated using Eq. 6.11, where V is the value function as used in a Dynamic Programming (DP) formulation. This equation is from the optimal control literature and is used to relate the Pontryagin Minimum Principle (PMP) approach to the DP approach. The mesh for the *SOC* state is uniform and is denoted as ΔSOC.

$$\begin{aligned}\lambda^*(t) &= \frac{\partial V^*}{\partial z^*} \\ &= \frac{V^*(SOC^*(t) + \Delta SOC) - V^*(SOC^*(t))}{\Delta SOC}\end{aligned} \tag{6.11a}$$

The co-states associated with the control constraints have the following analytical expression associated with them (Eq. 6.12). This expression is a result of the interpretation of the co-states (or Lagrange multipliers) as a shadow price of satisfying a certain constraint.

$$\mu_i^*(t) = \frac{\partial F_c^*}{\partial \eta_i(t)} \tag{6.12}$$

Since μ_{3c} and μ_{3d} are associated with an inequality constraint, they are equal to zero when the constraints are inactive. When the constraints are active, we simulate the optimal solution with a small modification of a constraint ($\partial \eta_i(t)$) at that time step to simulate the change in the optimal objective (∂F_c^*). The ratio of these changes is used in Eq. 6.12. In this manner all the necessary co-states required to calculate the coupling term are obtained. This is feasible because the charge/discharge constraints are active only during a few time steps (10 time steps at the most from a total of 4200 steps). The coupling term is thus calculated as

$$\Gamma = \sum_{k=0}^{T_{EOL}} \left(\frac{\partial f_{SOC}}{\partial x_p}\lambda^*(k) + \frac{\partial \eta_{3c}}{\partial x_p}\mu^*_{3c}(k) + \frac{\partial \eta_{3d}}{\partial x_p}\mu^*_{3d}(k) \right) \tag{6.13}$$

Utilizing the Coupling Term

Once the coupling term is obtained as demonstrated in the previous section, we can obtain the total gradient of the combined design and control problem which is defined in Eq. 6.14 below. To obtain the system level optimal solution we use this gradient.

$$\text{Total Gradient} = \left(\frac{dF_p}{dx_p} + \frac{dh_p^T}{dx_p}\alpha + \frac{dg_p^T}{dx_p}\beta + \Gamma \right) \tag{6.14}$$

This gradient can be used in many ways to either directly obtain the optimum or guide an optimization solver. The most obvious method is to use the gradient in a gradient-based solver to obtain the optimal design and control. This approach was used in chapter 5 to obtain the combined optimal beam design. The gradient was calculated and used with *fmincon* in MATLAB. The resulting solution was a system level optimal solution (Fig. 5.5) and this solution was obtained through fewer iterations (Fig. 5.4) than previous methods. The reduced computational effort was due to the ease of calculating the coupling term which represented the gradient of the control objective with respect to the design. To optimize the PHEV powertrain, we do not use this approach as gradient based methods do not guarantee system level optimality. Furthermore, we have only one design variable (the battery size x_p), so we explore simpler methods.

Another method of using the gradient is to guide non-gradient based optimization methods such as Genetic Algorithms (GA) and Simulated Annealing (SA) as demonstrated in [73]. The gradient can also be used in a hybrid optimization algorithm as demonstrated in [129].

Since we have only one design variable, we will calculate the optimal control solution for a range of designs in the design space and try to obtain the designs which have a zeros total gradient. Equivalently, we will calculate the coupling term by optimizing the control for a range of designs and verify where the condition in Eq. 6.15 is satisfied.

$$\Gamma = -\left(\frac{dF_p}{dx_p} + \frac{dh_p^T}{dx_p}\alpha + \frac{dg_p^T}{dx_p}\beta \right) \tag{6.15}$$

6.5 Optimization Conditions

The objective in our optimization problem is to minimize total CO_2 emissions produced during the battery design process and during its use in a PHEV. We assume a driving behavior with two identical 23.9 mile trips (Fig. 6.2), one at 8 AM and the other at 5 PM, everyday

through the EOL of the battery. We wish to demonstrate our method under these driving assumptions, but the method can be utilized for any number and nature of the trips.

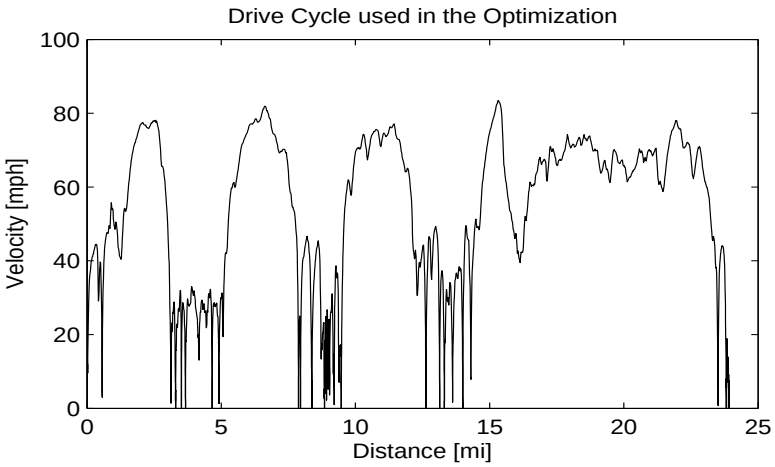

Figure 6.2 Drive Cycle Velocity graphed as a Function of Distance.

We consider grid mix conditions from a day in the NYISO region. These conditions result in the CO_2 emissions rate as shown in the first sub-plot of Fig. 6.3. These conditions are chosen for the following two reasons. First, the CO_2 rate in NYISO region is in the range 300-500 g/kWh compared to a 550-800 g/kWh range in Michigan (Fig. 3.1) and 650-800 g/kWh range from gasoline consumption. This is mainly due to the large fraction of hydro, nuclear and natural gas power plants in the NYISO region. The CO_2 production from gasoline during driving ranges from 650-800 g/kWh depending on the engine type and driving conditions. Thus the optimal solution in the case of NYISO grid conditions in order to minimize CO_2 emissions is to charge as much as possible and use as much electricity for propulsion. Second, the high CO_2 rate during the initial part of the day implies that it is not optimal to charge at those times during the day. These preliminary insights make it easier to analyze and understand the optimal solution as demonstrated in the results section. Again, our optimization method is applicable to any chosen grid mix conditions. To demonstrate this we also obtain a set of optimal results for grid conditions that we have used in chapters 3 and 4 to reflect the CO_2 emissions from the Michigan grid (Fig. 6.4).

The end of life of a PHEV battery is the time when the battery capacity drops down to 80% depth of discharge as compared to a new battery [130, 131]. Studies have shown that depending on the Lithium chemistry used, this could mean anywhere between 3000-5000 discharge cycles [130, 131]. Furthermore, depending on the supervisory control strategy, the utility factor of the battery, defined as the ratio of battery usage to engine fuel usage, will vary. It is expected that the battery life has to be at least 100000 miles in order for consumer

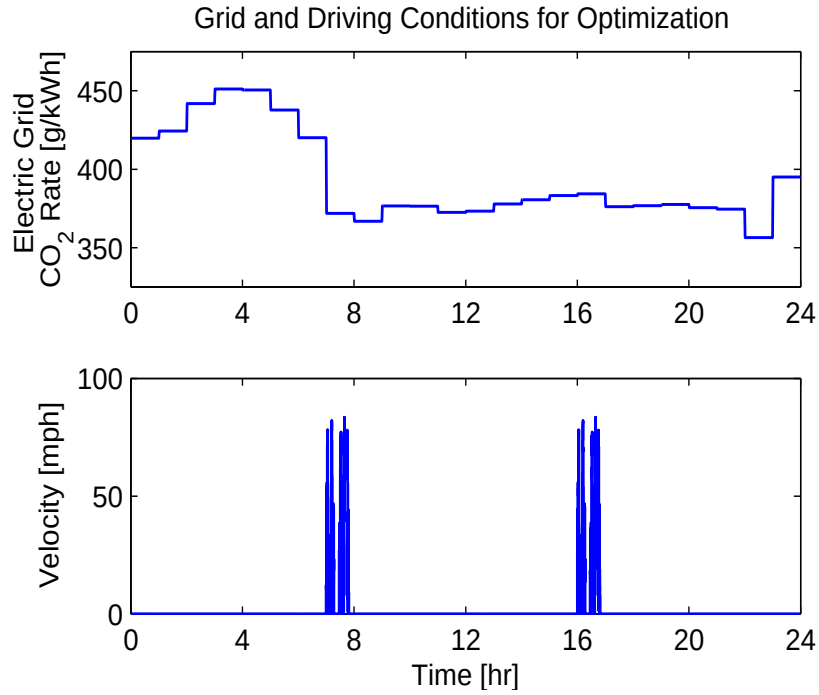

Figure 6.3 24 hour plot of Grid CO_2 Rate and Driving Trips used in the Optimization. (The 24 hour period begins at 1AM, hence 8AM is the 7th hour in the graph above)

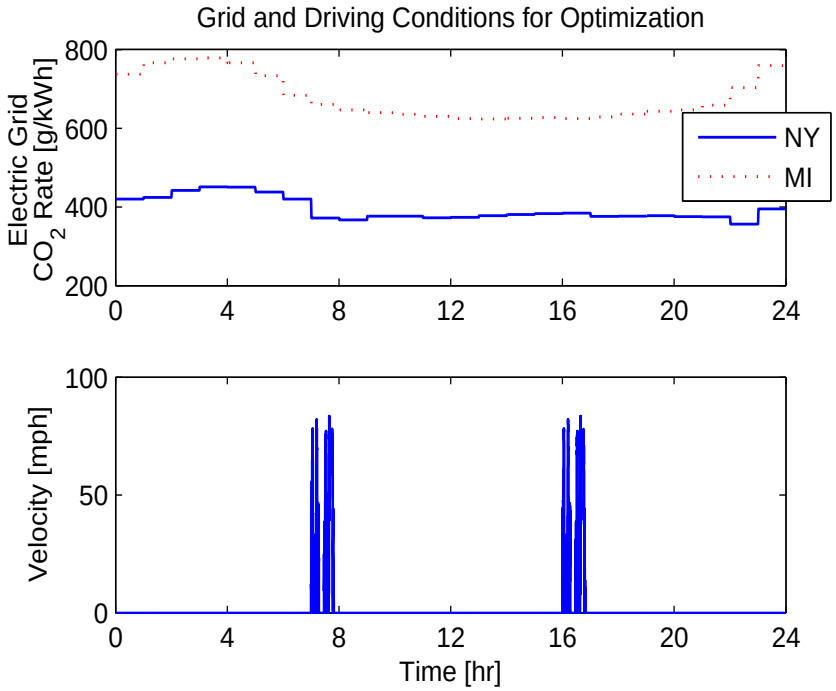

Figure 6.4 24 hour plot of Grid CO_2 Rate (for chosen days on NYISO region and Michigan) and Driving Trips.

acceptance of PHEV technology. Since the focus of this study is the optimization method and not the underlying assumptions, we demonstrate how to use the optimization method under two cases, one where the PHEV battery reaches its EOL at 100000 miles and another at 200000 miles.

6.6 Results

The optimization results were obtained by solving the problem in Eq. 6.3 with the conditions described in Fig. 6.3. In this section, we discuss three aspects of the results.

- The values of the coupling term and its significance in capturing the dependence of the optimal control solution on the battery size.
- Optimal battery sizes under different design assumptions (EOL at 100000 mi. and 200000 mi.).
- Comparison of optimal battery sizing results under the NYISO grid assumptions (Fig. 6.3) vs. the Michigan grid mix assumptions (Fig. 6.4).

Table 6.1 shows the values of the coupling term at different battery sizes. The coupling term is equal to the gradient of the optimal attainable control objective, as explained in sections 5.3 and 6.4.1 and analytically proven in Appendix D. A negative value of the coupling term means that increasing the battery size would result in lower CO_2 emissions through optimal charging and power management of the PHEV and *vice versa*. Thus the negative values of coupling term for smaller battery sizes in Table 6.1 indicate some restrictions on the optimal control trajectories that would be alleviated by increasing the battery size.

Table 6.1 Coupling Term Values at Different Battery Sizes (EOL at 100000 mi.)

Total Battery Size [kWh]	**Coupling Term [kg/kWh]**
11.29	-107.1
11.56	-98.14
13.29	-52.81
16.61	7.441
17.94	24.34

In Fig. 6.5, the optimal *SOC* trajectories for the smaller batteries indicate grid charging before the first trip as there is insufficient battery energy for the first trip (which occurs at hour 7). This first section of the day is the least favorable time to charge due to the high CO_2 rate on the grid. However, the large battery (17.9 kWh) does not need to charge during this period. This indicates that the smaller battery sizes restrict the range of possible optimal control actions (under our driving and grid mix assumptions). Thus, for smaller batteries the coupling term suggests that there are possible improvements, or increased flexibility of the control actions with increasing battery size. It should also be noted that even the smallest battery is not charged to the fullest extent or utilized at the highest *SOCs*. This is because the on-road power demand constraint results in the need for a 11.29 kWh battery, thus resulting in an over-sized battery in terms of transferring electric energy from the grid to transportation.

The coupling term is positive for larger battery sizes in table 6.1, which means that increasing the battery size results in an increased value of the optimal control objective or increased emissions from the use phase of the PHEV. This indicates that a 17.9 kWh does not provide any additional flexibility for carrying cleaner electrical energy, while increasing the mass and consequently the on-road power requirements. Indeed, Fig. 6.5 shows that for the larger battery there is no battery charging at times of high CO_2 production rate on the

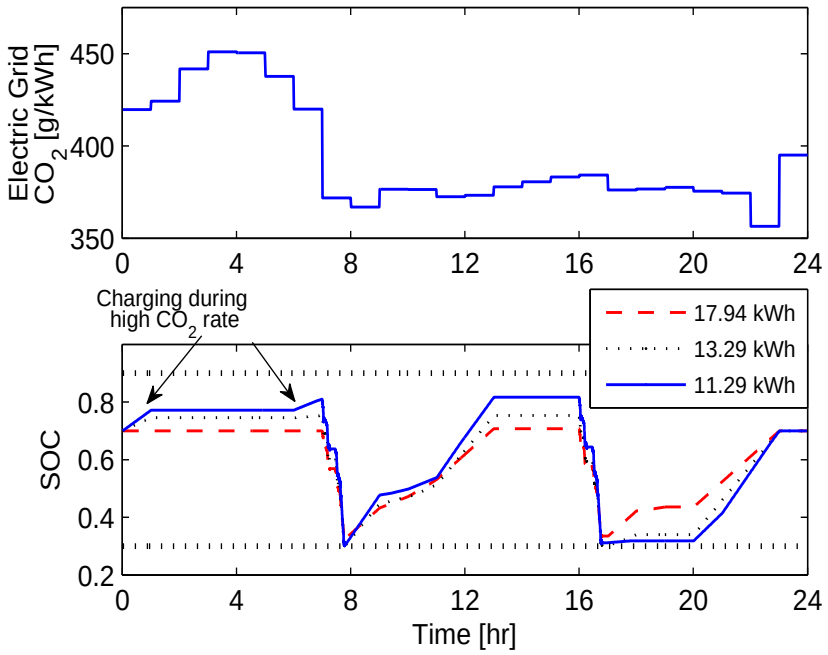

Figure 6.5 Optimal 24 hour Trajectories for different Battery sizes.

grid. These inferences are true only for the particular grid mix and driving patterns assumed here but demonstrate the power of evaluating the coupling term.

Before, obtaining the combined optimal battery size utilizing the coupling term, we provide some insight into the use of the modified KKT condition (Eq. 5.6) or the total gradient in Eq. 6.14. From a high-level perspective, the problem of optimizing battery size for CO_2 emissions in a PHEV involves mitigating the tradeoffs between at least three main competing phenomena. First, larger batteries require more CO_2 for production. Second, a larger battery also means a heavier vehicle, with more overall energy needs and therefore potentially more trip CO_2 emissions. Finally, a larger battery gives a PHEV more electric energy storage capacity, and more freedom in choosing when to charge with grid electricity. This means that the PHEV is potentially able to reduce its CO_2 emissions by charging with grid electricity, and timing that charging process to coincide with periods when grid CO_2 levels are low. The second and third effects are captured by the coupling term. Ultimately, the process of optimizing PHEV battery size for CO_2 emissions involves finding that particular size at which the drawbacks and benefits of a larger battery are balanced. This is precisely the condition represented by the total gradient in Eq. 5.6.

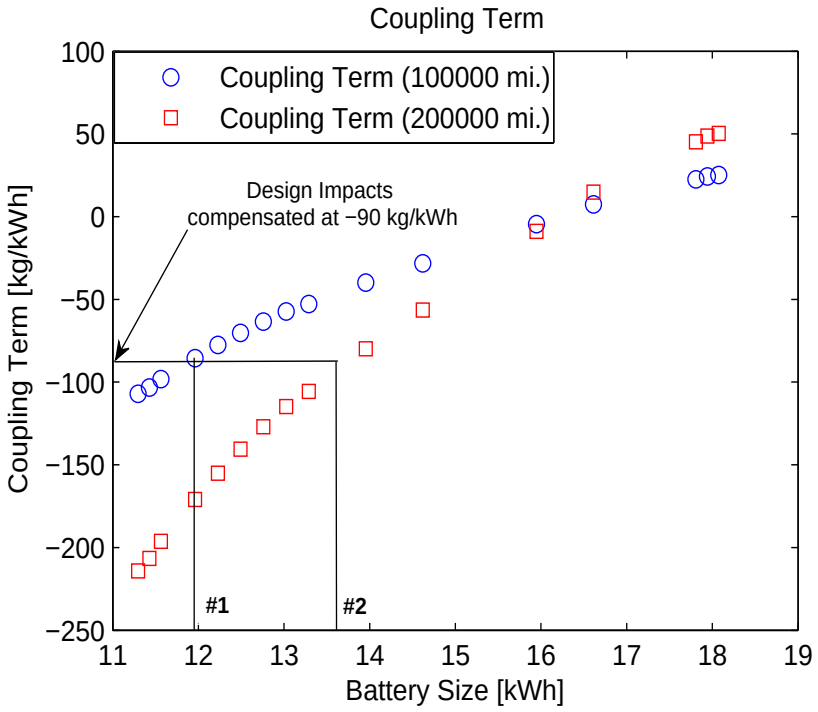

Figure 6.6 Coupling Term Values for different EOL assumptions and Optimal Battery sizes

The coupling term was evaluated for different battery sizes, by solving the optimal control problem at these battery sizes and graphed in Fig. 6.6. Utilizing Eq. 6.15, we obtain the battery sizes at which the coupling term negates the design impacts as the combined

Table 6.2 Coupling Term Values at Different Battery Sizes under Michigan grid assumptions

Total Battery Size [kWh]	**Coupling Term [kg/kWh]**
11.29	189.9
17.94	232.8

optimal battery size. Depending on the CO_2 emissions assumptions during the design phase, (in Fig. 6.6 we assume 90 kg of CO_2/kWh), we obtain battery sizes #1 (11.96 kWh) and #2 (13.62 kWh) respectively as the combined optimum for EOL at 100000 mi. and 200000 mi. Previous combined optimization efforts [66, 71, 77] cite computational effort as a major hindrance with optimization runs lasting several days on multiple cores. Each point in Fig. 6.6 is obtained through control optimization which is solved in less than 2 hours, producing the combined optimal solution in less than a day of computation on a single quad core machine. Through the insight provided by the coupling term, we obtain the optimal values in a computationally efficient manner.

Finally, we obtain the coupling term values for the Michigan grid mix assumptions, which is coal intensive and hence has high CO_2 production rates. The optimal control

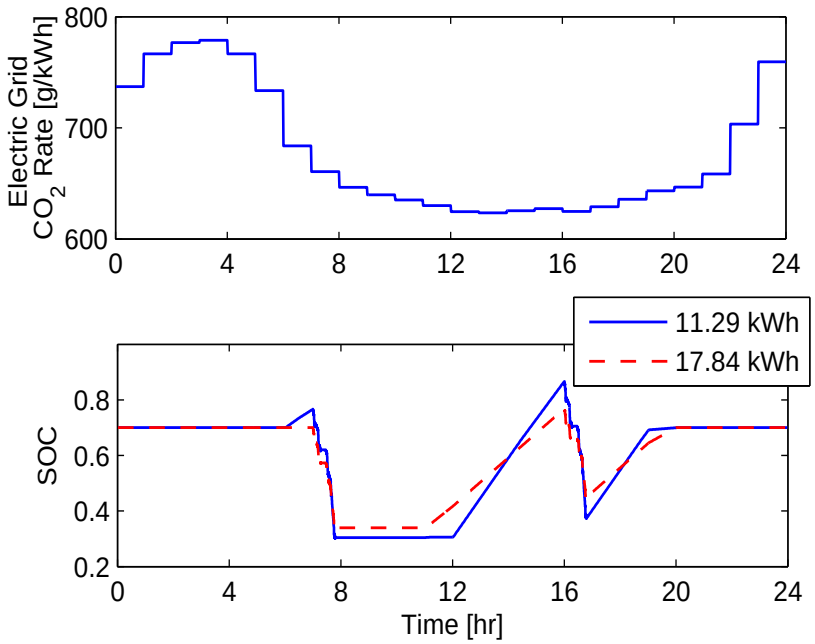

Figure 6.7 Coupling Term Values for different EOL assumptions and Optimal Battery sizes

solution and the associated coupling term is calculated at the lowest and the highest battery sizes. These numbers are reported in Table 6.2 and the trajectories are graphed in Fig. 6.7. As discussed above, positive coupling term values indicate that increasing the battery size results in higher CO_2 from control actions. The coupling term is positive at both the highest and the lowest possible battery sizes. At the lowest battery size, we observe in Fig. 6.7 that there is a small amount of charging before the first trip. Since the CO_2 production from gasoline usage is in the 650-800 g/kWh range additional battery capacity is not as beneficial and it results in increased vehicle mass. Another observation is that significant amounts of charging occurs before the second trip. Since the CO_2 levels are the lowest and almost constant over a sufficiently long period of time before the second trip there are no restrictions on charging before the second trip. Thus additional battery capacity has no benefits. At the largest battery size, the same considerations as for the NYISO case explained above are effective. Thus, under a CO_2 intensive grid the coupling term indicates that the smallest possible battery size is the optimal.

6.7 Summary

In this chapter, the computationally efficient combined design and control optimization method developed in chapter 5 is applied for the optimization of a PHEV powertrain. The major contributions of this work are the methods to calculate and obtain the coupling term, and its subsequent utilization to obtain the combined optimal battery sizes with low computational effort. Since the co-states are not instrumental to obtain the optimal control solution, the literature has not elaborated on their calculation. In this paper we demonstrate their calculation. The procedure for calculating the coupling term once these co-states are obtained is also explained in detail.

The results report the combined optimal battery sizes under different assumptions. It is shown that the coupling term captures the dependence of the optimal control solution on the battery size (the design variable) in an elegant way. The insights provided by the coupling term are emphasized. For example, a positive coupling term value for a particular battery size implies that increasing the battery size produces no improvement in the optimal control solution. We utilized the coupling term to obtain the battery sizes for which the combined design and control gradient is zero, by including the design impacts of manufacturing a battery. It is shown that a larger battery size with increased energy capacity is not the combined optimal solution.

Chapter 7
Conclusion

7.1 Summary

The development of algorithms to obtain the optimal design and control solutions for nonlinear dynamic systems in a computationally efficient manner is presented in this dissertation. These optimization methods highlight possible synergistic interactions between the PHEV, the electric grid and transportation from an individual PHEV's perspective. The methods have been shown to be flexible to accommodate different grid mix scenarios and driving behaviors and expose the relevant tradeoffs between battery sizing, charging and power management depending on the objectives and conditions.

In chapter 2, challenges in the implementation of DDP for a series PHEV powertrain model are resolved through a backward looking model implementation. The performance of two supervisory control strategies for PHEVs, namely Blending and EV/CS was compared using this algorithm. The results showed that there is no significant difference in the performance (in $ costs) of these two control strategies in most cases (esp. when gasoline is more expensive per mile than electricity).

Chapter 3 develops optimal control algorithms capable of addressing both; optimal charging and optimal power management in a single framework. The results show that it is necessary to consider such an approach to optimally charge and drive a PHEV. Depending on the objective and constraints, it is shown that it is not always optimal to fully charge the battery before every driving trip as assumed in the literature. This framework is also capable of exploring tradeoffs that might result from usage of a PHEV for grid related services through a restricted charging study.

Chapter 4 extends this integrated algorithm to consider multiple objectives - CO_2 emissions and $ costs. The concept of crowding distance from the EA literature is used to retain fewer number of points to represent the Pareto front at every state discretization and every time step. This refinement of the Pareto front significantly reduces the computational time and memory requirements making the problem feasible while retaining optimality. The

algorithm generates an optimal Pareto front with good spread ranging from one extremal point to the other. For the grid mix and driving behavior assumed, we exposed tradeoffs related to both the objectives.

Chapter 5 presents a novel approach to the optimization of a dynamic systems design and control. This approach is computationally efficient through the use of a coupling term which also captured the dependence between the optimal design and optimal control. The algorithm was demonstrated by solving a beam mass reduction and vibration attenuation problem. Chapter 6 applied this algorithm for optimal battery sizing and supervisory control of a PHEV. The challenges related to the calculation of the coupling term considering the nonlinear constraints and dynamics of the PHEV powertrain were resolved. The results report the combined optimal battery sizes under different assumptions. It is shown that the coupling term captures the dependence of the optimal control solution on the battery size (the design variable) in an elegant way. The results also indicate that a larger battery size with increased energy capacity is not always the optimal solution.

In summary, this dissertation contributes to the literature on optimization methods and provides solutions for optimal PHEV design and control. These methods are effective because they enable resolving combined objectives, and practical owing to their computational efficiency. Innovative strategies outlining their application by exploiting knowledge of the PHEV's dynamics and usage are presented. Several unanswered questions related to the use and design of PHEVs have been answered using these methods. Our approaches considered interactions between different systems in obtaining the optimal solutions, thereby pushing the envelope in both the optimization literature and the PHEV literature.

7.2 Perspectives on Future Research

Several research challenges related to optimal control and design of PHEVs were addressed in this dissertation. Nonetheless, numerous research challenges and topics exist.

Considering the Future Grid: Though we undertook certain steps to incorporate the impacts of PHEV usage on the electric grid and optimized the PHEV design and control, we assumed the grid in its current state. It is understood that with increased amount of renewable power sources and the inclusion of electric propulsion vehicles, the state of the grid will change. These changes might again influence the design and control decision for future auto-mobiles. Thus it is essential to develop and apply an optimization method that is capable of considering the PHEV impacts on the grid and *vice versa* in order to achieve maximum synergy on any objective.

Stochastic Optimal Solutions: Our research aimed at developing optimal control methods that could provide insights into the nature of the control actions and educate us. Chapters 2, 3, 4 develop deterministic algorithms that provided us with unprecedented insight regarding the necessary optimal actions and the possible tradeoffs for a given scenario. In order to utilize these insights and solutions, there is a need to extract rules from these solutions. Another way to obtain implementable solutions is to consider a wide array of grid mix and driving conditions through well understood distributions and obtain stochastic optimal solutions.

Battery Characterization: Battery technology will be instrumental in making PHEVs a reality. In this dissertation, we used a simple equivalent circuit model to represent the battery dynamics. We assumed that the *SOC* is always accurately known and that there are no degradation costs. In reality, it will be essential for power management and charging control algorithms to accurately know the charge and health variables in order to perform optimally. Accurate models to estimate the amount of battery charge and state of health have to be developed and these models need to be simplified or reduced in order to be usable for controls and optimization.

Battery Sizing and Control for Demand side Services: Several assumptions were made in the dissertation regarding the battery dynamics and its usage. It is necessary to use the algorithms developed in this dissertation with more accurate models of a battery's dynamics and its usage. For example, utilizing accurate battery dynamics models will impose more constraints on battery usage and hence influence its sizing. Battery energy usage for demand side services such as regulation and spinning reserves would also dictate different tradeoffs for battery sizing.

Consumer Expectations vs. Utility Expectations: PHEVs are expected to charge from a cleaner grid and bring cleaner (and maybe cheaper) energy for transportation. This is under the assumption that the PHEV owners charge at certain times of the day when the grid is cleaner and/or least stressed. These are some expectations from the utilities. PHEV consumers meanwhile might have different needs such as using PHEVs not just for trips to work, charging at fast rates before their trips and minimizing their operating costs. The alignment of these objectives and the objectives of several other stakeholders is not obvious. Thus it is necessary to manage and refine the objectives and constraints used in the optimization based on consumer surveys and the expectations of the utilities.

Multi-Objective Optimization for Combined Design and Control: Chapter 4 extends the control optimization algorithm developed in chapter 3 to consider multiple objectives in a computationally efficient manner. It is obvious that these multiple objectives also arise at a system level resulting in the need for a combined battery size and control optimum. Most

physical systems are also required to satisfy multiple objectives. Thus it is necessary to obtain combined optimization algorithms capable of elegantly handling multiple objectives.

Appendices

Appendix A
Backward Looking Powertrain Model

In order for a function to be invertible we have to show that the function representing the forward looking powertrain model (f in Eq. 2.14) satisfies the following two conditions. First, f must be one-to-one (i.e. given a current state we have to show that each input $u(k) \in U$, results in a unique future state $x(k+1) \in Z$, where U and Z are defined in Eqs. 2.11 and 2.12). Secondly, we have to show that f is onto (i.e. that the inputs in U span the set Z). The second condition (the onto relation) can be guaranteed by redefining the set Z to be only the reachable set from the set of inputs U. This means that only transitions to feasible future states will be considered in the optimization. To show the one-to-one mapping, the equations representing the function f are explained in detail below.

Figure A.1 is a diagram describing the relationship between the powertrain components. This is a forward looking representation that we will use to show the one-to-one dependence

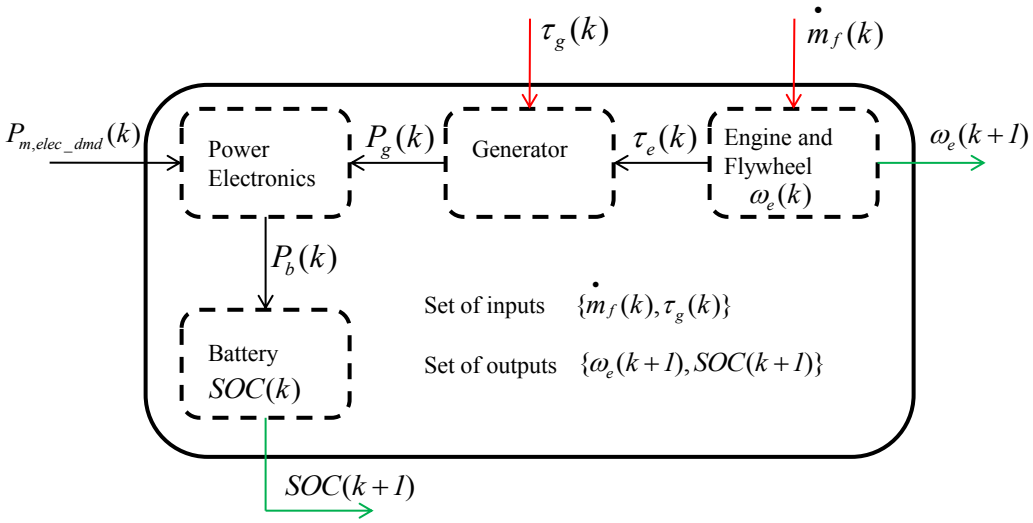

Figure A.1 Representation of Forward Looking Powertrain Model and the Interaction between Components

between the set of inputs $\{\dot{m}_f(k),\ \tau_g(k)\}$, and the set of outputs $\{\omega_e(k+1), SOC(k+1)\}$.

The motor electrical power demand is an external input that the supervisory controller has to satisfy. This electrical power demand is calculated using Eqs. 2.3 - 2.5. Assuming that the losses in the power electronics are negligible, the battery power demand (P_b) is related to motor electric power demand ($P_{m,elec,dmd}$) and the generator power output (P_g) by Eq. A.1

$$P_b(k) = P_{m,elec}(k) + P_g(k) \tag{A.1}$$

At every time step k, for a given $P_{m,elec,dmd}$, P_b is dependent only on P_g. The generator power is in turn dependent on generator torque (τ_g), which is an input and the generator speed (ω_g), which is proportional to the engine speed (ω_e), which is a state. For a given, $\omega_e(k)$ and $\tau_g(k)$, we have a unique value of $P_g(k)$ from Eq. A.2 below. A unique value of $P_g(k)$ for every $\tau_g(k)$ is guaranteed because of the monotonic relationship between these variables due to the nature of the generator efficiency map. This monotonic relationship between $P_g(k)$ and $\tau_g(k)$ is graphically verified and shown in Fig. A.2.

$$\eta_g(k) = f_g(\tau_g(k), \omega_g(k)) \tag{A.2a}$$
$$P_g(k) = \eta_g(k)\tau_g(k)\omega_g(k) \tag{A.2b}$$

Since P_g is uniquely determined by $\tau_g(k)$ and P_b is uniquely determined by P_g, every input $\tau_g(k)$ results in a unique value of $P_b(k)$.

The equations describing battery dynamics are given in Eq. A.3.

$$I_b(k) = \frac{V_{oc}(k) - \sqrt{V_{oc}^2(k) - 4R_i(k)P_b(k)}}{2R_i(k)} \tag{A.3a}$$
$$SOC(k+1) = SOC(k) - \frac{I_b(k)\Delta t}{Q_{max}} \tag{A.3b}$$

There is a monotonic relationship between P_b and I_b, as well as between I_b and $SOC(k+1)$. Thus every battery power input P_b, results in a unique $SOC(k+1)$, for a given $SOC(k)$. From the above arguments, we conclude that every generator torque input $\tau_g(k)$ results in a unique future state of charge $SOC(k+1)$ for a given pair of current states $\{\omega_e(k+1), SOC(k+1)\}$.

To model the engine and flywheel dynamics and to show that each pair of inputs $\{\dot{m}_f(k),$

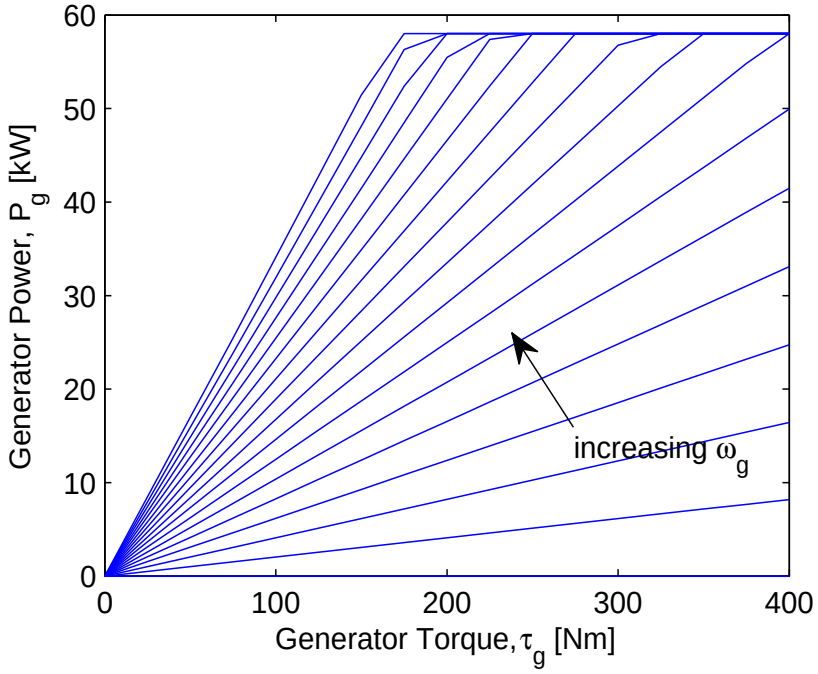

Figure A.2 Monotonic relationship between Generator Torque and Generator Power output

$\tau_g(k)\}$ results in a unique value of future engine speed state $\omega_e(k+1)$, given a current engine speed $\omega_e(k)$, we use Eq. A.4.

$$\tau_e(k) = f_e(\dot{m}_f(k), \omega_e(k)) \tag{A.4a}$$

$$\omega_e(k+1) = \omega_e(k) + \frac{\tau_e(k) - \tau_g(k)}{J_{flwhl}} \tag{A.4b}$$

Again the map (f_e) is graphically verified to be one-to-one in Fig. A.3 and hence results in a unique engine torque $\tau_e(k)$ for every fuel flow rate input($\dot{m}_f(k)$), given $\omega_e(k)$.

From our above discussion we have shown that every generator torque input $\tau_g(k)$ results in a unique future state of charge $SOC(k+1)$ for a given pair of current states $\{\omega_e(k)$, $SOC(k)\}$. For this $\tau_g(k)$ and pair of current states $\{\omega_e(k)$, $SOC(k)\}$, every fuel flow rate input($\dot{m}_f(k)$) results in a unique torque produced by the engine and hence a unique $\omega_e(k+1)$. In other words it is possible to obtain the same $\omega_e(k+1)$ for two different sets of inputs, but the $SOC(k+1)$ is uniquely decided by each $\tau_g(k)$. This means that the pair of future states $\{\omega_e(k+1), SOC(k+1)\}$ is uniquely determined by each input pair $\{\dot{m}_f(k)$, $\tau_g(k)\}$.

This ensures that when the forward looking powertrain model is inverted, for every future state considered in the backward looking model we can obtain the set of inputs required

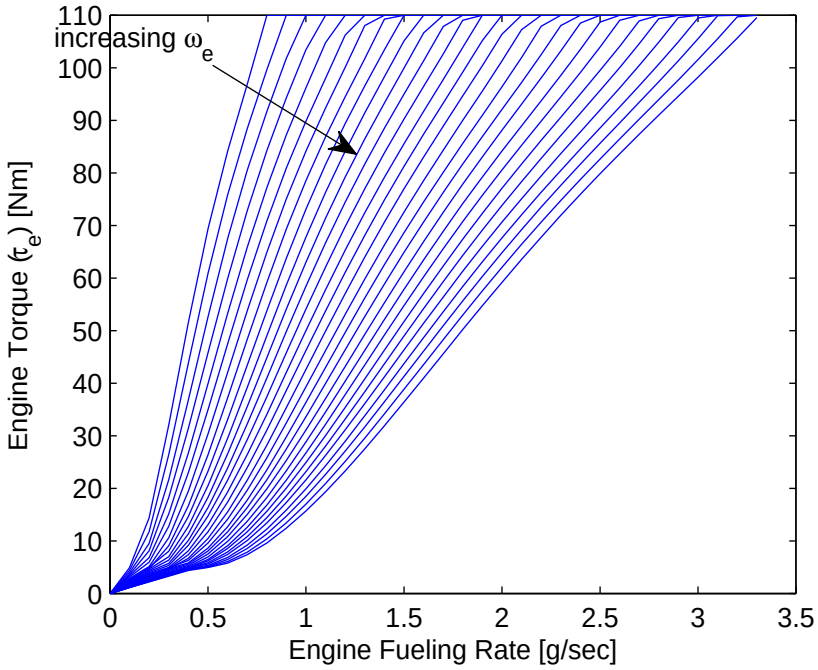

Figure A.3 Monotonic relationship between Engine Fueling Rate and Engine Torque output

to transition to that future state, and the set of inputs will be uniquely determined. Thus ensuring the existence of the function g, representing the backward looking model in Eq. 2.13.

Appendix B

Optimal Power Management Results

Tables B.1 - B.3 (below) present the results of the optimal Power Management studies from Chapter 2 in full detail.

Table B.1 Consumption Results for Highway Cycle

	Optimal Blending			Optimal EV/CS		
Gas and Electricity Prices	Gas [kg]	Electric [kWh]	Total ($)	Gas [kg]	Electric [kWh]	Total ($)
1$/gal, 10 c/kWh	4.44	0	1.55	4.57	0	1.59
1.2$/gal, 10 c/kWh	3.89	2.23	1.85	3.34	4.66	1.86
1.5$/gal, 10 c/kWh	2.54	7.95	2.12	2.57	7.95	2.14
2.5$/gal, 10 c/kWh	2.54	7.95	2.99	2.57	7.95	3.02
4$/gal, 10 c/kWh	2.54	7.95	4.31	2.57	7.95	4.35

Table B.2 Consumption and Cost Results for Optimal Solutions $c_G = 1$\$/gal, $c_E = 10$ c/kWh

Cycle	Distance	Optimal Blending			Optimal EV/CS		
	Miles	Gas [kg]	Electric [kWh]	Total ($)	Gas [kg]	Electric [kWh]	Total ($)
short 1	7.3	0.37	0	0.13	0	1.52	0.15
short 2	24.03	1.43	0	0.50	0	5.69	0.57
medium 1	34.43	2.41	0	0.84	1.45	4.15	0.92
medium 2	44.2	2.86	0	0.99	2	3.61	1.05
long	62.49	4.44	0	1.55	4.57	0	1.59

Table B.3 Consumption and Cost Results for Optimal Solutions $c_G = 2.5$\$/gal, $c_E = 10$ c/kWh

Cycle	Distance	Optimal Blending			Optimal EV/CS		
	Miles	Gas [kg]	Electric [kWh]	Total ($)	Gas [kg]	Electric [kWh]	Total ($)
short 1	7.3	0	1.52	0.15	0	1.52	0.15
short 2	24.03	0	5.69	0.57	0	5.69	0.57
medium 1	34.43	0.52	7.73	1.22	0.54	7.72	1.24
medium 2	44.2	0.93	7.73	1.58	0.96	7.7	1.6
long	62.49	2.54	7.95	2.99	2.56	7.95	3.02

Appendix C

Derivation of Combined Design and Control Optimality Conditions

Consider the combined plant/controller optimization problem in Eq. (5.3). Assuming there exists an optimal solution to this problem, the solution must , by definition satisfy all feasibility constraints, *i.e.*

$$\begin{aligned} h_p(x_p^*) = 0, g_p(x_p^*) \leq 0, \dot{z}^* = f(z^*(t), u^*(t), t, x_p^*), \\ \eta(u^*(t), t, x_p^*) \leq 0, \Psi(z^*(T^*), T^*) = 0, z^*(t_0) = z_0 \end{aligned} \tag{C.1}$$

Furthermore, assuming the optimization objective and constraints to be continuous and differentiable, and assuming the optimum to be a regular point, we define Lagrange multipliers $(\alpha, \beta, \lambda(t), \mu(t), \nu)$, such that the following complementary slackness conditions are met at the optimum:

$$\begin{aligned} \alpha^* \neq 0, \beta^* \geq 0, \beta^{*T} g_p(x_p^*) = 0, \lambda^*(t) \neq 0 \\ \mu^*(t) \geq 0, \mu^*(t)\eta(u^*(t), t, x_p^*) = 0, \nu^* = 0 \end{aligned} \tag{C.2}$$

The Lagrange multipliers can be used to define an augmented (Lagrangian) cost function J_{aug} that will be stationary with respect to the plant deign variables, controller state and

input variables, and the Lagrange multipliers at the optimum, *i.e.*

$$\begin{aligned} J_{aug} =& w_p\big(F_p + \alpha^T h_p(x_p) + \beta^T g_p(x_p)\big) \\ &+ w_c\Bigg[\Phi(z(T),T) + \nu^T \Psi(z(T),T) \\ &+ \int_0^T \Big(L(z(t),u(t),t) + \mu^T(t)\eta(u(t),t,x_p) \\ &+ \lambda^T(t)\big(f(z(t),u(t),t,x_p) - \dot{z}(t)\big)\Big)dt\Bigg] \end{aligned} \tag{C.3}$$

Now, define the following Hamiltonian cost functional:

$$H(z(t),u(t),t,x_p,\lambda(t)) = L(z(t),u(t),t) + \lambda^T f(z(t),u(t),t,x_p) \tag{C.4}$$

Rewriting the augmented cost function in terms of this Hamiltonian gives:

$$\begin{aligned} J_{aug} =& w_p\big(F_p + \alpha^T h_p(x_p) + \beta^T g_p(x_p)\big) \\ &+ w_c\Bigg[\Phi(z(T),T) + \nu^T \Psi(z(T),T) \\ &+ \int_0^T \Big(H(z(t),u(t),t,x_p,\lambda(t)) + \mu^T(t)\eta(u(t),t,x_p) \\ &- \lambda^T(t)\dot{z}(t)\Big)dt\Bigg] \end{aligned} \tag{C.5}$$

Using Leibniz's integral rule to derive an expression for the variation in J_{aug} in terms of

variations in the plant and controller design variables around their optimal values gives

$$
\begin{aligned}
dJ_{aug} = & \left[w_p \left(\frac{dF_p}{dx_p} + \frac{dh_p^T}{dx_p}\alpha + \frac{dg_p^T}{dx_p} \right) \right. \\
& + w_c \int_0^T \left(\frac{\partial H}{\partial x_p} + \frac{\partial \eta^T}{\partial x_p}\mu \right) \Bigg]^T dx_p \\
& + w_c \left[\frac{\partial \Phi}{\partial z} + \frac{\partial \Psi^T}{\partial z}\nu \right]_{t=T}^T dz(T) \\
& + w_c \left[\frac{\partial \Phi}{\partial T} + \frac{\partial \Psi^T}{\partial T} + H - \lambda^T \dot{z} + \mu^T \eta \right]_{t=T} dT \\
& + w_c \int_0^T \left[\frac{\partial H^T}{\partial z}\delta z(t) + \left(\frac{\partial H}{\partial u} + \frac{\partial \eta^T}{\partial u}\mu \right)^T \delta u(t) \right. \\
& \left. + \left(\frac{\partial H}{\partial \lambda} - \dot{z} \right)^T \delta\lambda - \lambda^T \delta\dot{z} \right] dt
\end{aligned}
\tag{C.6}
$$

Integrating the last term on the RHS in Eq. (C.6) by parts, to eliminate the variations in $\dot{z}$, the above equation reduces to

$$
\begin{aligned}
dJ_{aug} = & \left[w_p \left(\frac{dF_p}{dx_p} + \frac{dh_p^T}{dx_p}\alpha + \frac{dg_p^T}{dx_p} \right) \right. \\
& + w_c \int_0^T \left(\frac{\partial H}{\partial x_p} + \frac{\partial \eta^T}{\partial x_p}\mu \right) \Bigg]^T dx_p \\
& + w_c \left[\frac{\partial \Phi}{\partial z} + \frac{\partial \Psi^T}{\partial z}\nu - \lambda \right]_{t=T}^T dz(T) \\
& + w_c \left[\frac{\partial \Phi}{\partial T} + \frac{\partial \Psi^T}{\partial T} + H - \lambda^T \dot{z} + \mu^T \eta \right]_{t=T} dT \\
& + w_c \int_0^T \left[\left(\frac{\partial H^T}{\partial z} + \dot{\lambda} \right) \delta z(t) \right. \\
& \left. + \left(\frac{\partial H}{\partial u} + \frac{\partial \eta^T}{\partial u}\mu \right)^T \delta u(t) + \left(\frac{\partial H}{\partial \lambda} - \dot{z} \right)^T \delta\lambda \right] dt
\end{aligned}
\tag{C.7}
$$

Setting the variations in the augmented cost function to zero for all variations in the optimization variables and assuming a fixed (finite or infinite) time horizon for the optimal control subproblem, produces the following stationarity conditions at the combined opti-

mum. It should be noted that the control objective functional $L(z(t),u(t),t)$ has no explicit dependence on the design variable x_p.

$$\left[\frac{dF_p}{dx_p}+\frac{dh_p^T}{dx_p}\alpha+\frac{dg_p^T}{dx_p}\beta+\frac{w_c}{w_p}\int_0^T\left(\frac{\partial f^T}{\partial x_p}\lambda+\frac{\partial \eta^T}{\partial x_p}\mu\right)dt\right]^*=0 \tag{C.8}$$

$$\left[\frac{\partial \Phi}{\partial z}+\frac{\partial \Psi}{\partial z}\nu-\lambda\right]^*_{t=T}=0 \tag{C.9}$$

$$\left[\frac{\partial H}{\partial z}+\dot{\lambda}\right]^*=0 \tag{C.10}$$

$$\left[\frac{\partial H}{\partial u}+\frac{\partial \eta^T}{\partial u}\mu\right]^*=0 \tag{C.11}$$

The stationarity conditions Eqs. (C.8-C.11), along with the feasibility conditions Eq. (C.1) and the complementary slackness conditions Eq. (C.2) gives the complete set of first-order necessary conditions for combined plant and controller optimality as presented in Section 5.3.

Appendix D

Coupling Term and the Gradient of the Optimal Control Objective

We define the control objective in Eq. (D.1)

$$F_c(z(t),u(t),x_p) = \Phi(z(T),T) + \int_0^T (L(z(t),u(t),t)dt \tag{D.1}$$

Notice that the control objective is dependent on the control variables $(z(t),u(t))$, and the plant design (x_p). Consider the augmented control objective, defined using the appropriate Lagrange multipliers

$$\begin{aligned} F_{c,aug}(z(t),u(t),x_p) =& \Phi(z(T),T) + \nu^T \Psi(z(T),T) \\ &+ \int_0^T \{L(z(t),u(t),t) \\ &+ \lambda^T(t) f(z(t),u(t),t,x_p) \\ &+ \mu^T(t)\eta(u(t),t,x_p)\} \, dt \end{aligned} \tag{D.2}$$

For any chosen plant design (x_p), at the optimal control solution, we have (the superscript $^{\#}$ signifies optimal *control* solution only and not combined optimal)

$$F_c(z^{\#}(t),u^{\#}(t),x_p) = F_{c,aug}(z^{\#}(t),u^{\#}(t),x_p) \tag{D.3}$$

Since Eq. (D.3) holds $\forall x_p$

$$\begin{aligned} &\frac{\partial F_c(z^{\#}(t),u^{\#}(t),x_p)}{\partial x_p} = \frac{\partial F_{c,aug}(z^{\#}(t),u^{\#}(t),x_p)}{\partial x_p} \\ &\text{or simply} \quad \frac{\partial F_c^{\#}}{\partial x_p} = \frac{\partial F_{c,aug}^{\#}}{\partial x_p} \end{aligned} \tag{D.4}$$

Now, consider the total differential of $F_c^{\#}$,

$$\frac{dF_c^{\#}}{dx_p} = \frac{\partial F_c^{\#}}{\partial x_p} + \frac{\partial F_c^{\#}}{\partial z^{\#}}\frac{\partial z^{\#}}{\partial x_p} + \frac{\partial F_c^{\#}}{\partial u^{\#}}\frac{\partial u^{\#}}{\partial x_p} \tag{D.5}$$

For the optimal control solution, we have variations of the optimal control objective with respect to the variations in the state and input trajectories equals zero, *i.e.*

$$\begin{aligned} &\frac{\partial F_c^{\#}}{\partial z^{\#}} = 0, \quad \frac{\partial F_c^{\#}}{\partial u^{\#}} = 0 \\ &\Rightarrow \frac{dF_c^{\#}}{dx_p} = \frac{\partial F_c^{\#}}{\partial x_p} \end{aligned} \tag{D.6}$$

From Eqs. (D.4) and (D.6), we have

$$\frac{dF_c^{\#}}{dx_p} = \frac{\partial F_{c,aug}^{\#}}{\partial x_p} \tag{D.7}$$

Taking the partial differential of Eq. (D.3) with respect to x_p, we get

$$\frac{\partial F_{c,aug}^{\#}}{\partial x_p} = \int_0^T \left(\frac{\partial f^T}{\partial x_p}\lambda^{\#} + \frac{\partial \eta^T}{\partial x_p}\mu^{\#} \right) dt \tag{D.8}$$

From Eq. (D.7) and (D.8), we have,

$$\frac{dF_c^{\#}}{dx_p} = \int_0^T \left(\frac{\partial f^T}{\partial x_p}\lambda^{\#} + \frac{\partial \eta^T}{\partial x_p}\mu^{\#} \right) dt \tag{D.9}$$

Hence we have shown the equality of the coupling terms described in Eqs. (5.9) and (5.10), *i.e.*, the gradient of the optimal attainable control objective with respect to the plant design is equal to the coupling term.

Bibliography

[1] Thomas H. Bradley, Andrew A. Frank, "Design, Demonstrations and Sustainability Impact Assessments for Plug-in Hybrid Electric Vehicles", *Renewable and Sustainable Energy Reviews*, 13, pp. 115-128, 2009.

[2] W. Kempton, J. Tomic, "Vehicle-to-Grid Power Fundamentals: Calculating Capacity and Net Revenue", *Journal of Power Sources*, 144, 1, pp. 268-279, 2005.

[3] W. Kempton, J. Tomic, "Vehicle-to-Grid Power Implementation: From Stabilizing the Grid to Large Scale Implementation", *Journal of Power Sources*, 144, 1, pp. 280-294, 2005.

[4] T-K. Lee, Z. Filipi, "Simulation based Assessment of Plug-in Hybrid Electric Vehicle Behavior during Real-World 24-Hour Missions", *SAE World Congress*, 2010-01-0827.

[5] R. Patil, B. Adornato, Z. Filipi, "Design Optimization of a Series Plug-in Hybrid Electric Vehicle for Real-World Driving Conditions", *SAE Int. J. Engines*, 3, 1, pp.655-665, 2010.

[6] S. J. Moura, D. S. Callaway, H. K. Fathy, J. L. Stein, "Tradeoffs between Battery Energy Capacity and Stochastic Optimal Power Management in Plug-in Hybrid Electric Vehicles", *Journal of Power Sources*, 195, 9, pp. 2979-2988, May 2010.

[7] S. Sojoudi, S. H. Low, "Optimal Charging of Plug-in Hybrid Electric Vehicles in Smart Grids", *IEEE Power and Energy Society General Meeting*, 2011.

[8] N. Rotering, M. Ilic, "Optimal Charge Control of Plug-in Hybrid Electric Vehicles in Deregulated Electricity Markets", *IEEE Transactions on Power Systems*, 26, 3, Aug. 2011.

[9] A. Y. Saber, G. K. Venayagamoorthy, "Intelligent Unit Commitment with Vehicle-to-Grid - A Cost-Emission Optimization", *Journal of Power Sources*, 195, 3, pp. 898-911, 2010.

[10] Scott Moura, "Techniques for Battery Health Conscious Power Management via Electrochemical Modeling and Optimal Control", PhD Dissertation, University of Michigan, Ann Arbor, 2011.

[11] M. Armand, J.M. Tarascon, "Building Better Batteries", Nature, 451, pp.652-657, 2008.

[12] C.-S. Shiau, C. Samaras, R. Hauffe J. Michalek, "Impact of Battery Weight and Charging Patterns on the Economic and Environmental Benefits of Plug-in Hybrid Vehicles , *Energy Policy*, 37, pp.2653-2663, 2009.

[13] V. Gungor, "Opportunities and Challenges of Wireless Sensor Networks in Smart Grid", *IEEE Transactions on Industrial Electronics*, 57, 10, pp.3557-3564, 2010.

[14] P. McDaniel, "Security and Privacy Challenges in the Smart Grid", *IEEE Security and Privacy*, 7, 3, pp.75-77, 2009.

[15] R.E. Brown, “Impact of Smart Grid on Distribution System Design”, *IEEE Power and Energy General Society Meeting*, 2008.

[16] D. Callaway, I. Hiskens, “Acheiving Controllability of Electric Loads”, *Proceedings of the IEEE*, 99, 1, pp. 184-199, Jan. 2011.

[17] F. Orecchini, A. Santiangeli, “Beyond Smartgrids The need of Intelligent Energy Networks for a Higher Global Efficiency through Energy Vectors Integration”, *Interantional Journal of Hydrogen Energy*, 36, 13, pp. 8126-8133, 2011.

[18] A.S. Masoum, S. Deilami, P.S. Moses, A. Abu-Siada,, “Impacts of Battery Charging rates of Plug-in Electric Vehicle on Smart Grid Distribution Systems”, *IEEE Innovative Smart Grid Technologies Conference Europe (ISGT Europe)*, 2010.

[19] S. Hadley, A. Tsvetkova, “Potential Impacts of Plug-in Hybrid Electric Vehicles on Regional Power Generation”, Oak Ridge National Laboratory Report, TM-2007/50, Jan. 2008.

[20] S. Blumsack, C. Samaras, P. Hines, “Long-Term Electric System Investments to Support Plug-in Hybrid Electric Vehicles”, *IEEE Power and Energy Society General Meeting*, 2008.

[21] Climate Analysis Indicators Tool, World Resources Institute (WRI), http://cait.wri.org/figures.php?page=/US-FlowChart

[22] P.J. Balducci, “Plug-in Hybrid Electric Vehicles Marker Penetration Scenarios”, Pacific Northwest National Laboratory Report, PNNL-17441, 2008.

[23] J. Axsen, K. Kurani, “The Early U.S. Market for PHEVs: Anticipating Consumer Awareness, Recharge Potential, Design Priorities and Energy Impacts”, Institute of Transportation Studies Report, UCD-ITS-RR-08-22 , University of California, Davis, Aug. 2008.

[24] B. Kramer, S. Chakraborty, B. Kroposki, “A Review of Plug-in Vehicles and Vehicle-to-Grid Capability”, *IEEE Conference on Industrial Electronics*, 2008.

[25] T. Markel, A. Simpson, “Plug-In Hybrid Electric Vehicle Energy Storage System Design”, *Advanced Automotive Battery Conference*, 2006.

[26] A. Brahma, Y. Guezennec, G. Rizzoni, “Dynamic Optimization of Mechanical/Electrical Power Flow in Parallel Hybrid Electric Vehicles”, *5th International Symposium on Advanced Vehicle Control*, Aug. 2000.

[27] C.C. Lin, H. Peng, J. W. Grizzle, J. Kang. “Power Management Strategy for a Parallel Hybrid Electric Truck”, *IEEE Transactions on Control Systems Technology*, 11, 6, pp. 839-849, Nov. 2003.

[28] L. Serrao, S. Onori, G. Rizzoni, “ECMS as a Realization of Pontryagin’s Minimum Principle”, *American Control Conference*, 2009.

[29] A. Rousseau, S. Pagerit, D. Gao, "Plug-in Hybrid Electric Vehicle Control Strategy Parameter Optimization", *23rd International Electric Vehicle Symposium*, 2007.

[30] Ed Tate, J.W. Grizzle, Huei Peng, "SP-SDP for Fuel Consumption and Tailpipe Emissions Minimization in an EVT Hybrid", *IEEE Transactions on Control Systems Technology*, 18 , 3, 2010, pp. 673 - 687.

[31] Rajit Johri, A. Salvi, Z. Filipi, "Optimal Energy Management for a Hybrid Vehicle Using Neuro-Dynamic Programming to Consider Transient Engine Operation", *ASME Dynamic Systems and Control Conference*, 2011.

[32] S. Stockar, V. Marano, M. Canova, G. Rizzoni, L. Guzzella, "A Control Study for the Energy Management of Plug-in Hybrid Electric Vehicles with Applications to Real-World Driving Cycles", *IEEE Transactions on Vehicular Technology*, accepted.

[33] D. F. Opila, X. Wang, Ryan McGee, Brent Gillespie, J.A. Cook, J.W. Grizzle, "Incorporating Drivability Metrics into Optimal Energy Management Strategies for Hybrid Vehicles Part 1: Model, Methods, and Government Test Cycles", *IEEE Transactions on Control Systems Technology*, preprint.

[34] Scott Moura, J. Stein, H. Fathy, "Battery Health Conscious Power Management in Plug-in Hybrid Electric Vehicles via Electrochemical Modeling and Stochastic Control", submitted to *IEEE Transactions on Control Systems Technology*.

[35] P. Tulpule, V. Marano, G. Rizzoni, "Effects of Different PHEV Control Strategies on Vehicle Performance", *American Control Conference*, 2009.

[36] S. J. Moura, H. K. Fathy, D. S. Callaway, J. L. Stein, "A Stochastic Optimal Control Approach for Power Management in PHEVs", *IEEE Transactions on Control Systems Technology*, 19, 3, pp. 545-555, May 2011.

[37] E.D.Tate, M. O. Harpster, Peter J. Savagian, "The Electrification of the Automobile: From Conventional Hybrid, to Plug-in Hybrids, to Extended-Range EVs", *SAE World Congress*, 2008-01-0458.

[38] S. Bashash, S. J. Moura, J.C. Forman, H.K. Fathy, "Plug-in Hybrid Electric Vehicle Charge Pattern Optimization for Energy Cost and Battery Longevity", *Journal of Power Sources*, 196, pp. 541-549, 2011.

[39] Zhongjing Ma, D. Callaway, I. Hiskens, "Decentralized Charging Control for Large Populations of PHEVs: Application of the Nash Uncertainty Equivalence Principle", *IEEE Multi-Conference on Systems and Control*, 2010.

[40] Yixing Xu, Le Xie, C. Singh, "Optimal scheduling and operation of load aggregator with electric energy storage in power markets", *North American Power Symposium*, 2010.

[41] K. Clement, E. Haesen, J. Driesen, "Coordinated Charging of Multiple Plug-in Hybrid Electric Vehicles in Residential Distribution Grids", *IEEE Power Systems Conference and Expo*, 2009.

[42] C. Ahn, C.-T. Li, Huei Peng, "Decentralized charging algorithm for electric vehicles connected to smart grid", *American Control Conference*, 2011.

[43] A. Kashyap, D. S. Callaway, "Controlling Distributed Energy Constrained Resources for Power System Ancillary Services , *Proceedings of the 11th International Conference for Probabilistic Methods Applied to Power Systems*, 2010.

[44] Y. Ota, H. Taniguchi, T. Nakajima, K. M. Liyanage, J. Baba, A. Yokoyama, "Autonomous distributed V2G (vehicle-to-grid) considering charging request and battery condition", *International Conference on Industrial and Information Systems*, 2009.

[45] E. Traut, C. Hendrickson, E. Klampfl, Y. Liu, J. Michalek, "Optimal design and allocation of electrified vehicles and dedicated charging infrastructure for minimum greenhouse gas emissions , *NAS Transportation Research Board Annual Meeting*, Jan. 2011.

[46] G. Ripaccioli, D. Bernardini, S. Di Cairano, A. Bemporad, I.V. Kolmanovsky, "A Stochastic Model Predictive Control Approach for Series Hybrid Electric Vehicle Power Management", *American Control Conference*, 2010.

[47] H. Ali Borhan, A. Vahidi, Phillips. M. A., Ming L. Kuang, I.V. Kolmanovsky, "Predictive Energy Management of a Power-Split Hybrid Electric Vehicle", *American Control Conference*, 2009.

[48] A. Piccolo, L. Ippolito, Vincenzo Gal, A. Vaccaro, "Optimization of Energy Flow Management in Hybrid Electric Vehicles via Genetic Algorithms", *IEEE/ASME International Conference on Advanced Intelligent Mechatronics*, 2001.

[49] M. Salman, N. J. Schouten, N. A. Kheir, "Fuzzy Logic Control for Parallel Hybrid Vehicles", *IEEE Transactions on Control Systems Technology*, 10, 3, pp. 460-468, May 2002.

[50] O. Sundstrm, L. Guzzella, Patrik Soltic, "Torque-Assist Hybrid Electric Powertrain Sizing: From Optimal Control Towards a Sizing Law", *IEEE Transactions on Control Systems Technology*, 18, 4, pp. 837-849, July 2010.

[51] D. Kum, H. Peng, N. Bucknor, "Optimal Control of the Plug-In HEV for Fuel Economy under Various Travel Distances", *6th IFAC Symposium on Advances in Automotive Control*, 2010.

[52] Ryan Wiser, G. Barbose, "Renewable Portfolio Standards in the United States, Lawrence Berkeley National Laboratory Report, LBNL 154E, April 2008.

[53] S. Awerbuch, "Portfolio based Electricity Generation Planning: Policy Implications for Renewables and Energy Security", *Mitigation and Adaptation Strategies for Global Change*, 11, pp. 693-710, 2006.

[54] S.L Andersson, A.K. Elofsson, M.D. Galus, L. Goransson, S. Karlsson, F. Johnsson, G. Andersson, "Plug-in hybrid electric vehicles as regulating power providers: Case studies of Sweden and Germany", *Energy Policy*, 38, pp.2751-2762, 2010.

[55] C. D. White, K. M. Zhang, "Using Vehicle-to-Grid Technology for Frequency Regulation and Peak-Load Reduction", *Journal of Power Sources*, 196, pp. 3972-3980, 2011.

[56] P. Ramadass, B. Haran, P. Gomadam, R. White, B. Popov, "Development of rst principles capacity fade model for Li-ion cells", *J. Electrochem. Soc.*, 151, 2, pp. 196203, 2004.

[57] V. Paladini, T. Donateo, Arturo de Risi, D. Laforgia, "Super-capacitors Fuel-cell Hybrid Electric Vehicle Optimization and Control Strategy Development", *Energy Conversion and Management*, 48, 11, pp. 3011-3008, 2007.

[58] J. Wu, C. H. Zhang, N. X. Cui, "PSO Algorithm based Parameter Optimization for HEV Powertrain and its control strategy", *International Journal of Automotive Technology*, 9, 1, pp. 53-69, 2008.

[59] Carlos Coello, Gary Lamont, David Veldhuizen, "Evolutionary Algorithms for Solving Multi-Objective Problems", 2nd edition, Springer Publishing, 2007.

[60] K. Deb, A. Pratap, S. Agarwal, T. Meyarivan, "A Fast and Elitist Multiobjective Genetic Algorithm: NSGA-II", *IEEE Transactions on Evolutionary Computation*, 6, 2, pp. 182-197, Apr 2002.

[61] R.T. Marler, J.S. Arora, "Survey of Multiobjective Optimization Methods for Engineering", *Structural and Multidisciplinary Optimization*, 26, pp. 369-395, 2004.

[62] Linda Gaines, Roy Cuenca, " Costs of Lithium-Ion Batteries for Vehicles", Argonne National Laboratory Report, ANL/ESD-42, 2000.

[63] H. K. Fathy, J. A. Reyer, P.Y. Papalambros, A.G. Ulsoy, "On the Coupling between the Plant and Controller Optimization Problems". *Proceedings of the American Control Conference*, 2001.

[64] M. J. Smith, K. M. Grigoriadis, R. E. Skelton, "Optimal Mix of Active and Passive Control in Structures". *Journal of Guidance, Control, and Dynamics*, 15, 4, pp. 912-919, 1992.

[65] T. T. Soong, G. P. Cimellaro, "Future Directions in Structural Control", *Structural Control and Health Monitoring*, 16, pp.7-16, 2009.

[66] M. Kim, H. Peng., "Power management and design optimization of fuel cell/battery hybrid vehicles". *Journal of Power Sources*. 165, 2, pp.819-832, 2007.

[67] Rao S. S., "Combined Structural and Control Optimization of Flexible Structures". *Engineering Optimization*, 13, pp.1-16, 1988.

[68] F. N. Eastep, N. Khot, R. Grandhi, "Improving the Active Vibrational Control of Large Space Structures Through Structural Modifications". *Acta Astronautica*, 15, 6/7, pp.383-389, 1987.

[69] J. Rakowska, R. Haftka, L. Watson, "Multi-Objective Control-Structure Optimization via Homotopy methods". *SIAM Journal of Optimization*, 3, 3, pp. 654-667, 1993.

[70] D. L. Peters, P. Y. Papalambros, A. G. Ulsoy, "On measures of Coupling between the Artifact and Controller Optimal Design Problems". *Proceedings of the IDETC/CIE*, 2009.

[71] A. C. Pil, H. H. Asada, "Integrated Structure/Control Design of Mechatronic Systems Using a Recursive Experimental Optimization Method". *IEEE/ASME Transactions on Mechatronics*, 1, 3, pp.191-203, 1996.

[72] T Ravichandran, David Wang, Glenn Heppler, "Simultaneous plant-controller design optimization of a two-link planar manipulator". *Mechatronics*, 16, pp. 233242, 2006.

[73] Lee Kyu-Yeul, Roh Myung-Il, "An Efficient Genetic Algorithm using Gradient Information for Ship Structural Design Optimization", *Ship Technology Research*, 48, pp. 161-170, 2001.

[74] R. Patil, Z. Filipi, H. Fathy, "Computationally Efficient Combined Design and Control Optimization using a Coupling Measure", *IFAC Symposium on Mechatronic Systems*, 2010.

[75] R. Patil, B. Adornato, Z. Filipi, "Impact of Naturalistic Driving Patterns on PHEV Performance and System Design", *SAE Powertrains Fuels and Lubricants Meeting*, 2009.

[76] H. K. Fathy, "Combined Plant and Control Optimization: Theory Strategy and Applications", PhD Thesis, University of Michigan, Ann Arbor, MI, 2002.

[77] Z. Filipi, L. Louca, B. Daran, C.-C. Lin, U. Yildir, B. Wu, M. Kokkolaras, D. Assanis, H. Peng, P. Papalambros, J. Stein, D. Szkubiel, R. Chapp, "Combined optimization of design and power management of the hydraulic hybrid propulsion system for the 6 by 6 medium truck", *Int. J. of Heavy Vehicle Systems*, 11, 3/4, pp. 372-402, 2004.

[78] Philip Sharer, A. Rousseau, D. Karbowski, S. Pagerit, "PHEV Control Strategy: Comparison between EV and Charge-Depleting Options", *2008 SAE World Congress*, 2008-01-0460.

[79] Pierluigi Pisu, G. Rizzoni, "A Comparative Study of Supervisory Control Strategies for Hybrid Electric Vehicles, *IEEE Transactions on Control Systems Technology*, 15, 3, May 2007.

[80] M. Komatsu, T. Takaoka, T. Ishikawa, Y. Gotouda, "Study on the Potential Benefits of Plug-in Hybrid Systems", *2008 SAE World Congress*, 2008-01-0460.

[81] V. Freyermuth, E. Fallas, A. Rousseau, "Comparison of Powertrain Configuration for Plug-in HEVs from a Fuel Economy Perspective", *SAE World Congress*, 2008-01-0461.

[82] D. Bertsekas, "Dynamic Programming and Optimal Control", chapter 6, Vol 2, Belmont, MA: Athena Scientific, 1995.

[83] Warren B. Powell, "Approximate Dynamic Programming: Solving the Curses of Dimensionality", 1st edition, Wiley-Interscience, Sept 2007

[84] O. Sundstrm, D. Ambhl, L. Guzzella, "On Implementation of Dynamic Programming for Optimal Control Problems with Final State Constraints", *Oil & Gas Science and Technology Rev. IFP*, 65, 1, pp. 91-102, 2010.

[85] Tate, Edward Dean, Jr., "Techniques for hybrid electric vehicle controller synthesis", PhD Dissertation, University of Michigan, Ann Arbor, Aug 2007.

[86] Rakesh Patil, Hosam Fathy, Zoran Filipi, "Comparison of Optimal Supervisory Control Strategies for a Series PHEV Powertrain", *ASME Dynamic Systems and Control Conference*, 2011.

[87] http://www.transportation.anl.gov/modeling_simulation/PSAT/index.html

[88] B. Adornato, R. Patil, Z. Filipi, Z. Baraket, T. Gordon, "Characterizing Naturalistic Driving Patterns for Plug-in Hybrid Electric Vehicle Analysis", *IEEE Vehicle Power and Propulsion Conference*, 2009.

[89] Road Departure Crash Warning System Field Operational Test: Methodology and Results , University of Michigan Transportation Research Institute, 2006.

[90] J. Kelly, G. Keoleian, I. Hiskens, "Evaluation of Economic and Capacity Factor Electricity Dispatch Models for Estimating Air Pollutant Emissions", in review.

[91] R. Sioshansi, P. Denholm, "Emission impacts and benefits of plug-in hybrid electric vehicles and vehicle-to-grid services", *Environ. Sci. Technol.*, 43, 4, pp. 11991204, 2009.

[92] http://www.nada.org/Publications/NADADATA/2007, National Automobile Dealers Association 2007 Data.

[93] http://www.epa.gov/otaq/climate/420f05001.htm, EPA Emission Facts: Average Carbon Dioxide Emissions Resulting from Gasoline and Diesel Fuel.

[94] Ali Ipakchi, Farrokh Albuyeh, "Grid of the Future", *IEEE Power and Energy Magazine*, 7, 2, 2009, pp. 52-62.

[95] Han Sekyung, Han S., Sezaki Kaoru, "Development of an Optimal V2G Aggregator for Frequency Regulation", *IEEE Trans. on Smart Grid*, 1, 1, 2010, pp. 65-72.

[96] W. Short, P. Denholm, "A preliminary assessment of plug-in hybrid electric vehicles on wind energy markets", NREL Technical Report, TP-620-39729, April 2006.

[97] http://www.nrel.gov/wind/systemsintegration/ewits.html, Eastern Wind Integration and Transmission Study (EWITS).

[98] S. Stockar,; V. Marano, G. Rizzoni, L. Guzzella, "Optimal control for Plug-in Hybrid Electric Vehicle applications", *American Control Conference*, 2010.

[99] I. Kolmanovsky, M. van Nieuwstadt, J. Sun, "Optimization of Complex Powertrain Systems for Fuel Economy and Emissions", *IEEE Conference on Control Applications*, 1999.

[100] D. Kum, H. Peng, "Supervisory Control of Parallel Hybrid Electric Vehicles for Fuel and Emission Reduction", *ASME Journal of Dynamic Systems, Measurement and Control*, 133, 6, 2011.

[101] S. J. Moura, J. C. Forman, S. Bashash, J. L. Stein, and H. K. Fathy, "Optimal Control of Film Growth in Lithium-Ion Battery Packs via Relay Switches", *IEEE Transactions on Industrial Electronics*, 58, 8, pp. 3555-3566, 2011.

[102] H. G. Daellenbach, C. A. De Kluyver, "Note on Multi Objective Dynamic Programming", *The Journal of the Operational Research Society*, 31, 7, pp. 591-594, 1980.

[103] F.Szidarovszky, M. Gershon, A. Bardossy, "Application of Multiobjective Dynamic Programming to Regional Natural Resource Management", *Applied Mathematics and Computation*, 24, 4, pp.281301, 1987.

[104] M. A. Abo-Sinna, M. L. Hussein, "An Algorithm for Generating Efficient Solutions of Multiobjective Dynamic Programming Problems", *European Journal of Operations Research*, 80, 1, pp.156-165, 1995.

[105] https://www.midwestiso.org/MarketsOperations/Prices/Pages/Prices.aspx

[106] http://www.eia.gov/electricity/monthly/epm_table_grapher.cfm?t=epmt_5_4_b

[107] R. Patil, J. Kelly, Z. Filipi, H. K. Fathy, "Framework for the Integrated Optimization of Charging and Power Management in Plug-in Hybrid Electric Vehicles", *American Control Conference*, 2012.

[108] J. A. Reyer, P. Y. Papalambros, "Combined Optimal Design and Control With Application to an Electric DC Motor". *Journal of Mechanical Design, Transactions of the ASME*, 124, pp. 183-191, 2002.

[109] V. S. Shabde, Karlene A. Hoo, "Optimum controller design for a spray drying process". *Control Engineering Practice*, 16, 5, pp. 541-552, 2008

[110] J. Bauman, M. Kazerani, "A Comparative Study of Fuel Cell Battery, Fuel Cell Ultracapacitor, and Fuel Cell Battery Ultracapacitor Vehicles". *IEEE Transactions on Vehicular Technology*, 57, 8, pp. 760-769, 2008.

[111] N. Shidore, P. Maxime, "Interdependence of System Control and Component Sizing for a Hydrogen fueled Hybrid Vehicle", *Future Transportation Technology Conference*, 2005.

[112] Y. Zhu, Jinhao Qiu, Hejun Du, Junji Tani. "Simultaneous Structural-control Optimization of a Coupled Structural-acoustic Enclosure",*Journal of Intelligent Material Systems and Structures*, 14, April/May, 2003.

[113] Z. Wang, S. Chen, W. Han,"Integrated Structure and Control Optimization of Intelligent Structures", *Engineering Structures*, 21, pp.183-191, 1999.

[114] M. Milman, M. Salama, R. E. Scheid, R. Bruno, "Combined Control-Structure Optimization", *Computational Mechanics*, 8, pp.1-18, 1991.

[115] S. F. Alyaqout, P. Y. Papalambros, A. G. Ulsoy, "Quantification and use of system coupling in decomposed design optimization", *Proceedings of the ASME IMECE*, 2005.

[116] Sten Karlsson, "Optimal Size of PHEV Batteries from a Consumer Perspective Estimation Using Car Movement Data and Implications for Data Harvesting", *Electric Vehicle Symposium 24*, 2009.

[117] J. Liu, "Modeling, Configuration and Control Optimization of Power-Split Hybrid Vehicles", PhD Dissertation, University of Michigan, Ann Arbor, 2007.

[118] C-S. Shiau, N. Kaushal, C.T. Hendrickson, S. Peterson, J. Whitacre, J. Michalek, "Optimal Plug-in Hybrid Electric Vehicle Design and Allocation for Minimum Life Cycle Cost, Petroleum Consumption, and Greenhouse Gas Emissions , *ASME Journal of Mechanical Design, Special Issue on Sustainability*, 132, 9, pp. 1-11.

[119] J. Kelly, J. S. MacDonald, G. Keoleian, "Time-dependent Plug-in Hybrid Electric Vehicle Charging based on National Driving Patterns and Demographics", *Applied Energy*, 94, pp.395-405, 2012.

[120] D. Assanis, G. Delagrammatikas, R. Fellini, Z. Filipi, J. Liedtke, N. Michelena, P. Papalambros, D. Reyes, D. Rosenbaum, A. Sales, M. Sasena, "An Optimization Approach to Hybrid Electric Propulsion System Design", *Mechanics of Structures and Machines*, 27, 4, pp. 393-421, 1999.

[121] N. Murgovski, L. Johannesson, J. Sjberg, Bo Egardt, "Component Sizing of a Plug-in Hybrid Electric Powertrain via Convex Optimization", *Mechatronics*, 22, pp. 106-120, 2012.

[122] K. Ishihara, N. Kihira, N. Terada, T. Iwahori, "Environmental Burdens of Large Lithium-ion Batteries Developed in a Japanese National Project", www.electrochem.org/dl/ma/202/pdfs/0068.PDF, Central Research Institute of Electric Power Industry, Tokyo.

[123] J. L. Sullivan, L. Gaines, "A Review of Battery Life-Cycle Analysis: State of Knowledge and Critical Needs", Argonne National Laboratory Report, ANL/ESD/10-7, 2010.

[124] H. Kamath, "Lithium Ion Batteries for Electric Transportation: Costs and Markets", http://www.arb.ca.gov/msprog/zevprog/2009symposium/presentations/kamath.pdf, Symposium at California Air Resources Board, 2009.

[125] C. Samaras, K. Meisterling, "Life Cycle Assessment of Greenhouse Gas Emissions from Plug-in Hybrid Vehicles: Implications for Policy", *Environmental Science and Technology*, 42, pp.3170-3176, 2008.

[126] S. Golbuff, "Design Optimization of a Plug-In Hybrid Electric Vehicle", *SAE World Congress*, 2007-04-16.

[127] R. Strengel, "Optimal Control and Estimation", Dover Publications, 1994.

[128] V.N. Afanasev, V.B. Kolmanovskii, V.R. Nosov, "Mathematical Theory of Control System Design", Kluwer Academic Publishers, 1989.

[129] S.K. Porandla, W.D. Gao, "Design Optimization of a Parallel Hybrid Electric Powertrain", *IEEE Vehicle Power and Propulsion Conference*, 2005.

[130] A.A. Pesaran, T. Markel, "Battery Requirements for Plug-in Hybrid Electric Vehicles - Analysis and Rationale", *Electric Vehicle Symposium 23*, 2007.

[131] E. Wood, M. Alexander, T. Bradley, "Investigation of Battery end-of-life conditions for Plug-in Hybrid Electric Vehicles", *Journal of Power Sources*, 196, pp. 5147 5154, 2011.